MONITORING BIOLOGICAL PROCESSES AND INTERACTIONS AT LIPID MEMBRANES USING ION CHANNEL-BASED SENSORS AND MEMBRANE MICROARRAYS

by

Sheereen Majd Zarringhalam Araghy

A dissertation submitted in partial fulfillment
of the requirements for the degree of
Doctor of Philosophy
(Biomedical Engineering)
in The University of Michigan
2009

Doctoral Committee:

Associate Professor Michael Mayer, Chair
Associate Professor L. Jay Guo
Associate Professor Shuichi Takayama
Assistant Professor Mohamed E. H. El-Sayed

Human beings are members of a whole,

In creation of one essence and soul.

If one member is afflicted with pain,

Other members unease will remain.

If you have no sympathy for human pain,

The name of human you cannot retain.

Sa'di of Shiraz

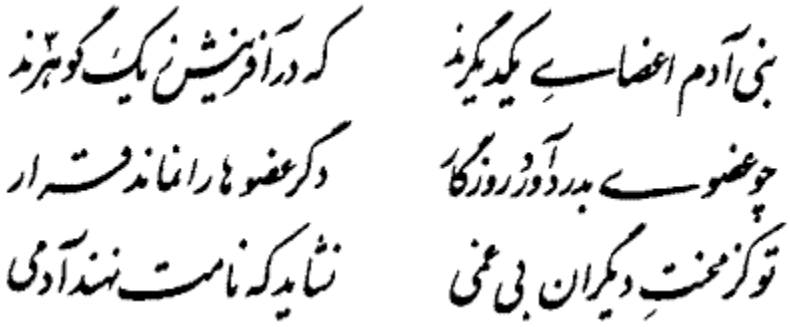

DEDICATION

This thesis is dedicated to my parents, who have raised me to be the person I am today. Thank you for all the unconditional love, guidance, and support that you have always given me!

Also, this thesis is dedicated to my husband who has been a great source of motivation and inspiration for me.

ACKNOWLEDGMENTS

I would like to formally thank:

Dr. Michael Mayer, my research advisor, for his excellent guidance and advice throughout the course of this PhD. I have learned so much, and without you, this would not have been possible. Thank you so much for believing in my abilities, supporting me, and making this journey such a great experience for me!

Dr. Shuichi Takayama, Dr. Mohamed El-Sayed, and Dr. Jay Guo, for serving on my dissertation committee. Thank you for your valuable insight and guidance.

Eric C. Yusko, for assisting in data collection, analysis, and for valuable discussions.

Anna M. Sauer, Nirmish Singla, Alexander D. MacBriar, Jessica S. Wang, and Nashmia Khalid, for assisting in data collection and analysis.

My lab mates in the Biomembrane Lab, for their friendships and support. The last few years have been quite an experience and you have all made it a memorable time of my life. I will miss all of you! Good luck to each of you in your future endeavors.

My parents, for their never-ending love and support in all my efforts, and for giving me the foundation to be who I am. Thank you, Mom and Dad!

My sisters, Nooshin and Simin, and my brother, Afshin, for their love and support throughout the years. Thank you for the laughing and the fighting, and everything in between!

My in-laws, for their support and understanding through the past few years.

And finally my husband, Mohammadreza, for always being there for me. Thank you for your continual love, support, and patience as I went through this journey! I could not have made it through without you by my side.

TABLE OF CONTENTS

LIST OF FIGURES

LIST OF TABLES

ABSTRACT

Many cellular processes involve molecular interactions at the cell membrane. Due to the complexity of living cells, these interactions are usually studied on model membranes. This thesis introduces two platforms based on model membranes for studying biological interactions and processes on cell membranes.

In the first part of this thesis, we employed planar lipid bilayers to develop a novel, label-free, and sensitive assay for monitoring the activity of phospholipases D and C that are critical for cell signaling. The activities of these enzymes typically change the surface charge of the membrane. The present assay employs the ion channel-forming peptide gramicidin A to probe these changes and, hence, to monitor the activity of these phospholipases *in situ* and in real-time. Quantitative results from this assay, allowed us to investigate the kinetics of the heterogeneous catalysis of these enzymes.

In addition we applied this gramicidin-based sensor to monitor the binding of two therapeutic drugs to various bilayers. Quinine, an anti-malaria agent, and imipramine, an anti-depressant, are positively-charged under physiological conditions and, once bound to a membrane, alter the membrane surface charge. The present assay probes these changes and makes it possible to quantify these binding events.

In the second part of this work, we developed a technique that employs topographically-patterned hydrogel stamps to fabricate arrays of membranes and

membrane proteins for screening of membrane interactions. This method takes advantage of the porous, hydrated, and biocompatible nature of hydrogels to print spatially-addressable arrays of membranes in a rapid and parallel fashion. We employed this method for two distinct approaches; one approach takes advantage of the storage capability of agarose stamps and minimizes the required time and amount of membrane preparations by generating multiple copies of a membrane array. The other approach takes advantage of on-stamp preconcentration of cellular membrane fragments to generate arrays of multilayered-membranes with high contents of proteins and enhances detection sensitivity. We used these arrays for screening the interactions of a protein (annexin V) and an anti-inflammatory drug (nimesulide) with various bilayers. We also carried out ligand-binding assays on these arrays and showed that the stamped membrane proteins retained their binding activity.

Chapter 1

Introduction and Background

All prokaryotic and eukaryotic cells are surrounded with a plasma membrane that not only defines the shape and structure of the cell but also acts as a selective barrier with a crucial role in communication between the inside and outside of the cell.[1-3] Many of fundamental processes in cells such as signal transduction and cell proliferation involve membranes at some point. Biomembranes have, consequently, been implicated in a variety of disease states including cancer[4] and Alzheimer's disease.[5,6] Interest in biomembranes, their function, and their dynamics have constantly grown in a number of fields including biology, biochemistry, biophysics, immunology, and pharmacology. Elucidating cellular mechanisms by studying different aspects of membranes on natural cell membranes is extremely difficult due to the complexity of living systems and hence, benefits from representative model membranes.[1,3] These model membranes can be categorized into three main groups of lipid monolayers, lipid bilayers,[1] and lipid vesicles.[7]

This thesis describes two novel platforms based on lipid bilayer model membranes for studying molecular processes and interactions on membranes. The first part of this work presents an ion channel-based sensor for monitoring the activity of membrane-active enzymes and for binding of bioactive molecules at the surface

membranes. The second part of this work introduces a straightforward approach to fabricate arrays of lipid bilayers and arrays of membrane proteins for screening of lipid-protein interactions and drug-membrane interactions.

In the following chapter, this introduction focuses first on a general background on biological membranes and model membranes by discussing "Biological and Model Membranes", and then it focuses on the two parts of the thesis by discussing the two following topics:

- "Planar Lipid Bilayer Systems for Sensing Membrane Interactions"
- "Arrays of Supported Membranes for Screening Membrane Interactions"

1.1. Biological and Model Membranes

1.1.1. Historical View on Biological Membranes

In the mid-nineteenth century, Wilhelm Pfeffer, a plant physiologist, recognized the presence of a semipermeable membrane around the cytoplasm while he was studying osmosis in plant cells.[1,3] Later, additional evidence confirmed the existence of a selective barrier around the cell, the so called the plasma membrane,.

Soon after this discovery, work by Overton on the flux of different molecules into cells provided evidence for the lipid nature of cell membranes.[1,3,8] In his studies, Overton found a strong correlation between the influx of molecules into cells and their partition coefficient between oil and water.

In 1925, Gorter and Grendel showed that lipid molecules in an erythrocyte cell membrane form a bimolecular (bilayer) structure.[1,3,8] Despite all the later modifications of this model, the basic lipid bilayer structure of membranes proposed by Gorter and Grendel has remained unchanged ever since.

In 1935, Davson and Danielli proposed a model in which proteins coated the surfaces of the lipid bilayer and formed a three-layered protein-lipid bilayer-protein structure.[1,3,8] While accepted for the next 30 years, this model was slightly modified to account for the functional diversity in membranes.

In 1970, Singer and Nicolson proposed the fluid mosaic model[9] that described the membrane as a fluid lipid bilayer in which proteins are embedded and can diffuse freely.[1,3,8] The fluid mosaic model was the first model to address the fluidity of natural membranes. Within the past few decades, extensive research on membranes demonstrated

the complexity of natural membranes compared to the simple fluid mosaic model and led to several modifications of this model. Table 1-1 shows an overview of the experimental evolution that led to the current understanding of biomembranes as summarized by Tien *et al.*.[1]

Table 1-1. The lipid bilayer concept and its experimental evolution. This table is taken from Tien *et al.* [1] and the references refer to the citations of original work.

Year	Observer(s)	Experimental finding and insight
1665	R. Hooke	Microscopic observation of cork, Hooke coined the word "cell" which we use today
1672	R. Hooke [1]	"Black holes" in soap bubbles
1704	I. Newton [2]	Thickness of blackest soap films: 9.5 nm
1877	W. Pfeffer	Artificial osmometer and plasma membrane
1890s	E. Overton [4]	Olive oil/water partition coefficient and lipoid nature of cell membrane
1917	I. Langmuir [5]	The monolayer technique; orientation of "soapy" (amphipathic) molecules at interfaces
1920s	H. Fricke [4]	Electrical measurements of red blood cells; plasma membrane less than 10 nm thick
1925	E. Gorter and F. Grendel [7]	Red blood cells covered by two lipid monolayers; the bilayer leaflet model was specifically put forth
1940s	Davson and Danielli [5]	A protein–lipid bilayer-protein sandwich model, a novel proposal
1950s	Robertson [8]	Electron micrsoscopy — the unit membrane concept
1961	Rudin et al. [9–11]	The BLM technique for lipid bilayer reconstitution
1965	Bangham et al. [13]	Liposomes, vesicles with lipid bilayer structures

The present view of biomembranes, proposes that the basic structure of all membranes is a lipid bilayer assembly in which lipid molecules can diffuse. Embedded in, or peripherally associated with, this fluid lipid bilayer are many other components including proteins and carbohydrates.

Moreover, that natural membranes exhibit transverse and lateral asymmetry that is important for their function.[3] Recently, it has become clear that the composition of membranes (in terms of type and ratio of lipids, proteins, and hydrocarbons) varies significantly from one cell type to another, depending on the functional role of the

membrane.[3] The function of the vast number of different lipids is not fully understood; the novel field of lipidomics attempts to elucidate these functions.[3]

1.1.2. Membrane Components

Plasma membranes are composed of three major components: lipids, proteins, and carbohydrates.[10]

Bilayer-forming lipids are amphiphilic molecules that self assemble into a bilayer structure with their hydrophobic fatty acyl chains associated together in the interior of the bilayer and their polar headgroups facing the aqueous environment on either side of the bilayer.

In most natural membranes, proteins constitute the largest weight fraction of the membrane. Membrane proteins can be grouped into two distinct categories of integral proteins and peripheral proteins. Integral or transmembrane proteins contain hydrophobic domains which enable them to pass through the hydrophobic core of the lipid bilayer, whereas peripheral proteins only bind to the surface of the membrane.

Carbohydrates, that form the third major component of biomembranes, are often coupled to lipid or protein molecules forming glycolipids and glycoproteins. Glycolipids and glycoproteins are usually found on the outer leaflet of cell membranes with their hydrocarbate portion located in the extracellular space where they act as cell surface receptors.

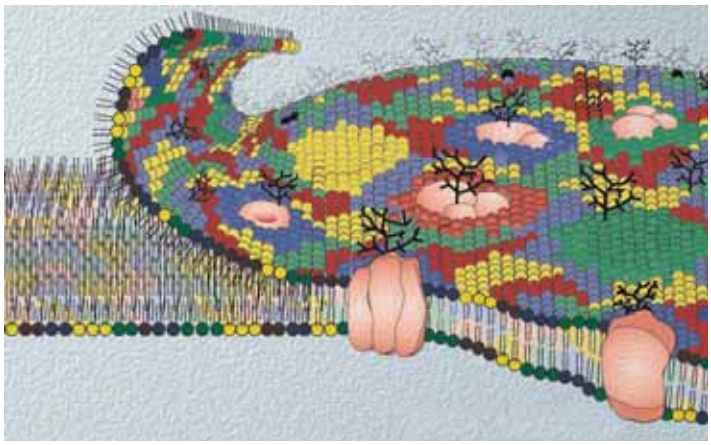

Figure 1-1. Current understanding of the fluid mosaic model for biomembranes, which shows the lipid bilayer in more detail (different lipid species are shown in different colors) with associated membrane proteins and carbohydrates. This figure is adopted from Edinin *et al.* [8].

1.1.3. Model Membranes

The significant role of biomembranes in biology has driven the development of several experimental models for studying biomembranes. These model membranes include lipid monolayers, planar lipid bilayers,[1,11] supported lipid bilayers,[2,10,12] and lipid vesicles.[1,7] Each of these model membranes has advantages and disadvantages as discussed below.

Lipid monolayers, referring to a single layer of lipid molecules that self assemble at the air-water interface, comprised the first model membrane developed for studying different aspects of biomembranes.[1] Given the fundamental lipid bilayer structure in all biomembranes, lipid monolayers mimic only half of a natural membrane and hence, are not ideal models. Models based on a lipid bilayer, therefore, resemble natural membranes better than those based on lipid monolayers.

Planar lipid bilayers are free-standing lipid bilayers that typically span over a small pore in a hydrophobic partition between two aqueous compartments (Figure 1-2).[1,2,11] Electrical access to both sides of these bilayers makes them well suited for electrical measurements across membranes.[11] These systems are not, however, mechanically stable.[13]

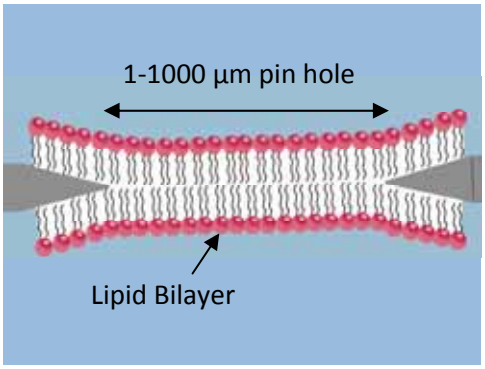

Figure 1-2. Schematic representation of a planar lipid bilayer. These lipid bilayers typically span a pin hole with a diameter of 1-1000 µm in a hydrophobic support.

In supported lipid bilayers, a solid substrate that supports the lipid bilayer (Figure 1-3), provides mechanical stability and makes these systems one of the most robust yet fairly realistic models for biological membranes.[1,2,10,14,15] The applicability of surface detection methods in these systems, makes them particularly attractive for studying molecular interactions at the membrane.[2,10,16] The main drawback of these models is undesired interactions between the membrane components (e.g. lipids and proteins) with the supporting substrate.[2,10]

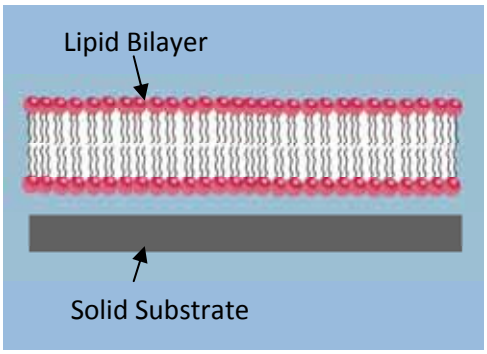

Figure 1-3. Schematic diagram of a solid-supported lipid bilayer.

Lipid vesicles, also called liposomes, are spherical shells made of a lipid bilayer (Figure 1-4).[1] Among the present model membranes, liposomes mimic the inherent spherical shape of natural membranes the best. These membranes are particularly useful for biophysical studies of biomembranes such membrane fusion,[17] curvature,[18] and domain formation.[19,20]

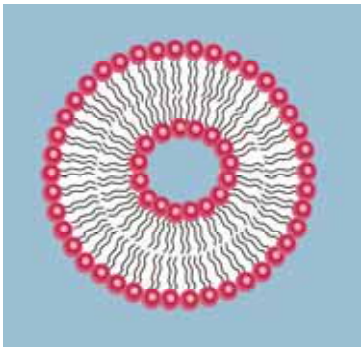

Figure 1-4. Schematic of a lipid vesicle.

While the bilayer in these model membranes is free-standing, lack of electrical access to both sides of the bilayer limits the application of vesicles in electrical probing of membranes and proteins such as ion channels (unless the liposome is accessed with a patch pipette).[11]

1.2. Planar Lipid Bilayer Systems for Sensing Membrane Interactions

This part of the introduction focuses on planar lipid bilayers as model membranes and discusses the fabrication, characterization, and some of the applications of these model membranes. At the end of this section, the main goal of the first part of this thesis is discussed.

In the 1960s Muller *et al.* developed the first planar lipid bilayer system to investigate the electrical properties of a bilayer.[21,22] In this system a lipid bilayer is suspended over a small hole in a partition between two compartments with aqueous solutions. Electrical access to both sides of the bilayer in these systems makes these platforms attractive for electrophysiological studies. Compared to solid-supported bilayers, these free-standing bilayers avoid direct interactions with an underlying substrate and hence, are advantageous for investigation of integral membrane proteins (e.g. ion channels).[2,11] These bilayers have, however, limited lifetime (typically a few hours) due to their poor mechanical stability.[2] This short-term stability limits the application of planar lipid bilayers to relatively short experiments in a controlled laboratory environment. Several recent developments have addressed this issue and strengthened these bilayers. Examples of such strategies include: employing micro pores with diameters below 15 μm[23-25] and sandwiching bilayers between hydrogels.[26-28]

1.2.1. Fabrication of Planar Lipid Bilayers

While several different techniques generate planar lipid bilayers, traditional methods for fabrication of these bilayers include the “painting” method and the “folding” method.[2,3,11]

In the "painting" method[21] a free-standing lipid bilayer is formed by painting a concentrated solution of lipids dissolved in an organic solvent over a small orifice (sub-millimeter diameter) in a nonpolar septum (e.g. Teflon) which separates two aqueous compartments. As the excess solvent disperses to the rim of the pore in the nonpolar septum, lipid molecules self-assemble to a bilayer structure across the orifice. The "painting" method, developed by Mueller and Rudin,[21] has a drawback of producing bilayers that contain uncertain amounts of solvent, such as decane or heptane.

In the "folding" technique,[29] a lipid bilayer forms over a small orifice in a nonpolar septum from opposing two lipid monolayers that were previously formed at an air-water interface. Although in comparison with painted bilayers, folded bilayers are often named "solvent-free", these bilayers also contain small traces of the organic solvent that is required to pretreat the pore (typically hexadecane or squalene).[11]

1.2.2. Biophysical Characterization of Planar Lipid Bilayers

Formation of planar lipid bilayers can be followed by optical microscopy.[2,3,11] Observing this process by an optical microscope for the first time, Mueller *et al.* noted that as the bilayer thins out, a black spot gradually spreads over the film resulting in a black lipid bilayer at the end.[21,22] This dark appearance is due to the destructive interference of the reflected light from water-lipid interface and the phase-shifted light from the lipid-water interface.[2,11] Referring to their appearance under optical microscopy, the term black lipid membrane (BLM) is also used for planar lipid bilayers.[2,3,11]

Planar lipid bilayers are usually probed for their electrical characteristics (e.g. capacitance and conductance). A lipid bilayer is an insulator with a specific capacitance

of 0.6-1 μF cm^{-2}.[11,24] As a result, even a slight defect or pore in the bilayer can be detected by an increase in conductance. Given an estimate of bilayer surface area, the thickness of the bilayer can also be monitored through its capacitance.

1.2.3. Planar Lipid Bilayers for Membrane Studies

Planar lipid bilayers are particularly attractive platforms for electrical measurements across the membrane.[1-3,11] Since their development, these model membranes have been used for studies of different membrane-active molecules such as peptides,[30] proteins,[31,32] and other ion channel-forming biomolecules. These membranes have also been employed for discovery of channel blockers and possible new therapeutics.[33,34]

In recent years, planar lipid membranes with embedded protein pores have received increasing attention for the development of chemo- and biosensors.[2,23,35] Among current applications of these channel-based sensors are: monitoring protein-ligand interactions,[13,36,37] monitoring chemical reactions,[38,39] pH-sensing,[40] probing surface charge,[41-43] and detection of binding and unbinding of organic molecules into modified protein channels.[44-46] Protein pores commonly used for these sensors include alamethicin,[13] α-hemolysin,[45-53] and gramicidin channels.[36-38,40-42]

The goal of the first part of this thesis was to develop an ion channel-based sensor to monitor the activity of surface-active enzymes and other membrane active compounds. To address this goal, we introduced a gramicidin-based assay to monitor and quantify the activity and enzyme kinetics of two membrane-active enzymes, phospholipases C and D, on planar lipid bilayers (chapters 2 and 3). We also present a gramicidin-based platform

to screen and quantify the binding of bioactive molecules including therapeutic compounds to lipid bilayers (chapter 4).

Gramicidin A is a natural channel-forming peptide with a molecular weight of 1.9 kDa that is secreted from the bacterium *Bacillus brevis*.[54] This small peptide self-incorporates into lipid bilayers and upon a reversible head-to-head dimerization forms an aqueous pore with a diameter of 4 Å and a length of 25 Å through the bilayer.[54] The channel forming kinetics of gA pores in a lipid bilayer are evidenced by stepwise changes in conductance, where each step increase illustrates the formation of one gA pore and each step decrease shows the dissociation of a pore. Gramicidin channels are cation selective and facilitate the transmembrane flux of monovalent cations.[54,55]

Previous work on gA pores has demonstrated that the kinetics of gA channels such as their lifetime and opening frequency, depend strongly on the recording buffer as well as the composition of the lipid bilayer that surrounds the channel.[41,56] These kinetics can, hence, reveal information about the environment surrounding the gA channel. As a result, gA channels, in native and chemically derivatized form, have attracted increasing interest as nanosensors to sense membrane surface charge,[42,43] pH at the membrane surface,[40] ligand-protein interactions,[36,37] lipid-protein interactions,[57] and chemical reactions that lead to derivatization of the which a gA derivative.[38,39]

Here we present the first attempt to employ native gramicidin channels to monitor, *in situ* and in real time, the activity of membrane-active enzymes on membranes and to screen binding of bioactive compounds to lipid bilayers. This part of the thesis addresses the following specific aims within the chapters 2 to 4:

- Chapter 2 and 3: To develop a sensitive, label-free, and quantitative assay that proceeds *in situ* an in real time to monitor the enzymatic activity of membrane-active enzymes. To employ the results of this assay to investigate the kinetics of heterogeneous catalysis of these surface-active enzymes by elucidating kinetic constants.
- Chapter 4: To develop a novel, label-free, and quantitative platform to detect binding of membrane active molecules to planar lipid bilayers, and to demonstrate the potential of this platform to quantify binding of pharmaceutical compounds.

1.3. Arrays of Supported Membranes for Screening Membrane Interactions

This part of the introduction focuses on supported lipid membranes and arrays of supported membranes as model membranes, and discusses the fabrication, characterization, and some of the applications of these model membranes. At the end of this section, the main goal of the second part of this thesis is discussed.

Unlike planar lipid bilayers, supported lipid bilayers are mechanically stable. While the supporting substrate provides unique mechanical stability for these lipid bilayers, the presence of a thin (1-2 nm) layer of water between the lipid bilayer and the substrate retains the mobility of lipid molecules within these model membranes.[15,58] In addition, supported membranes are accessible to a wide range of surface-specific analytical techniques, such as atomic force microscopy (AFM),[59,60] surface plasma resonance (SPR),[16] and total internal reflection (TIRF) microscopy.[16] Since their development by Tamm and McConnell in the 1980s,[15] supported lipid bilayers have received increasing attention as one of the most robust yet realistic models for natural membranes.[2,14,16,61,62]

Supported lipid bilayers form and remain on solid supports due to a number of different forces, including van der Waals, electrostatic, hydration, and steric forces.[2,12,63-65] In these systems, therefore, surface properties of the substrate are crucial and strongly influence the quality of the bilayer. Studies have shown that bilayers of high quality (with minimal defects) and high lipid mobility form on hydrophilic and clean surfaces.[2,12] Examples of hydrophilic substrates that are commonly used in this field include glass,[15] quartz,[15] mica,[66] and oxidized silicon.[15] Although these surfaces can support fluid and defect-free bilayers, they are not ideal substrates for bilayers that contain transmembrane

proteins with large peripheral domains.[2,61,67] If the peripheral domain of a protein exceeds 1-2 nm (the thickness of the water film between the bilayer and the supporting substrate), then the protein is likely to interact with the substrate which can cause an irreversible denaturation of the protein.[2] Researchers have addressed this issue by developing polymer cushioned supported bilayer systems in which a cushion of polymer on the substrate elevates the bilayer to provide space for the peripheral domains of integral proteins (Figure 1-5).[67-69] This cushion, hence, protects the protein from direct interactions with the substrate. Various polymer cushions have been employed for this purpose, as summarized by Castellana *et al.,*[2] these include "dextran, cellulose, chitosan, polyelectrolytes, and lipopolymer tethers".

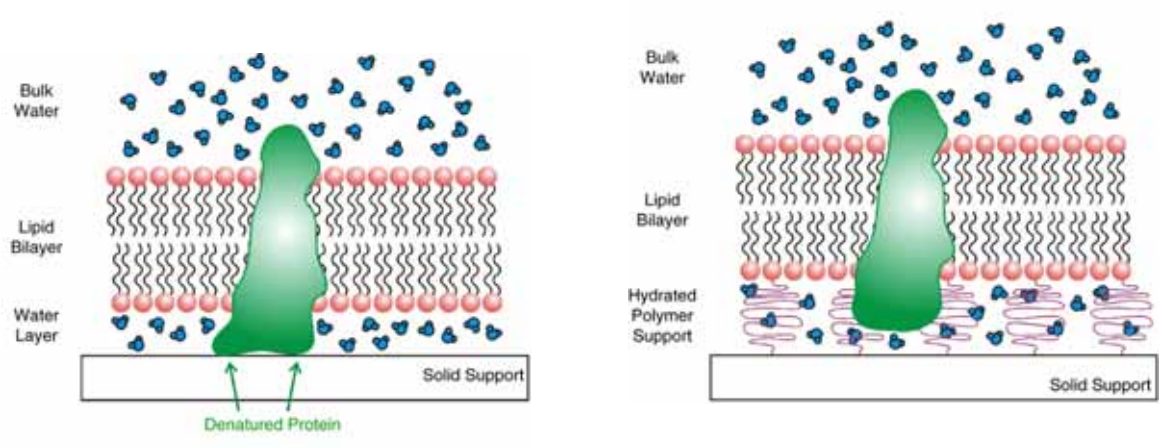

Figure 1-5. Peripheral domains of transmembrane proteins can become immobilized and denatured on a solid support. A polymer cushion helps shield the protein from the substrate. This figure is adopted from Castellana e*t al.*[2].

1.3.1. Formation of Supported Lipid Bilayers

Supported lipid bilayers can be formed by three main techniques ,including the Langmuir-Blodgett/Langmuir-Schaefer method,[15,70] the vesicle fusion method,[71] and the Langmuir-Blodgett/vesicle fusion method.[72]

The Langmuir-Blodgett/Langmuir-Schaefer (LB/LS) technique, developed by Tamm and McConnel in 1984,[15,70] is the oldest method of fabricating solid-supported lipid bilayers. This technique forms a lipid bilayer in two steps. First, a lipid monolayer is formed by spreading lipids at an air-water interface, [73] and a clean, hydrophilic substrate is vertically pulled through this lipid monolayer. This process leads to deposition of the first leaflet of the bilayer onto the substrate (LB method). In the second step, the substrate, already coated with one monolayer, is horizontally pushed through another lipid monolayer at the air-water interface (LS method), completing the formation of a lipid bilayer on the surface (Figure 1-6a). This technique can create bilayers with transverse asymmetry.[74] Also, incorporation of small peptides into the first or second monolayer at the air-water interface results in a supported lipid bilayer that contains these peptides. Incorporation of large transmembrane proteins, however, is not feasible by this method due to the possible exposure of proteins to air and their consequent deactivation.[72]

Vesicle fusion[71,75] is the simplest and most common method for the formation of supported lipid bilayers.[2] In this method, a solution of small or large unilamellar liposomes is exposed to a clean, hydrophilic surface for 1–60 min. At the end of the incubation time, excess liposomes are washed away, leaving behind a supported lipid bilayer behind (Figure 1-6b). Incorporation of membrane proteins into these membranes

is, in principle, relatively straightforward and only requires application of proteoliposomes (liposomes that contain integral membrane proteins) instead of pure liposomes.[76] Moreover, polymer cushioned supported bilayers can be fabricated using the vesicle fusion method by replacing the bare substrate with a polymer-coated substrate. The liposomes and proteoliposomes used in this technique can be prepared in various ways including sonication[77] and extrusion[78] for liposomes and the detergent-dialysis procedure for proteoliposomes.[76]

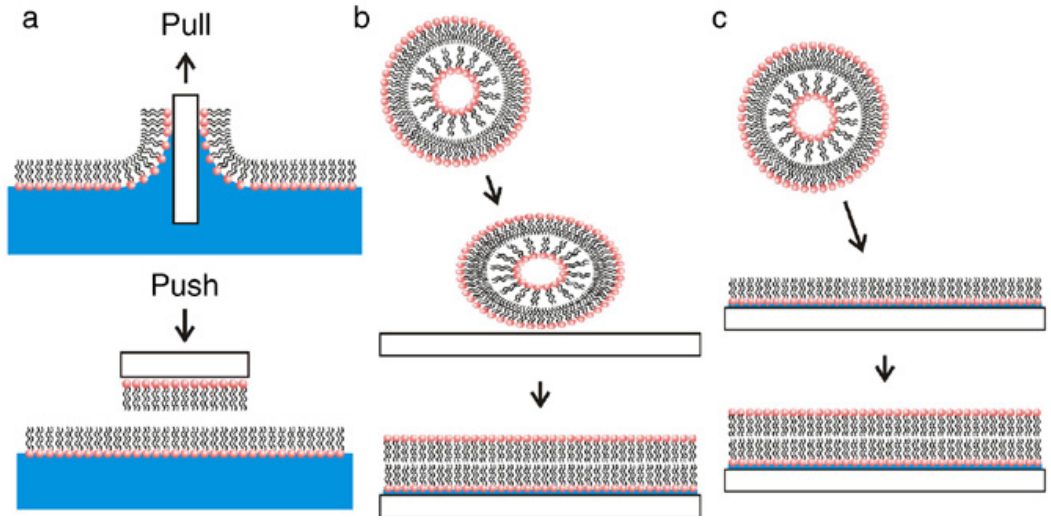

Figure 1-6. Common techniques for the formation of supported lipid bilayers. (a) The Langmuir–Blodgett technique is carried out by pulling a hydrophilic substrate through a lipid monolayer followed by the Langmuir-Schaefer technique that involves pushing the substrate horizontally through another lipid monolayer. (b) In the vesicle fusion method, vesicles in solution adsorb and spontaneously fuse to the surface to form a solid supported lipid bilayer. (c) The Langmuir-Blodgett/vesicle fusion is a combination of the Langmuir–Blodgett and vesicle fusion processes. This figure is taken from Castellana *et al.*[2].

In vesicle fusion, vesicles (also called liposomes) first adsorb to the surface, fuse with each other, and then rupture and spread on the surface, creating small patches of lipid bilayers.[2,12,65] Coalescence of these small bilayer patches forms a large and continuous lipid bilayer (Figure 1-7).[12,63,64,79,80] Despite attempts to understand the exact mechanism of this process, vesicle fusion on hydrophilic surfaces is still not completely understood. Considerable work on this topic has, however, revealed a number of factors that affect the progression of each of the adsorption, fusion, and spreading steps. These factors, as stated by Castellana *et al.*,[2] include "the vesicle composition, size, surface charge, surface roughness, surface cleanliness, solution pH, ionic strength, and the osmotic pressure of the vesicles".[2,12,63,64,79,80]

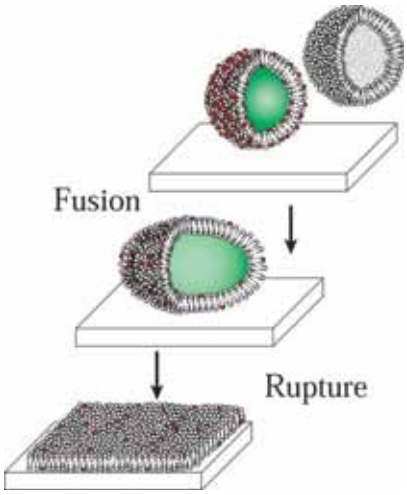

Figure 1-7. Schematic of the proposed mechanism of formation of lipid bilayer in vesicle fusion method. Adsorbed vesicles fuse with themselves until a critical size is reached and then rupture to form bilayer patches. This figure is taken from Johnson *et al.*[63].

Due to the coalescence mechanism of bilayer formation, the vesicle fusion technique often produces bilayers with more defects compared to those produced by LB/LS method. This technique is also usually limited to the production of symmetric lipid bilayers.

The combination of the two aforementioned techniques results in the Langmuir-Blodgett/vesicle fusion method for fabrication of supported lipid bilayers.[72] Similar to the LB/LS method, this method creates a supported lipid bilayer in two steps. In the first step, a lipid monolayer is transferred from the air-water interface to the substrate by the LB technique. In the second step, fusion of liposomes onto the monolayer-coated substrate forms the upper leaflet of the bilayer.

This method is unique in that it has advantages of both the LB/LS and the vesicle fusion methods. For instance, compared to vesicle fusion, this technique forms bilayers with fewer defects and can create lipid bilayers with transverse asymmetry in lipid composition.[81] Furthermore, transmembrane proteins can be incorporated into these supported membranes[72] in the second step by fusing proteoliposomes to form the second leaflet of the bilayer, although not all proteins may remain functional during the process.

1.3.2. Biophysical Characterization of Supported Lipid Bilayers

Supported lipid bilayers are often characterized in terms of their quality, structure, fluidity, and electrical properties.

One of the most common techniques for probing the overall quality of supported bilayers is epifluorescence microscopy.[2] This comparably simple microscopy method is useful in detecting large (i.e. micrometer sized) inhomogeneous and defective areas

within a supported membrane; it requires to add a small fraction (typically ≤1 mol%) of a fluorescently-labeled lipid to the bilayer.

Detection of nanometer-size defects, however, is not feasible by epifluorescence microscopy and necessitates higher-resolution imaging techniques such as atomic force microscopy (AFM).[59,66] This type of microscopy probes the height profile of the membrane on the surface and is commonly used to monitor nanometer-size defects in supported bilayers.[59] This unique approach also distinguishes between single bilayer and multiple bilayer structures in a supported membrane and can detect lateral phase separation in lipid bilayers.[60]

Structural details, such as transverse or lateral organization of supported bilayers, can be studied with a number of different techniques including neutron reflectivity,[58] Fourier transform infrared spectroscopy (FTIR),[82] sum frequency vibrational spectroscopy (SFVS),[83] and fluorescence interface contrast microscopy (FLIC).[81]

Fluidity is one of the key features of natural membranes and its changes influence important physiological functions such as signal transduction.[84,85] Thus, to resemble natural membranes, model membranes such as supported lipid bilayers should be fluid. The significance of fluidity in membranes has driven the development of several techniques for measuring membrane fluidity. Fluorescence recovery after photobleaching (FRAP)[60] is one of the most common methods for quantifying lateral diffusion in cell membranes as well as in model membranes. In this method, a beam of high-intensity light (ideally from a laser) is used to photobleach, irreversibly, a population of fluorophores in a small region within a fluorescently-labeled membrane. Recovery of fluorescence in the

bleached area due to the lateral diffusion of intact, fluorophore-labeled lipids is then monitored and used to calculate the diffusion coefficient, *D*, of the lipids.[86,87]

Other techniques to probe membrane fluidity include fluorescence anisotropy,[88] environmentally-sensitive fluorescent probes (i.e. molecular rotors),[89] fluorescence correlation spectroscopy (FCS),[87] and single particle tracking (SPT).[90]

As mentioned before, a lipid bilayer is an excellent electrical insulator with a specific capacitance of 0.6-1 μF cm^{-2}.[3] In natural membranes, however, a variety of channels and pores embedded in the lipid bilayer facilitate the transport of ions and determine the overall conductance of the cell membrane. In model lipid membranes without embedded channel proteins, therefore, any change in conductance is a measure of existing defects in the bilayer.[11] While for most current applications of supported lipid bilayers, electrical properties and conductance of the bilayer are not critical, for some applications such as sensor development,[2,62] these properties are important. The electrical characterization of supported lipid bilayers is often conducted by impedance spectroscopy.[91,92] In this method, the target lipid bilayer is supported by a conductive substrate (e.g. gold) that acts as an electrode. A second electrode is placed in the aqueous media around the bilayer and the impedance of the system is measured for an applied A/C voltage in a range of frequencies. Electrical properties of the bilayer (including its capacitance and conductance) are then determined by evaluating the entire electrical circuit in the system.[91] For the evaluation, the lipid bilayer in this electrical circuit is represented by a parallel combination of a resistor and a capacitor.[91,92]

1.3.3. Supported Lipid Bilayers for Membrane Studies

Interest in supported lipid bilayers includes studies on the dynamic structure of membranes,[58,69] lipid-protein interactions,[69] ligand-receptor interactions,[16,69,93,94] development of membrane-based biosensors,[2,14,62,95,96] and drug discovery.[97] Selected examples of applications of supported bilayers in these studies are discussed below.

Studies on lipid rafts are often performed on supported lipid bilayers. Lipid rafts, i.e. cholesterol and sphingolipid (SL) enriched domains in the plasma membrane,[19,60,98,99] attract much interest due to their possible role in a broad range of biological processes and, hence, in a number of diseases.[100-102] Several research groups have investigated phase separation and formation of raft-like lipid domains in supported lipid bilayers by epifluorescence microscopy, atomic force microscopy (AFM),[59,60] and near-field scanning optical microscopy (NSOM).[99]

Research on membrane fusion has also employed supported membrane platforms.[103,104] Understanding the mechanism of membrane fusion is important due to the central role of this process in events such as vesicle trafficking, membrane biogenesis, fertilization, and virus entry.[103,104] Recently, several groups have studied protein-mediated fusion of vesicles with supported lipid bilayers by surface-sensitive techniques such as total internal reflection fluorescence microscopy (TIRFM)[103] and Fourier transform infrared (FTIR) spectroscopy.[104]

Interactions between proteins and lipids influence the function of both the proteins and the lipids and are thus critical for many cellular functions.[16,105] These interactions in supported lipid bilayers have been studied by a number of techniques such as epifluorescence microscopy,[106] atomic force microscopy (AFM),[107,108] surface plasma

resonance (SPR),[16,109] impedance spectroscopy,[109] total internal reflection fluorescence microscopy (TIRFM),[16] attenuated total reflection FTIR spectroscopy,[16] and fluorescence resonance energy transfer (FRET).[110] Such interactions have also been investigated by monitoring lateral diffusion of lipids and proteins by techniques such as fluorescence recovery after photobleaching (FRAP)[111-113] and fluorescence correlation spectroscopy (FCS).[114]

1.3.4. Arrays of Membranes and Membrane Proteins

Membrane arrays provide a unique platform to study different aspects of membranes with various compositions under identical conditions and in a parallel fashion. These arrays are, hence, of interest for performing multiplexed, high-information-content assays in both academic and industrial membrane research.[94,97,113,115,116] Arrays of lipid membranes with and without functional transmembrane proteins have been applied for investigating lipid-protein interactions,[106] protein-protein interactions,[113] and drug-membrane interactions.[97,115,116] Due to the medical significance of transmembrane proteins, as the largest group of current therapeutics targets,[116,117] arrays of membrane proteins are particularly attractive for the pharmaceutical industry. Therefore, the ability to pattern arrays of membranes and membrane proteins has become essential.

Arrays of supported lipid bilayers can be produced by different approaches as briefly described here. In one such method, arrays of lipid bilayers can be formed by fusing lipid vesicles onto a partitioned substrate. This technique requires substrates with

patterned barriers, which can be made by standard photolithography[118,119] or microcontact printing with poly(dimethylsiloxane) (PDMS)[120] stamps.[121,122]

Alternatively, arrays of membranes can be created from an existing continuous membrane. Using this approach, a membrane array can be produced when a topographically patterned PDMS stamp removes selected areas of a continuous bilayer. This process is followed by adsorption of a protein, as a barrier, onto these cleared areas.[121,122]

Formation of an array of lipid bilayers from a continuous bilayer can also be addressed by erasing selective regions of a bilayer by high intensity deep-UV illumination through a photomask under aqueous solution.[123]

Furthermore, creating membrane arrays from a continuous membrane can be accomplished by the polymer lift-off method.[124,125] In this method, a thin patterned film of polymer is first deposited onto the substrate and after formation of a continuous bilayer on the substrate, the film is peeled off to leave behind an array of bilayers.

As a third approach, microcontact printing by PDMS stamps can print arrays of lipid bilayers on bare substrates. In this technique, plasma oxidation of the PDMS stamp renders the surface of the stamp hydrophilic; a supported lipid bilayer is formed on the PDMS stamp by vesicle fusion and then is transferred to a clean substrate upon short and close contact to transfer an array of bilayers onto this substrate.[122] As mentioned previously, a PDMS stamp can also remove selective regions of an existing supported bilayer and transfer these bilayer regions onto a clean substrate to create an array of lipid bilayers.[121,122]

While useful for some applications, these established techniques are limited in their ability to vary the membrane composition from one spot to another within one array. Considering the main advantage of membrane arrays, i.e. providing a platform for parallel studies on various membrane compositions in parallel, arrays of membranes with various membrane compositions present a more attractive class of membrane arrays in this field. Existing methods to fabricate such "multi-composition" arrays include:

i) Selective photobleaching of lipid bilayer spots in an array of identical lipid bilayers to produce an array of bilayers with limited differentiation in composition of photobleached and non-photobleached fluorescent lipids (Figure 1-8a).[126,127]

ii) Microcontact printing of spots of bilayers of the same composition but different sizes onto a substrate with patterned corrals. Backfilling these corrals with a solution of vesicles of a different composition results in an array of lipid bilayers with a gradient in the two lipid components (Figure 1-8b).[122,126]

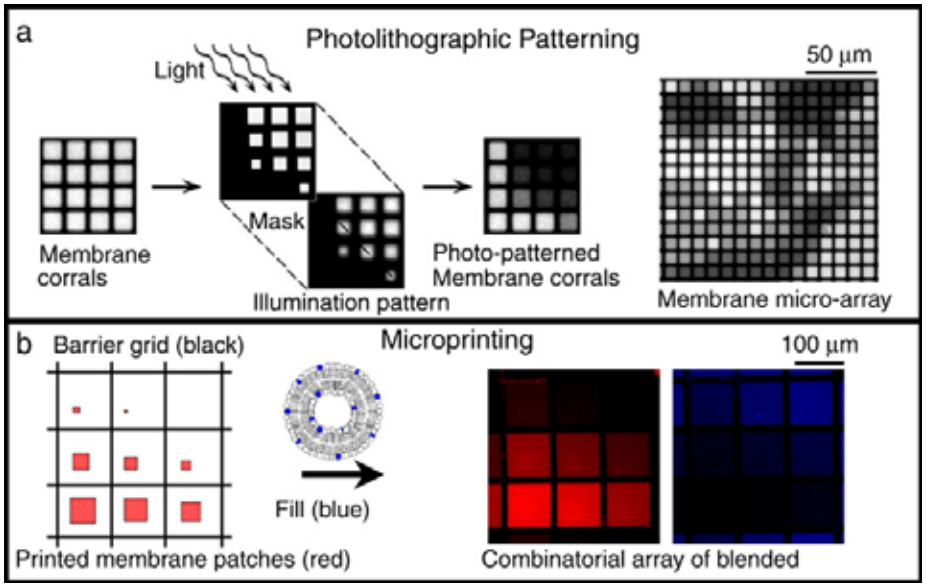

Figure 1-8. (a) Composition array generated by photopatterning. A mask is used to selectively bleach different-sized areas of a membrane array. After diffusive mixing within each corral, a concentration array is observed. (b) Concentration arrays fabricated by microcontact printing of different-sized bilayer patches. After printing, the empty space in each corral is backfilled with small unilamellar vesicles (SUV) to form a continuous bilayer in each corral. Shown here is an epifluorescence image of printed Texas Red labeled membranes backfilled with Cascade Blue labeled lipids. The red image is shown on the left and the blue on the right. This figure is taken from Castellana *et al.*[2].

iii) Flowing of two different liposome solutions within the laminar flow regime inside a microfluidic channel (with a wall of patterned glass) to produce arrays of membrane spots with a gradient in their lipid components that depends on the position of the corral inside the channel (Figure 1-9).[126,128]

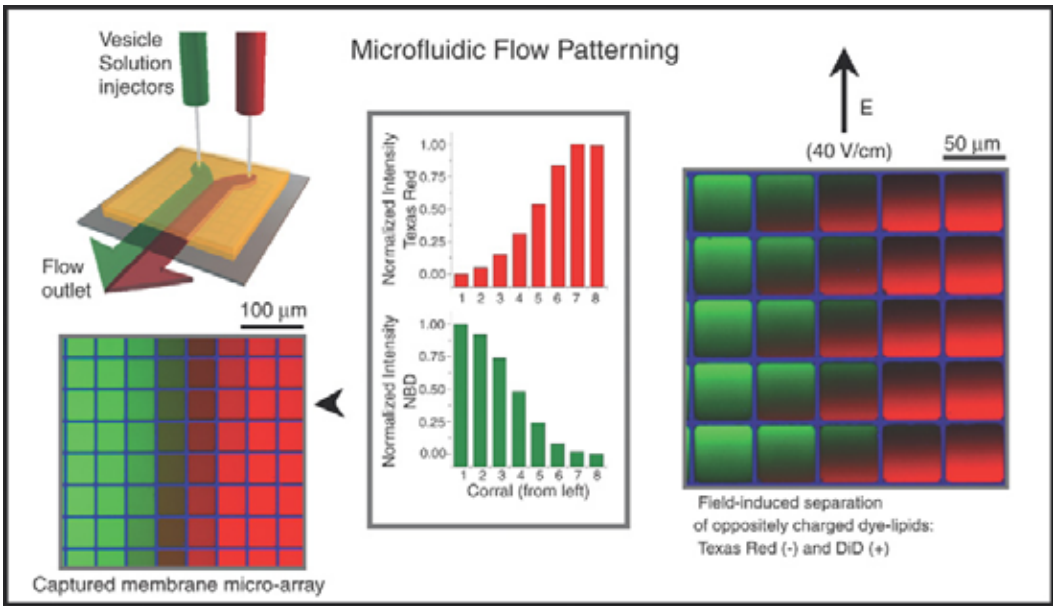

Figure 1-9. Concentration array formed by laminar flow in a microfluidic channel. Diffusive mixing in a microchannel under laminar flow conditions provides a concentration gradient of different dye-labeled vesicles. The concentration of vesicles in the gradient is reflected by the surface concentration of each membrane in the resultant array. The array shown is a mixture of Texas Red labeled lipids (shown in red) and NBD labeled lipids (shown in green). Since the dyes have opposite charges, they can be separated in an electric field as shown in the panel on the right. This figure is taken from Castellana *et al*.[2].

iv) Pipetting of small droplets of different liposome solutions into individual corrals of a substrate with patterned barriers (Figure 1-10).[129] Compared to the other methods, this method has the capability to create membrane arrays with an unlimited number of compositions. Production of membrane arrays by this method has been facilitated by employing quill pin printers.[113]

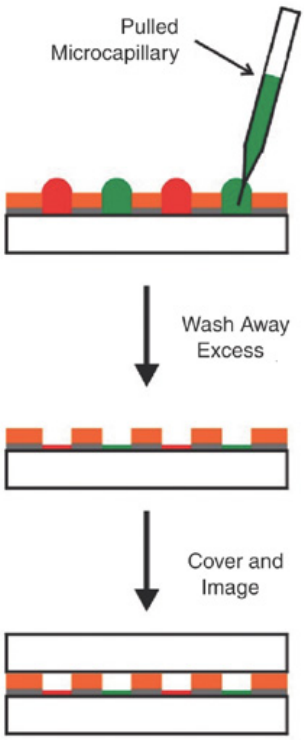

Figure 1-10. Array fabricated by pipetting of individual liposome solutions. A pulled microcapillary tip is used to fill individual corrals on a pre-patterned substrate. This figure is adopted from Castellana *et al*.[2].

Given the application of membrane arrays in today's academic and pharmaceutical research, an ideal fabrication method would create arrays of *fluid* lipid bilayers with *various compositions* in a *rapid* and *parallel* fashion *without* the need for *patterning the substrate* and with *minimal consumption* of lipid preparations. As described above, all current techniques with the capability of producing membrane arrays with various compositions require substrates with patterned corrals. Among these techniques, deposition of small droplets of vesicle solutions[64] onto a patterned substrate is

the only approach that allows fabrication of arrays with a large number of membrane compositions. This technique, however, transfers bilayers in a serial fashion (which in case of large and complex arrays can be time-consuming) unless combined with a quill pin printer.[113]

Despite the usefulness of the established techniques for production of arrays of lipid bilayers, not all of these methods are applicable for fabrication of arrays of lipid bilayers that contain membrane proteins. Fabrication of membrane protein arrays is much more challenging than fabrication of arrays of lipid bilayers due to the fragile nature of these proteins. This fragility requires membrane proteins to be embedded in a membrane environment in order to maintain their native conformations.[94,115,116]

Currently, arrays of membrane proteins are fabricated by deposition of small droplets of a proteoliposome solution onto surfaces.[94,115,116] This technique is able to create arrays with numerous different membrane proteins. In addition, robotic technology has turned this otherwise serial and time-consuming printing approach to a parallel and rapid approach.[94,115,116] The additional cost of robotic technology, however, limits its application in academic research laboratories. In addition, this method deposits nanoliter volumes of membrane preparations, which might lead to drying of the membranes and associated damage to the proteins, unless a controlled humidity environment is maintained.

The goal of the second part of this thesis was to develop a novel and straightforward technique to fabricate spatially addressable arrays of membranes and membrane proteins for screening molecular interactions on membranes. This technique should ideally meet the following requirements:

- produce arrays of fluid and functional membranes with and without integral membrane proteins.
- Transfer membrane arrays without the need for patterned substrates (ideally applicable on bare and coated surfaces).
- create arrays of membranes of various compositions (with no limitation in the number of components, including type of lipid and protein).
- pattern membrane spots of an array in a rapid and parallel fashion.
- prevent dehydration and denaturation of lipids and proteins during the fabrication process.
- minimize the consumption of precious membrane preparations.
- be low-tech and applicable even in a small research laboratory with limited resources.
- be expandable to automated and robotic formats for industrial applications.

To meet these characteristics, we introduce hydrogel-based microcontact printing for fabrication of arrays of supported lipid bilayers of well-defined compositions (chapter 5). We also introduce a novel approach for fabrication of membrane *protein* microarrays using hydrogel-based microcontact printing (chapter 6). In chapters 5 and 6, we discuss whether this novel approach meets presented approaches for all of the aforementioned requirements.

Microcontact printing by poly(dimethylsiloxane) (PDMS) stamps was developed originally to pattern non-polar alkane thiols onto gold surfaces.[120] Since then, this patterning method has found wide application in different fields such as material

science.[2] The stamps used are fabricated by molding PDMS against a lithographically patterned surface.[120] Because the surface of PDMS stamps is inherently hydrophobic, this method is best suited to transfer small non-polar molecules. In order to employ PDMS stamps for patterning hydrophilic materials, the surface of the stamp must be rendered hydrophilic.[130] Although several techniques have been developed to render the PDMS surface hydrophilic, these stamps are still not ideal for patterning hydrophilic materials such as proteins. In 1998, Martin *et al.* have introduced the concept of a "hydrogel stamper" as an alternative to PDMS stamps for stamping hydrophilic materials.[130] Hydrogels are hydrophilic polymers; stamps made of these polymers often contain more than 90% water.[130-133] In addition, hydrogel stamps are porous and can provide a hydrated and biocompatible reservoir for biomolecules.[130-133] These characteristics make hydrogel stamps ideal for patterning biomolecules. Hydrogel stamps have been employed to pattern a variety of soluble proteins (e.g. antibodies and cell adhesion factors)[130,131] as well as bacterial[133] and mammalian cells.[132] Hydrogel stamps have also been used for controlled etching[134] and reactive-patterning of solid surfaces.[135]

Here we present the first attempt to use hydrogel stamps to create arrays of fluid and functional membranes with and without integral membrane proteins for screening of membrane interactions within chapters 5 and 6.

References

1. H. T. Tien and A. L. Ottova, *Journal of Membrane Science* **189** (1), 83 (2001).
2. E. T. Castellana and P. S. Cremer, *Surface Science Reports* **61** (10), 429 (2006).

3. R. B. Gennis, *Gennis, R. B. Springer Advanced Texts in Chemistry: Biomembranes: Molecular Structure and Function. Xvii+533p. Springer-Verlag New York Inc.: Secaucus, New Jersey, USA; Berlin, West Germany. Illus*, XVII+533P (1989).

4. M. Gould and H. Nicholson, *Journal of Andrology* **30**, 52 (2009).

5. I. Peters, U. Igbavboa, T. Schutt et al., *Biochimica Et Biophysica Acta-Biomembranes* **1788** (5), 964 (2009).

6. M. Suwalsky, S. Bolognin, and P. Zatta, *Journal of Alzheimers Disease* **17** (1), 81 (2009).

7. Y. Onoue, T. Suzuki, M. Davidson et al., *Biochimica Et Biophysica Acta-Biomembranes* **1788** (6), 1332 (2009).

8. M. Edidin, *Nature Reviews Molecular Cell Biology* **4** (5), 414 (2003).

9. S. J. Singer and G. L. Nicolson, *Science* **175** (4023), 720 (1972).

10. M. Tanaka and E. Sackmann, *Nature* **437** (7059), 656 (2005).

11. M. Winterhalter, *Current Opinion in Colloid & Interface Science* **5** (3-4), 250 (2000).

12. R. P. Richter, R. Berat, and A. R. Brisson, *Langmuir* **22** (8), 3497 (2006).

13. M. Mayer, V. Semetey, I. Gitlin et al., *Journal of the American Chemical Society* **130** (4), 1453 (2008).

14. D. Anrather, M. Smetazko, M. Saba et al., *Journal of Nanoscience and Nanotechnology* **4** (1-2), 1 (2004).

15. L. K. Tamm and H. M. McConnell, *Biophysical Journal* **47** (1), 105 (1985).

16. S. Heyse, T. Stora, E. Schmid et al., *Biochimica Et Biophysica Acta-Reviews on Biomembranes* **1376** (3), 319 (1998).

17. F. Nomura, T. Inaba, S. Ishikawa et al., *Proceedings of the National Academy of Sciences of the United States of America* **101** (10), 3420 (2004).

18. G. Drin, J. Bigay, and B. Antonny, *M S-Medecine Sciences* **25** (5), 483 (2009).

19. S. L. Veatch and S. L. Keller, *Biophysical Journal* **85** (5), 3074 (2003).

20. S. L. Veatch, I. V. Polozov, K. Gawrisch et al., *Biophysical Journal* **86** (5), 2910 (2004).

21. P. Mueller, D. O. Rudin, H. T. Tien et al., *Nature* **194** (4832), 979 (1962).

22. P. Mueller, W. C. Wescott, D. O. Rudin et al., *Journal of Physical Chemistry* **67** (2), 534 (1963).

23. H. Bayley and P. S. Cremer, *Nature* **413** (6852), 226 (2001).

24. M. Mayer, J. K. Kriebel, M. T. Tosteson et al., *Biophysical Journal* **85** (4), 2684 (2003).

25. M. C. Peterman, J. M. Ziebarth, O. Braha et al., *Biomedical Microdevices* **4** (3), 231 (2002).

26. T. J. Jeon, N. Malmstadt, J. Poulos et al., presented at the 51st Annual Meeting of the Biophysical-Society, Baltimore, MD, 2007 (unpublished).

27. T. J. Jeon, J. L. Poulos, and J. J. Schmidt, *Lab on a Chip* **8** (10), 1742 (2008).

28. N. Malmstadt, L. J. Jeon, and J. J. Schmidt, *Advanced Materials* **20** (1), 84 (2008).

29. M. Montal and P. Mueller, *Proceedings of the National Academy of Sciences of the United States of America* **69** (12), 3561 (1972).

30. E. Bamberg, H. Alpes, H. J. Apell et al., *Journal of Membrane Biology* **50** (3-4), 257 (1979).

31. F. Gomezlagunas, A. Pena, A. Lievano et al., *Biophysical Journal* **56** (1), 115 (1989).

32. P. Van Gelder, F. Dumas, and M. Winterhalter, *Biophysical Chemistry* **85** (2-3), 153 (2000).

33. C. Frenkel, K. Weckbecker, H. C. Wartenberg et al., *Neuroscience Letters* **249** (2-3), 131 (1998).

34. P. W. Radke, C. Frenkel, and B. W. Urban, *European Journal of Anaesthesiology* **15** (1), 89 (1998).

35. E. Reimhult and K. Kumar, *Trends in Biotechnology* **26** (2), 82 (2008).

36. A. Hirano, M. Wakabayashi, Y. Matsuno et al., *Biosensors & Bioelectronics* **18** (8), 973 (2003).

37. S. Futaki, Y. J. Zhang, T. Kiwada et al., *Bioorganic & Medicinal Chemistry* **12** (6), 1343 (2004).

38. S. Blake, R. Capone, M. Mayer et al., *Bioconjugate Chemistry* **19** (8), 1614 (2008).

39. S. Blake, T. Mayer, M. Mayer et al., *ChemBioChem* **7** (3), 433 (2006).

40. V. Borisenko, Z. H. Zhang, and G. A. Woolley, *Biochimica Et Biophysica Acta-Biomembranes* **1558** (1), 26 (2002).

41. V. Aguilella, T. K. Rostovtseva, I. Vodyanoy et al., *Biophysical Journal* **72** (2), TH275 (1997).

42. R. Capone, S. Blake, M. R. Restrepo et al., *Journal of the American Chemical Society* **129** (31), 9737 (2007).

43. T. K. Rostovtseva, V. M. Aguilella, I. Vodyanoy et al., *Biophysical Journal* **75** (4), 1783 (1998).

44. O. Braha, B. Walker, S. Cheley et al., *Chemistry & Biology* **4** (7), 497 (1997).

45. S. Cheley, H. Z. Xie, and H. Bayley, *ChemBioChem* **7** (12), 1923 (2006).

46. L. Q. Gu, O. Braha, S. Conlan et al., *Nature* **398** (6729), 686 (1999).

47. Y. Astier, O. Uzun, and F. Stellacci, *Small* **5** (11), 1273 (2009).

48. S. Howorka, S. Cheley, and H. Bayley, *Nature Biotechnology* **19** (7), 636 (2001).

49. S. Howorka, J. Nam, H. Bayley et al., presented at the 48th Annual Meeting of the Biophysical Society, Baltimore, MD, 2004 (unpublished).

50. S. Howorka, J. Nam, H. Bayley et al., *Angewandte Chemie-International Edition* **43** (7), 842 (2004).

51. T. Luchian, S. H. Shin, and H. Bayley, *Angewandte Chemie-International Edition* **42** (17), 1925 (2003).

52. S. H. Shin and H. Bayley, *Journal of the American Chemical Society* **127** (30), 10462 (2005).

53. S. H. Shin, T. Luchian, S. Cheley et al., *Angewandte Chemie-International Edition* **41** (19), 3707 (2002).

54. O. S. Andersen, R. E. Koeppe, and B. Roux, *Ieee Transactions on Nanobioscience* **4** (1), 10 (2005).

55. Olaf S. Andersen, Roger E. Koeppe, II, and Benoit Roux, *Biological and Medical Physics, Biomedical Engineering*, 33 (2007).

56. H. J. Apell, E. Bamberg, and P. Lauger, *Biochimica Et Biophysica Acta* **552** (3), 369 (1979).

57. K. Eskesen, B. I. Kristensen, A. J. Jorgensen et al., *European Biophysics Journal with Biophysics Letters* **30** (1), 27 (2001).

58. S. J. Johnson, T. M. Bayerl, D. C. McDermott et al., *Biophysical Journal* **59** (2), 289 (1991).

59. D. M. Czajkowsky and Z. F. Shao, in *Atomic Force Microscopy in Cell Biology* (2002), Vol. 68, pp. 231.

60. T. V. Ratto and M. L. Longo, *Biophysical Journal* **83** (6), 3380 (2002).

61. T. Baumgart and A. Offenhausser, *Langmuir* **19** (5), 1730 (2003).

62. H. T. Tien and A. L. Ottova, *Electrochimica Acta* **43** (23), 3587 (1998).

63. J. M. Johnson, T. Ha, S. Chu et al., *Biophysical Journal* **83** (6), 3371 (2002).

64. P. S. Cremer and S. G. Boxer, *Journal of Physical Chemistry B* **103** (13), 2554 (1999).

65. T. H. Anderson, Y. J. Min, K. L. Weirich et al., *Langmuir* **25** (12), 6997 (2009).

66. J. A. N. Zasadzinski, C. A. Helm, M. L. Longo et al., *Biophysical Journal* **59** (3), 755 (1991).

67. J. Spinke, J. Yang, H. Wolf et al., *Biophysical Journal* **63** (6), 1667 (1992).

68. M. L. Wagner and L. K. Tamm, *Biophysical Journal* **79** (3), 1400 (2000).

69. M. L. Wanger and L. K. Tamm, *Biophysical Journal* **79** (1), 1400 (2000).

70. L. K. Tamm, *Klinische Wochenschrift* **62** (10), 502 (1984).

71. A. A. Brian and H. M. McConnell, *Proceedings of the National Academy of Sciences of the United States of America-Biological Sciences* **81** (19), 6159 (1984).

72. E. Kalb, S. Frey, and L. K. Tamm, *Biochimica Et Biophysica Acta* **1103** (2), 307 (1992).

73. I. Langmuir, *Transactions of the Faraday Society* **15** (3), 0062 (1920).

74. G. Csucs and J. J. Ramsden, *Biochimica Et Biophysica Acta-Biomembranes* **1369** (2), 304 (1998).

75. H. M. McConnell, T. H. Watts, R. M. Weis et al., *Biochimica Et Biophysica Acta* **864** (1), 95 (1986).

76. L. T. Mimms, G. Zampighi, Y. Nozaki et al., *Biochemistry* **20** (4), 833 (1981).

77. Y. Barenholz, D. Gibbes, B. J. Litman et al., *Biochemistry* **16** (12), 2806 (1977).

78. M. J. Hope, M. B. Bally, G. Webb et al., *Biochimica Et Biophysica Acta* **812** (1), 55 (1985).

79. C. Hamai, T. L. Yang, S. Kataoka et al., *Biophysical Journal* **90** (4), 1241 (2006).

80. B. Seantier and B. Kasemo, *Langmuir* **25** (10), 5767 (2009).

81. J. M. Crane, V. Kiessling, and L. K. Tamm, *Langmuir* **21** (4), 1377 (2005).

82. L. K. Tamm and S. A. Tatulian, *Quarterly Reviews of Biophysics* **30** (4), 365 (1997).

83. J. Liu and J. C. Conboy, *Journal of the American Chemical Society* **126** (27), 8376 (2004).

84. G. Deliconstantinos, *Anticancer Research* **7** (5), 1011 (1987).

85. G. S. Zubenko, U. Kopp, T. Seto et al., *Psychopharmacology* **145** (2), 175 (1999).

86. D. Axelrod, D. E. Koppel, J. Schlessinger et al., *Biophysical Journal* **16** (9), 1055 (1976).

87. E. I. Goksu, B. A. Nellis, W. C. Lin et al., *Langmuir* **25** (6), 3713 (2009).

88. M. Shinitzky and Y. Barenholz, *Biochimica Et Biophysica Acta* **515** (4), 367 (1978).

89. M. A. Haidekker, T. Brady, K. Wen et al., *Bioorganic & Medicinal Chemistry* **10** (11), 3627 (2002).

90. T. Schmidt, G. J. Schutz, W. Baumgartner et al., *Journal of Physical Chemistry* **99** (49), 17662 (1995).

91. C. Steinem, A. Janshoff, W. P. Ulrich et al., *Biochimica Et Biophysica Acta-Biomembranes* **1279** (2), 169 (1996).

92. S. Terrettaz, M. Mayer, and H. Vogel, *Langmuir* **19** (14), 5567 (2003).

93. C. Bieri, O. P. Ernst, S. Heyse et al., *Nature Biotechnology* **17** (11), 1105 (1999).

94. Y. Fang, A. G. Frutos, and J. Lahiri, *Journal of the American Chemical Society* **124** (11), 2394 (2002).

95. H. Kiefer, B. Klee, E. John et al., *Biosensors & Bioelectronics* **6** (3), 233 (1991).

96. E. Sackmann and M. Tanaka, *Trends in Biotechnology* **18** (2), 58 (2000).

97. J. T. Groves, *Current Opinion in Drug Discovery & Development* **5** (4), 606 (2002).

98. H. M. McConnell and M. Vrljic, *Annual Review of Biophysics and Biomolecular Structure* **32**, 469 (2003).

99. A. Ianoul, P. Burgos, Z. Lu et al., *Langmuir* **19** (22), 9246 (2003).

100. H. P. Cheng, K. S. Vetrivel, P. Gong et al., *Nature Clinical Practice Neurology* **3** (7), 374 (2007).

101. E. C. Jury, F. Flores-Borja, and P. S. Kabouridis, *Seminars in Cell & Developmental Biology* **18** (5), 608 (2007).

102. K. Simons and L. Rajendran, *Journal of Neurochemistry* **108**, 43 (2009).

103. Peter Hinterdorfer, Gwen Baber, and Lukas K. Tamm, *Journal of Biological Chemistry* **269** (32), 20360 (1994).

104. S. A. Tatulian, P. Hinterdorfer, G. Baber et al., *Embo Journal* **14** (22), 5514 (1995).

105. J. M. Sanderson, *Organic & Biomolecular Chemistry* **3** (2), 201 (2005).

106. S. Majd, D. J. Estes, and M. Mayer, *Calcium Binding Proteins* **1** (1), 26 (2006).

107. V. Gerke, C. E. Creutz, and S. E. Moss, *Nature Reviews Molecular Cell Biology* **6** (6), 449 (2005).

108. H. Mueller, H. J. Butt, and E. Bamberg, *Journal of Physical Chemistry B* **104** (18), 4552 (2000).

109. S. Terrettaz, T. Stora, C. Duschl et al., *Langmuir* **9** (5), 1361 (1993).

110. J. F. Tait, D. F. Gibson, and C. Smith, *Analytical Biochemistry* **329** (1), 112 (2004).

111. L. Cezanne, A. Lopez, F. Loste et al., *Biochemistry* **38** (9), 2779 (1999).

112. R. Gilmanshin, C. E. Creutz, and L. K. Tamm, *Biochemistry* **33** (27), 8225 (1994).

113. V. Yamazaki, O. Sirenko, R. J. Schafer et al., *Bmc Biotechnology* **5** (2005).

114. A. J. Garcia-Saez and P. Schwille, *Methods* **46** (2), 116 (2008).

115. Y. Fang, A. G. Frutos, and J. Lahiri, *ChemBioChem* **3** (10), 987 (2002).

116. Y. Fang, J. Lahiri, and L. Picard, *Drug Discovery Today* **8** (16), 755 (2003).

117. P. Ma and R. Zemmel, *Nature Reviews Drug Discovery* **1** (8), 571 (2002).

118. J. T. Groves, N. Ulman, and S. G. Boxer, *Science* **275** (5300), 651 (1997).

119. J. T. Groves, N. Ulman, P. S. Cremer et al., *Langmuir* **14** (12), 3347 (1998).

120. A. Kumar, H. A. Biebuyck, and G. M. Whitesides, *Langmuir* **10** (5), 1498 (1994).

121. L. A. Kung, L. Kam, J. S. Hovis et al., *Langmuir* **16** (17), 6773 (2000).

122. J. S. Hovis and S. G. Boxer, *Langmuir* **17** (11), 3400 (2001).

123. C. K. Yee, M. L. Amweg, and A. N. Parikh, *Advanced Materials* **16** (14), 1184 (2004).

124. R. N. Orth, J. Kameoka, W. R. Zipfel et al., *Biophysical Journal* **85** (5), 3066 (2003).

125. M. Wu, D. Holowka, H. G. Craighead et al., *Proceedings of the National Academy of Sciences of the United States of America* **101** (38), 13798 (2004).

126. J. T. Groves and S. G. Boxer, *Accounts of Chemical Research* **35** (3), 149 (2002).

127. L. A. Kung, J. T. Groves, N. Ulman et al., *Advanced Materials* **12** (10), 731 (2000).

128. L. Kam and S. G. Boxer, *Langmuir* **19** (5), 1624 (2003).

129. P. S. Cremer and T. L. Yang, *Journal of the American Chemical Society* **121** (35), 8130 (1999).

130. B. D. Martin, B. P. Gaber, C. H. Patterson et al., *Langmuir* **14** (15), 3971 (1998).

131. M. Mayer, J. Yang, I. Gitlin et al., *Proteomics* **4** (8), 2366 (2004).

132. M. M. Stevens, M. Mayer, D. G. Anderson et al., *Biomaterials* **26** (36), 7636 (2005).

133. D. B. Weibel, A. Lee, M. Mayer et al., *Langmuir* **21** (14), 6436 (2005).

134. S. K. Smoukov, K. J. M. Bishop, R. Klajn et al., *Advanced Materials* **17** (11), 1361 (2005).

135. C. J. Campbell, S. K. Smoukov, K. J. M. Bishop et al., *Langmuir* **21** (7), 2637 (2005).

Chapter 2

Gramicidin Pores Report the Activity of Membrane-Active Enzymes

Abstract

Phospholipases constitute a ubiquitous class of membrane-active enzymes that play a key role in signaling, proliferation, and membrane trafficking. Aberrant phospholipase activity is implicated in a range of diseases including cancer, inflammation, and myocardial disease. Characterization of these enzymes is therefore important, both for improving the understanding of phospholipase catalysis, and for accelerating pharmaceutical and biotechnological applications. This chapter describes a novel approach to monitor, *in-situ* and in real-time, the activity of phospholipase D (PLD) and phospholipase C (PLC) on planar lipid bilayers. This method is based on enzyme-induced changes in the electrical charge of lipid bilayers and on the concomitant change in ion concentration near lipid membranes. The approach reports these changes in local ion concentration by a measurable change in the ion conductance through pores of the ion channel-forming peptide gramicidin A. This enzyme assay hence takes advantage of the amplification characteristics of gramicidin pores to sense the activity of picomolar to nanomolar concentrations of enzyme without requiring labeling of substrates or products. The resulting method proceeds without the need for detergents, quantifies

enzyme activity on native lipid substrates within minutes, and provides unique access to both leaflets of well-defined lipid bilayers; this method also makes it possible to generate planar lipid bilayers with transverse lipid asymmetry.

2.1. Introduction

Phospholipases are membrane-active enzymes that catalyze the hydrolysis of specific ester bonds in phospholipids. These enzymes play a critical role in cell signaling, proliferation, and vesicle trafficking.[1-3] As a result, phospholipases are implicated in a range of diseases including cancer, inflammation, and myocardial disease.[1-4] To improve the understanding of these enzymes, characterization methods that monitor the activity of phospholipases *in situ*, in real time, and in a label-free fashion, would be useful. Due to the heterogeneous nature of catalytic reactions on lipid membranes it is, however, often challenging to monitor the activity of membrane-active enzymes.[5-7] Established methods to characterize phospholipases include pH-stat[5,8-10] and those assays that measure the absorbance,[7,8] fluorescence,[9,11] or radioactivity[3,7,12] of their enzymatic products. While radioactive and fluorescent assays offer high sensitivity, these assays are often not performed *in situ*, and the need for labeling of the substrate can limit the application or affect the results of these assays. Other assays employ coupled enzyme reactions[1,13,14] in which the optimum experimental condition may be limited by the second enzyme. More recently, liquid crystals were employed for label-free detection of phospholipase activity, however, this approach is not quantitative.[15,16]

Here, we describe a novel, label-free, rapid, and quantitative method to monitor, *in situ*, the activity of phospholipases D and C (PLD, PLC) on planar lipid bilayers. This approach offers high sensitivity by ion channel amplification[17-21] and employs planar lipid bilayers instead of micelles or liposomes. The assay hence provides access to both leaflets of a bilayer—a unique characteristic that makes this assay platform attractive for generating asymmetric lipid bilayers by adding different enzymes to each side of a membrane.

PLD cleaves the phosphodiester bond on the polar side of phospholipid headgroups (Figure 2-1a) while PLC cleaves the bond on the glycerol side (Figure 2-2).[1,3,7]

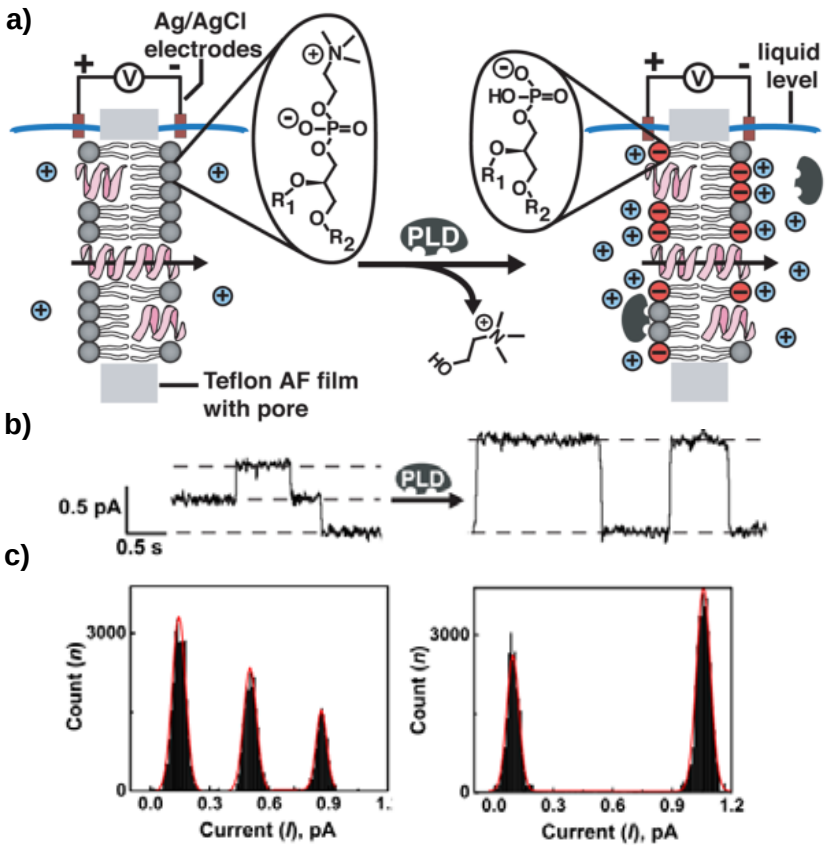

Figure 2-1. *In situ* monitoring of the activity of PLD on planar lipid bilayers by changes in single channel conductance of gA pores, γ. (a) As PLD hydrolyzes electrically neutral (zwitterionic) phosphatidylcholine (PC) lipids and produces choline and negatively-charged phosphatidic acid (PA) lipids,[1] accumulation of cations close to the membrane surface leads to a significant increase in γ.[18,22,23] (b) Current versus time recordings in the presence of 2 pM gA before and after addition of PLD. Current steps in these recordings represent opening and closing of individual gA pores. (c) Corresponding histograms of current amplitudes illustrate the PLD-induced increase in the mean step amplitude of currents through individual gA pores: 0.36 pA before addition of PLD (left panel) compared to 0.96 pA after addition of PLD (right panel). Dividing this amplitude by the voltage that was applied during the current recording (here 0.1 V), revealed γ = 3.6 pS before addition of PLD (left panel) and γ = 9.6 pS after addition of PLD (right panel).

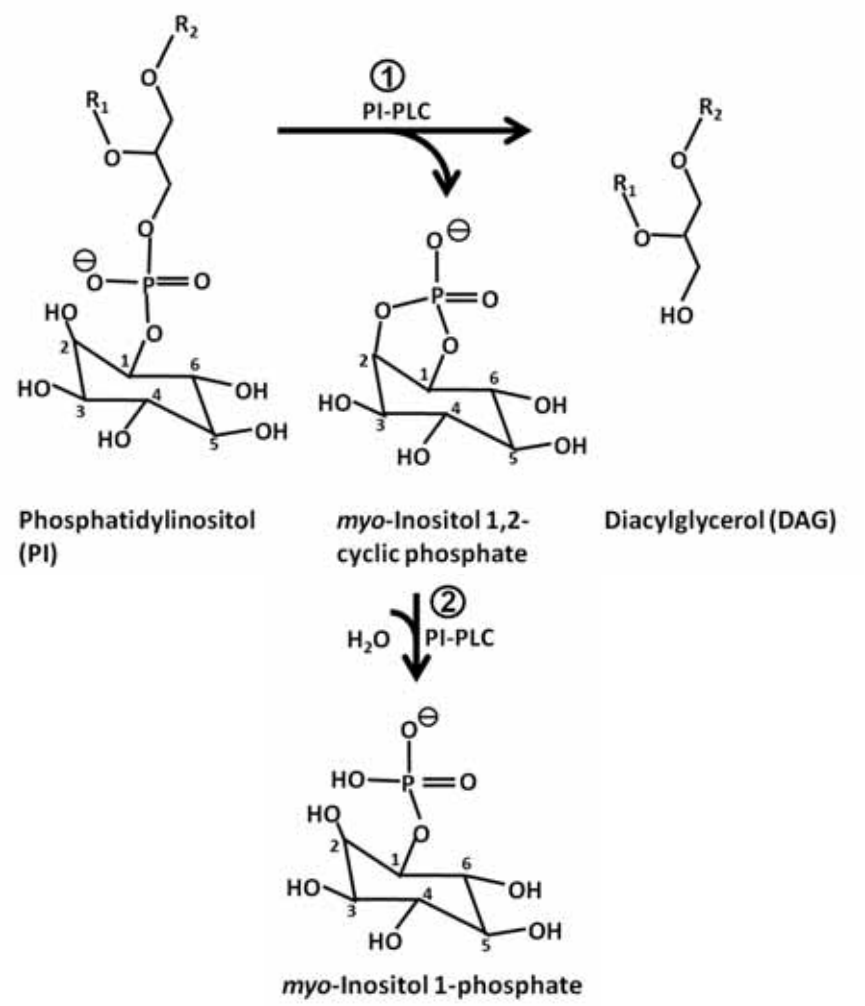

Figure 2-2. PI-PLC catalyzed hydrolysis of PI lipids proceeds in two steps. In the first reaction, PI-PLC catalyzes hydrolysis of PI to produce electrically neutral DAG lipids and soluble *myo*-inositol 1,2-cyclic phosphate and in the second, slower reaction PI-PLC hydrolyzes *myo*-inositol 1,2-cyclic phosphate to *myo*-inositol 1-phosphate.[12,24]

These phospholipases, therefore, modify the headgroup of phospholipids and, for many lipid substrates, this modification results in a change in the net charge of the lipid

molecule. At ionic strengths close to, or below the physiologic range, this enzyme-induced change in the electric charge on the lipids in a membrane results in a change of the local concentration of counter ions near the membrane surface[25] and can be detected by the channel-forming peptide gramicidin A (gA).[18,22,23,26] Hence, the enzyme assays introduced here, take advantage of the change in the single-channel ion conductance through gA pores, γ, in response to enzyme-catalyzed modifications of the charge of lipids.[18,22,23] Figure 2-1 illustrates this concept for PLD.

2.2. Results and Discussion

2.2.1. PLD Assay

In order to demonstrate the ability of this gA-based assay to detect the enzymatic activity of PLD, we formed planar lipid bilayers containing phosphatidylcholine (PC) lipids as substrate and monitored the changes in γ upon addition of PLD from cabbage (EC 3.1.4.4).[27] To relate the changes in γ to the changes in membrane composition, we first acquired a calibration curve (Figure 2-3a) of γ (in units of pS = 10^{-12} Ω^{-1}) as a function of the mole fraction of phosphatidic acid (X_{PA}, unitless); PA is the negatively-charged lipid product of PLD-catalyzed hydrolysis of neutral PC lipids (Figure 2-1a). Eq. (1), which resulted from the curve fit in Figure 2-3a, describes this calibration curve:[27]

$$\gamma = 3.50 \text{ pS} + (12.83 \text{ pS} \times X_{PA}) / (0.23 + X_{PA}) \, . \qquad (1)$$

Figure 2-3b demonstrates that the addition of PLD to both sides of a bilayer resulted in a time-dependent increase in γ. Interestingly, this increase progressed with an initial lag phase of slow change, followed by a rapid increase in γ. We attributed this lag phase (which lasted 5-9 min depending on the enzyme concentration) to a mixing time and delayed binding of PLD to PC membranes. Kuppe et *al.* have previously reported a similar lag phase of slow activity of PLD on PC bilayers. These authors demonstrated that Ca^{+}-induced formation of PA domains in PC membranes[27] is a key parameter that facilitates binding of PLD to the membrane surface and significantly increases the hydrolysis rate of PLD.[14]

To estimate the change in X_{PA} in membranes upon addition of PLD, we used Eq. (1). Figure 2-4 shows the linear, time-dependent changes in X_{PA} after the lag phase for different PLD concentrations. We defined the lag time as the interval from addition of PLD until X_{PA} reached a value of ~0.03. The inset in Figure 2-4 reveals that the rate of product formation (dX_{PA}/dt) increased linearly with an increase in enzyme concentration.

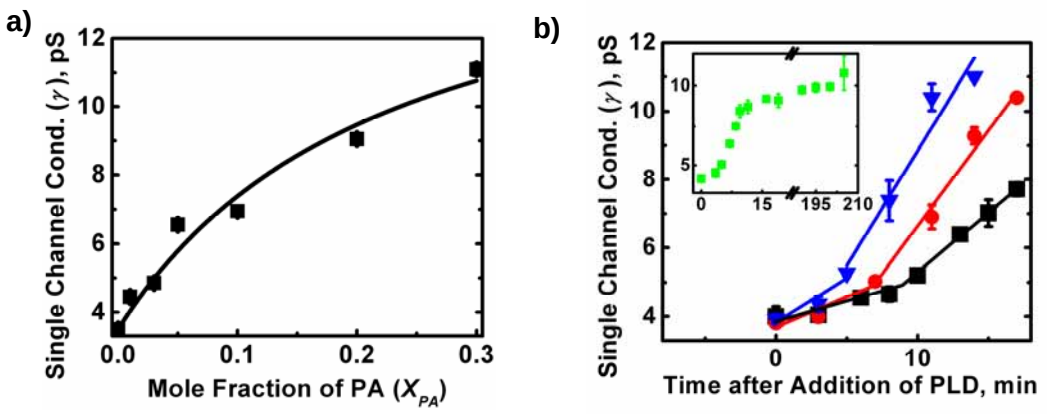

Figure 2-3. Single channel conductance of gA pores, γ, as a function of PA membrane content and as a function of time after addition of PLD. (a) Calibration curve of γ versus the mole fraction of negatively-charged PA lipids, X_{PA}, in PC membranes. The graph shows the best fit ($R^2 = 0.97$, $N = 7$) to a hyperbolic function[27] of the form $\gamma = \gamma_0 + (A \times X_{PA}) / (B + X_{PA})$, where A (pS) and B (unitless) are fitting parameters, and γ_0 (pS) is γ before the addition of PLD. (b) Time-dependent increase in γ upon addition of various conc. of PLD, including: (■) 2.3, (●) 3.1, and (▼) 5.2 units·mL^{-1} corresponding to PLD conc. of ~15-40 nM to a pure PC bilayer. The lines represent the best linear fits. For each PLD concentration, points within the lag phase and after the lag phase were fitted separately. Typically the slope after the lag phase was 2.6-3.1 fold larger than the slope during the lag phase. The inset shows the enzymatic hydrolysis by 4.2 units·mL^{-1} of PLD over an extended period of time. Error bars represent the standard error of the mean ($N \geq 3$). Ion channel recordings proceeded in an aqueous electrolyte containing 10 mM CsCl, 0.5 mM $CaCl_2$, and 10 mM cesium acetate at pH 5.5.

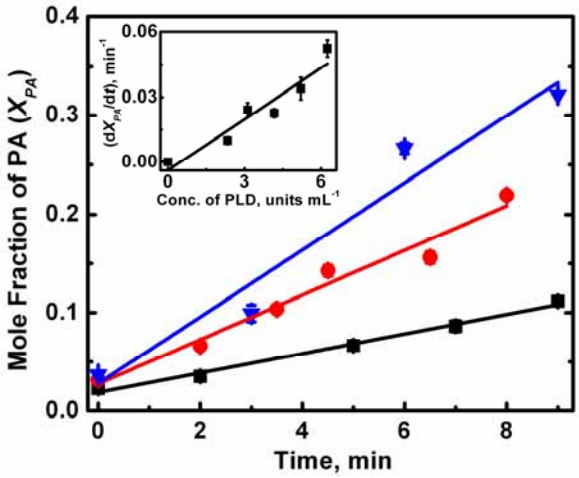

Figure 2-4. Graph showing the change in mole fraction of PA, X_{PA}, in PC membranes after addition of (■) 2.3, (●) 4.2, and (▼) 5.2 units·mL^{-1} PLD. The *x*-axis shows the time after the lag phase. The lines represent the best linear fits to the data. Error bars represent the standard error of the mean ($N \geq 3$). The inset depicts the slope from these linear fits, representing dX_{PA}/dt as a function of PLD concentration. Error bars in the inset show the error of the linear fits used to obtain dX_{PA}/dt.

2.2.2. Lag Phase in PLD Hydrolysis

Figure 2-5, which shows a plot of X_{PA} as a function of time, illustrates a clear biphasic behavior with two distinct linear slopes. In the first phase, defined as lag phase (the time interval from addition of PLD until X_{PA} reached a value of ~0.03), which started immediately after addition of PLD and typically continued for ~5-9 min, X_{PA} increased slowly with time in a linear fashion. Once the mole fraction of PA reached a value of ~0.03, the time-dependent increase of X_{PA} entered a second phase of linear change with a steeper positive slope. In the analysis performed here, we employed the linear slope of the second phase as the initial hydrolysis rate of PLD (Figure 2-4). The hydrolysis rate

after the lag phase was typically 3-6 fold higher than the hydrolysis rate during the lag phase.

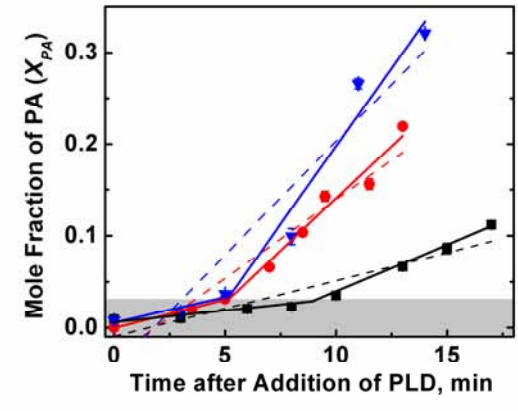

Figure 2-5. Biphasic change in mole fraction of PA, X_{PA}, in PC membranes after addition of (■) 2.3 (●) 4.2, and (▼) 5.2 units·mL^{-1} PLD. The graph shows the mean value of X_{PA} in planar lipid bilayers after addition of PLD. Error bars represent the standard error of the mean ($N \geq 3$). Dashed lines represent the best linear fits to the data (black: $X_{PA} = -0.009 + 0.006\ (min^{-1}) \times t\ (min)$, with N = 8, $R^2 = 0.86$, red: $X_{PA} = -0.031 + 0.017\ (min^{-1}) \times t\ (min)$, with N = 8, $R^2 = 0.91$, blue: $X_{PA} = -0.045 + 0.025\ (min^{-1}) \times t\ (min)$, with N = 6, $R^2 = 0.87$). The first part of the solid lines represents the best linear fits to the points in the lag phase (black: $X_{PA} = 0.006 + 0.003\ (min^{-1}) \times t\ (min)$, with N = 4, $R^2 = 0.85$, red: $X_{PA} = 0 + 0.006\ (min^{-1}) \times t\ (min)$, with N = 3, $R^2 = 1$, blue: $X_{PA} = 0.005 + 0.006\ (min^{-1}) \times t\ (min)$, with N = 3, $R^2 = 0.78$) and the second part of the solid lines represent the best linear fits to the points after the lag phase (black: $X_{PA} = -0.061 + 0.009\ (min^{-1}) \times t\ (min)$, with N = 4, $R^2 = 0.99$, red: $X_{PA} = -0.086 + 0.022\ (min^{-1}) \times t\ (min)$, with N = 6, $R^2 = 0.96$, blue: $X_{PA} = -0.142 + 0.034\ (min^{-1}) \times t\ (min)$, with N = 4, $R^2 = 0.93$). The gray area illustrates the lag phase.

2.2.3. Control Experiments

To confirm a functional dependence of γ on the enzymatic activity of PLD, we performed a control experiment with heat-denatured PLD and found no increase in γ (Figure 2-6a). Furthermore we monitored the changes in γ upon addition of PLD in the presence of two PLD inhibitors, resveratrol[3,28] and cyclosporine A.[29] Figure 2-6a shows that both inhibitors reduced the reaction rate significantly.

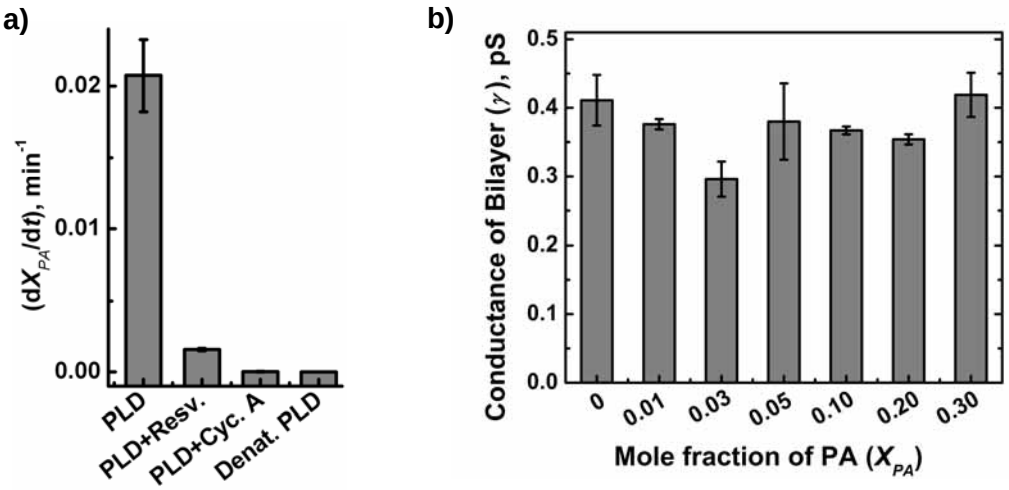

Figure 2-6. (a) Comparison of the initial velocity (dX_{PA}/dt) of PC hydrolysis by 4.2 units·mL^{-1} of PLD in the presence of two inhibitors, resveratrol (final conc. ~130 μM) and cyclosporin A (final conc. 5 μM), and after adding heat-denatured PLD. All error bars show the error of the linear fits used to obtain dX_{PA}/dt. (b) Effect of PA content in planar lipid bilayers on the conductivity through the bilayer in the *absence* of gA. Error bars represent standard error of the mean ($N \geq 3$).

We also examined the effect of the soluble product of the reaction, choline, on γ. During the experiments with PLD, the mole fraction of the enzymatic product PA

typically reached a final value of ~0.3 which corresponded to ~45 nanomoles of PA lipids and an average concentration of ~15 μM in a 3 mL compartment. We, therefore, estimated the concentration of the soluble product of this enzymatic reaction, choline, to be ≤ 15 μM and examined the effect of choline chloride on the conductance of gA within a final concentration range of 0-20 μM (in a buffer solution containing 10 mM CsCl and 10 mM cesium acetate with a pH of 5.5). These experiments revealed that the presence of 0-20 μM choline chloride did not significantly affect the single channel conductance of gA (change < 3%).

Hovis and co-workers have investigated the effect of ionic strength on the organization and topology of supported lipid bilayers composed of PC and PA lipids.[30,31] These authors demonstrated that lowering the ionic strength led to formation of PA-enriched domains in supported bilayers that contained more than 10 mol% PA. To examine the effect of such organizational change on the permeability of the planar lipid bilayers employed in this work, we probed the conductivity through PC bilayers that contained 0-30 mol% of PA lipids under the same condition as the enzymatic assay but in the *absence* of gramicidin pores. Figure 2-6b illustrates the mean conductance through the examined lipid bilayers with different PA contents but in the absence of gA. These results revealed small variations in conductance of these lipid bilayers (0.3-0.4 pS), however, we did not observe a trend of the change in conductance as a function of X_{PA}. As explained before, these small variations in conductance of ions through the bilayer membrane itself, did not affect the accuracy of the determination of the single channel conductance of gA pores since we based the analysis exclusively on step-changes in current which resulted from opening and closing of individual gA pores.

Together, these control experiments confirmed that the increase in γ upon addition of PLD was due to enzymatic activity and not due to artifacts.

2.2.4. Generation of Asymmetric Lipid Bilayers

To explore the potential of this assay platform to create asymmetric planar lipid bilayers, we exposed one side of a PC bilayer to active PLD and the other side to inactivated PLD. We hypothesized that asymmetric activity of the enzyme would create a planar bilayer with transverse asymmetry, in which one leaflet (exposed to active PLD) would contain the catalytic product, i.e. negatively-charged PA lipids, and the other leaflet (exposed to inactivated PLD) would retain unmodified substrate, i.e. neutral PC lipids. We have previously demonstrated that γ is affected only by the electric charges present near the *entrance* of gA channels and not by the charges near the *exit* of the pore.[18] Since gA is permeable to cations, the entrance of gA pores is always located in the positively polarized compartment of the bilayer setup. Hence, the entrance of gA channels can be switched from one compartment to the other based on the polarity of applied voltage. We, therefore, hypothesized that if asymmetric activity of PLD on the PC bilayer produces a bilayer with transverse lipid asymmetry, gA pores would have a large conductance when the polarity of the voltage would place the entrance of gA on the side of the negatively-charged leaflet (i.e., the side with active PLD), whereas gA pores would have a low conductance when the polarity of the voltage would place the entrance on the side of the neutral leaflet of the bilayer (i.e., the side with inactive PLD).

Figure 2-7b shows that, as expected, γ changed asymmetrically depending on the polarity of the applied voltage: at +100 mV, γ increased over time (with this polarity, the entrance of the gA pores was located on the side with active PLD), whereas γ did not increase significantly at -100 mV, when the polarity placed the gA entrance on the side with inactive PLD. We obtained inactivated PLD from a preparation that went through at least three freeze-thaw cycles, followed by extended storage at 4º C.

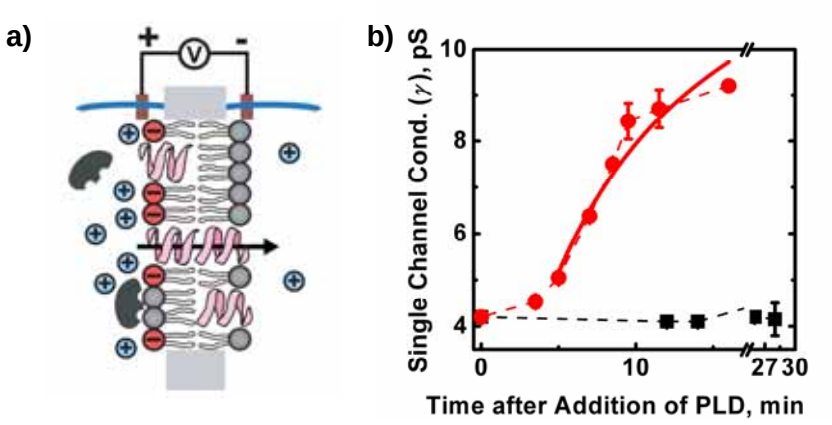

Figure 2-7. Generation of planar lipid bilayers with transverse asymmetry by addition of active PLD to one compartment of the bilayer setup and addition of inactive PLD to the other compartment. (a) Schematic representation of PLD-induced asymmetry in a bilayer. (b) Graph showing changes in γ when the polarity was such that (●) the entrance of gA pores was located in the compartment with 4.2 units·mL^{-1} active PLD, or (■) in the compartment with 4.2 units·mL^{-1} inactive PLD. Error bars represent the standard error of the mean ($N \geq 3$). The solid red curve illustrates the best fit ($R^2 = 0.93$, $N = 6$) of the points shown in red to Eq. (3). For this fit only data after the lag phase were included (the point at ~5 min corresponds to X_{PA} ~0.03 and marks the end of lag phase).

To describe the relationship between γ and the time after addition of PLD, we derived an equation to fit the data in Figure 2-7b. As shown by Eq. (1), γ is a hyperbolic function of the mole fraction of PA in the membrane, X_{PA}, while the relationship between X_{PA} and time, t, after addition of PLD can be described by a rate equation for pseudo-first order kinetics of the form:

$$X_{PA} = 1 - e^{-kt} \ , \tag{2}$$

where the fitting parameter k (min^{-1}) is a pseudo-first order rate constant of the overall reaction at a given concentration of PLD. Combining Eq. (1) and Eq. (2), we obtained the functional dependence of γ on the time t after addition of PLD:

$$\gamma = 3.50 \text{ pS} + \frac{12.83 \text{ pS} \times (1 - e^{-k(t-t_0)})}{0.23 + (1 - e^{-k(t-t_0)})} \ . \tag{3}$$

We introduced t_0 (min) in Eq. (3) to account for the lag phase. The solid red curve in Figure 2-7 illustrates the best fit of the six points shown in red after the lag phase to Eq. (3), with $k = 0.02$ min^{-1} and $t_0 = 3.16$ min for the best fit.

The strong difference between γ as a function of the polarity of the applied voltage in Figure 2-7b demonstrates the ability of the platform presented here to create asymmetric lipid bilayers by asymmetric addition of an enzyme to a symmetric planar bilayer. Although not demonstrated in this communication, we think that this capability is attractive since intracellular lipases process lipids in natural biomembranes with strong

transverse asymmetry. The assay developed here, may hence make it possible to study lipase activity in bilayers that are better models of physiologic membranes than liposomes or micelles. In addition, the capability of generating asymmetric lipid bilayers by exploiting lipase activity as demonstrated here, may be useful for studying the effect of transverse asymmetry on the activity of other membrane proteins, such as ion channels and transport proteins. And finally, the results from asymmetric addition of enzymes shown in Figure 2-7, provide additional evidence that the observed changes in γ were indeed due to the enzyme activity of phospholipase and not due to artifacts.

2.2.5. PLC Assay

In order to extend this label-free, ion channel-based approach of quantifying enzyme activity to another relevant enzyme, we monitored the activity of phosphatidylinositol-specific PLC (PI-PLC) from *Bacillus cereus* (EC 3.1.4.10). In this case, we recorded the changes in γ in PC bilayers that contained initially 10 % PI (i.e. $X_{PI,0} = 0.1$) upon addition of the PI-PLC enzyme.

In these experiments, as PI-PLC catalyzed the hydrolysis of negatively-charged PI lipids and produced neutral diacylglycerol (DAG) lipids[12] (Figure 2-2), the concentration of cations close to the membrane surface gradually decreased, leading to a measurable reduction of γ. Figure 2-8a shows a calibration curve of γ as a function of X_{PI}. Eq. (4), which resulted from the curve fit in Figure 2-8a, describes this calibration curve:

$$\gamma = 8.65 \text{ pS} + \frac{8.26 \text{ pS} \times X_{PI}}{0.07 + X_{PI}}. \quad (4)$$

Using Eq. (4), we estimated X_{PI} as a function of time after addition of PI-PLC. Figure 2-8b shows the decrease in X_{PI} after addition of ~40 and ~80 pM of PI-PLC. The initial slopes of the two resulting exponential fits in Figure 2-8a, differed by a factor of 2.1 and were hence close to the expected value of 2.0.

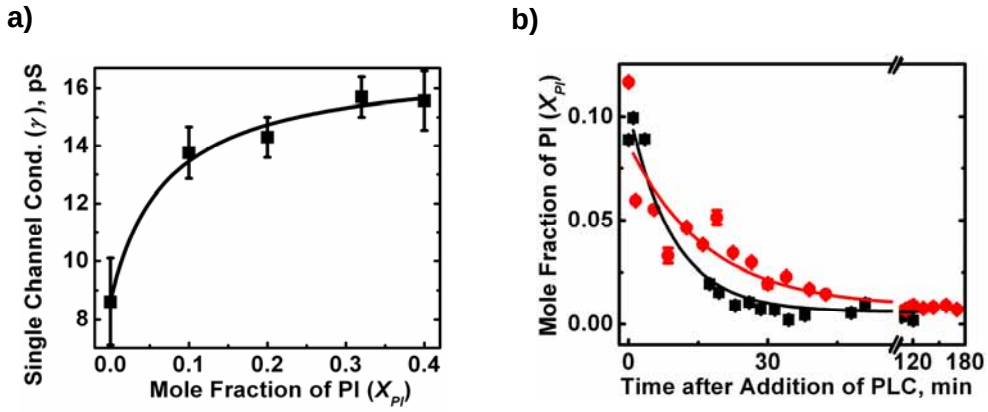

Figure 2-8. (a) Single channel conductance of gA, γ, as a function of the mole fraction of PI (X_{PI}) in PC membranes. The black curve corresponds to Eq. (4) and represents the best fit (R^2= 0.93, N = 5) to a hyperbolic function. (b) Decrease in X_{PI} of membranes after addition of (●) 0.0015 and (■) 0.0030 units·mL^{-1} PLC. The solid curves show the best fit of the data to an exponential decay of the form $X_{PI} = X_{PI,0} \times \exp(-k \times t)$, where $X_{PI,0} = 0.1$, while k (min^{-1}) is the fitting parameter at a given enzyme concentration, and t (min) is time. All error bars represent the standard error of the mean ($N \geq 3$). Single channel recordings proceeded in 20 mM KCl with 10 mM HEPES at pH 7.4.

2.2.6. Limit of Detection and Sensitivity of the Assay

The limit of detection (LOD) of the PLD assay and the PLC assay presented here, according to the definition of LOD = 3 × standard deviation (STD), is equal to a mole fraction of PA, X_{PA}, of 0.003 and to a mole fraction of PI, X_{PI}, of 0.078 respectively. We calculated the LOD for the PLD enzymatic assay considering a standard deviation of 0.05 pS for the conductance of gA in a PC bilayer. For this analysis, we employed Eq. (1) and standard error propagation rules to convert the smallest detectable change in the conductance of gA, γ, to the smallest detectable change in X_{PA} in the membrane as the detection limit of this assay. A similar approach for the PLC enzymatic assay, considering a standard deviation of 1.45 pS for the conductance of gA in a bilayer composed of PC and 10 mol% PI and employing Eq. (4) gave a value of 0.078 as the smallest detectable change in X_{PI} in the membrane as the detection limit of this assay.

We obtained this sensitivity with an ionic strength of ~21.5 mM; the sensitivity of the assay decreases with increasing ionic strength because the effect of electrostatic attraction of cations near a negatively-charged membrane surface will contribute relatively less to γ than the increased concentration of cations in the bulk solution.[18,22,23,27] Nevertheless, we and others showed previously that negatively-charged membranes still increase γ significantly at ionic strengths close to the physiologic range (e.g. at 100 mM KCl).[18,22,23]

2.2.7. Signal Amplification through Gramicidin A Pore

Ion channels are attractive for sensing applications due to their inherent amplification capability:[15,18,20-23,32-38] Opening of a single ion channel can lead to the flux of 10^3-10^6 ions per millisecond through the channel.[18] Previous studies have employed gA pores[26,39-45] to sense the electrical charge on the lipids surrounding the channel in the membrane.[18,22,23] These studies showed that a slight difference in the electrical charge on the lipid membrane can lead to an amplified change in single channel conductance of gA. The present assay took advantage of this amplifying effect of gA pores to detect the enzymatic activity of PLD and PLC. For instance, Figure 2-3a reveals that an increase of only 5% in the mole fraction of negatively-charged PA lipids in a PC membrane (i.e., a change from $X_{PA} = 0$ to $X_{PA} = 0.05$) led to an increase in single channel conductance of gA pores from $\gamma = 3.5$ pS to $\gamma = 6.5$ pS, corresponding to an increase of 86%. In this assay, therefore, gA pores offered an amplification factor of ~17 (0.86 / 0.05) for sensing the enzymatic activity of PLD.

2.3. Conclusion

In summary, this work presents a novel, label-free assay to monitor, in real time, the enzymatic activity of phospholipases D and C on planar lipid bilayers. This ion channel-based assay provides unique access to both leaflets of a bilayer, proceeds on membranes with well-defined lipid composition, and exploits amplification characteristics of an ion pore.[18] In addition, this assay detects enzyme activity within minutes at picomolar to nanomolar concentrations of enzyme on native lipid substrates

without requiring detergents or labels. Finally, this assay platform makes it possible to generate planar lipid bilayers with transverse lipid asymmetry.

2.4. Experimental Section

2.4.1. Materials

We purchased cesium acetate, resveratrol, and cyclosporin A from Sigma Aldrich; potassium chloride (KCl) from EMD Chemicals; cesium chloride (CsCl) from International Biotechnologies, Inc.; choline chloride from Fluka; calcium chloride ($CaCl_2$), pentane, and hexadecane from Fluka; and HEPES from Fisher Scientific. Gramicidin A (gA) was purchased as gramicidin D from Sigma Aldrich and purified by silica chromatography as described previously[46] to afford a final purity of 97% of gA. We purchased the following phospholipids form Avanti Polar Lipids, Inc.: 1,2-diphytanoyl-*sn*-glycero-3-phosphocholine (DiPhyPC), 1,2-diphytanoyl-*sn*-glycero-3-phosphate (sodium salt) (DiPhyPA), and 1,2-dioleoyl-*sn*-glycero-3-phosphoinositol (ammonium salt) (PI). Phospholipase D (PLD) from cabbage (EC 3.1.4.4) was obtained from Sigma Aldrich and phosphatidylinositol-specific phospholipase C (PI-PLC) from *Bacillus cereus* (EC 3.1.4.10) was purchased from Invitrogen.

2.4.2. Storage and Final Concentration of Enzymes

We received PLD as a lyophilized powder and immediately dissolved it in a buffer solution containing 10 mM CsCl, 0.5 mM $CaCl_2$, and 10 mM cesium acetate with

a pH of 5.5 (the same buffer was used for single channel recordings with this enzyme) to a final activity of 2,500 units mL^{-1}. We aliquoted and stored this PLD solution at -80º C until usage. According to Sigma Aldrich, one unit of PLD liberates 1.0 μmol of choline from L-α-phosphatidylcholine (egg yolk) per hour at pH 5.6 at 30 °C. The specific activity of this enzyme, provided by Sigma Aldrich, was more than 1670 units per milligram of protein. Assuming a pure enzyme and considering a molecular weight of ~92,000 Da,[47] a concentration of 1 unit mL^{-1} corresponds to a concentration of ~17.1 nM. We used this enzyme in a concentration range of ~15-40 nM in the bilayer chamber.

We received PI-PLC with an activity of 100 units mL^{-1} in a solution containing 20 mM Tris-HCl, pH 7.5, 1 mM EDTA, 0.01 % sodium azide, and 50% glycerol from Invitrogen, and stored it at -80º C. After thawing this enzyme preparation for the first time, we diluted it 10-fold in a buffer solution containing 20 mM KCl, 10 mM HEPES, pH 7.4 (this buffer was used for single channel recordings with this enzyme). We then aliquoted and stored the diluted enzyme solution at -80º C until usage. The unit definition for this enzyme, according to Invitrogen, is the amount of enzyme that converts 1 μmol of substrate to product per minute under the conditions of the assay. The specific activity of this enzyme, according to Invitrogen, was at least 1,000 units per milligram of protein. Assuming a pure enzyme and considering a molecular weight of ~35,000 Da, a concentration of 1 unit mL^{-1} corresponds to ~10.9 nM. We used this enzyme in a concentration range of ~43-86 pM in the bilayer setup. Therefore, with the standard bilayer setup used here, which had a volume of 3-4 mL, we were able to sense the activity of 172 femtomoles of PLC enzyme. It may be worth to point out that microfabricated bilayer setups[48-51] have the capacity of measuring single ion channel

conductance in volumes as small as 10 μL. Employing such miniaturized setups for the assays developed here, may make it possible to quantify the activity of 430 attomoles of PLC.

To minimize loss of enzyme activity due to storage of these enzymes in solution, we always thawed fresh aliquots of enzyme solutions shortly before addition to the bilayer setup.

2.4.3. Formation of Planar Lipid Bilayers

We formed planar lipid bilayers[52,53] with the "folding technique"[18,32] in a custom-made bilayer setup fabricated in Teflon with two compartments of 3 or 4 mL capacity. We separated these two compartments by a thin Teflon film that contained one aperture with a diameter of ~100 μm (Eastern Scientific Inc.). We used vacuum grease (Corning) to attach the Teflon film to the chamber and to create a water tight seal between the two compartments. To facilitate bilayer formation, we pretreated the area surrounding the aperture of the Teflon film on each side with 2 μL of 5% (v/v) hexadecane in pentane. After addition of 1 mL of appropriate electrolyte (see below) to each compartment, we spread 3-5 μL of a lipid solution in pentane (25 mg mL^{-1} for DiPhyPC or 5 mg mL^{-1} for mixtures containing 90 mol% DiphyPC and 10 mol% phosphatidylinositol) at the air-water interface of the electrolyte solution and raised the liquid level by adding another 2 or 3 mL (depending on the compartment size) of electrolyte. Raising the liquid level in these two compartments above the aperture in the Teflon film resulted in the formation of a lipid bilayer from apposition of two lipid monolayers as described originally by Montal

and Mueller[54]. If raising the liquid level did not immediately result in formation a bilayer over the aperture, we lowered the liquid level in one or both compartments, followed by raising the electrolyte solution again. We repeated this cycle until we obtained a bilayer with a minimum capacitance of 70 pF.

The electrolyte solution for the experiments with PLD contained 10 mM CsCl, 0.5 mM $CaCl_2$, and 10 mM cesium acetate at a pH of 5.5 (adjusted with HCl). For experiments with PLC, the electrolyte contained 20 mM KCl and 10 mM HEPES at a pH of 7.4 (adjusted with KOH). We chose electrolytes with low ionic strength for these single channel recordings because the charge-induced local increase in cation concentration close to a membrane affects the gA conductance more significantly under conditions of low ionic strength compared to conditions of high ionic strength.[18,22,23]

2.4.4. Single Channel Recordings

Once a stable lipid bilayer was obtained, we gradually added small volumes (0.1 μL) of a solution of 10 ng mL^{-1} gA in isopropanol (Acros Organics) to both compartments of the bilayer setup until one to six gA channels were inserted in the bilayer at the same time. We chose isopropanol as solvent for gA since tertiary alcohols are not substrates for PLD as opposed to primary and secondary alcohols. After each addition of gA, we mixed the bilayer chambers by stirring the solutions in both compartments for at least 3 min (we confirmed previously that a small droplet of food dye was completely mixed in the setup within 2 min of stirring). In these experiments the final concentration of gA in the bilayer chamber was in the range of 0.1-2.0 pM. This

range of gA concentration corresponds to 0.3-8 femtomoles of gA in the chamber with a volume of 3-4 mL; the total amount of lipid in each compartment was ~150 nanomoles, leading to a lipid to gA ratio of ~10^8. To measure the single channel conductance of gA pores,[55-59] we recorded current traces versus time while applying different voltages in the range of ±100 mV. We performed these single channel recordings in "voltage clamp mode" using Ag/AgCl pellet electrodes (Warner Instruments) in both compartments of the bilayer setup. Data acquisition and storage was carried out using a custom software written in Labview by Daniel J. Estes in combination with a Geneclamp 500 amplifier from Axon Instruments (set to a gain of 100 mV pA^{-1} and a filter cutoff frequency of 2 kHz). The data acquisition board (National Instruments) that was connected to the amplifier was set to a sampling frequency of 15 kHz. All recordings were carried out at a temperature of ~22º C.

We performed the analysis of the single channel current traces by computing histograms of the currents from the original current versus time traces with Clampfit 9.2 software (Axon Instruments). From these histograms, we extracted the mean current amplitude of gA channel opening and closing events. All conductance values were obtained from the slopes of current amplitudes versus voltage (I-V) curves (see the next section for more details on this analysis).

In order to reduce the noise in these single channel recordings, we mounted the bilayer setup on a low noise stir plate (Stir-2, Warner Instruments), which was placed on a bench top vibration isolation platform (50 BM-4, Minus K Technology) inside a Faraday cage from Warner Instruments. In addition, we found that we reached the

minimum noise level by placing the aforementioned setup on top of a second vibration isolation table (63-500 series from TMC) with a Faraday cage.

2.4.5. Monitoring Changes in gA Conductance Induced by Enzymatic Activity and Statistical Data Analysis

Upon addition of enzyme to a bilayer that contained gA pores, we recorded short (≤ 60 s) current traces at different applied voltages and at distinct points of time (Figure 2-9). To analyze these current versus time traces, we first obtained a histogram that represented the distribution of currents for each current trace (Figure 2-9). The difference in current between adjacent peaks in these histograms represented the current amplitude of single gA channel openings. These current amplitudes, therefore, reflect the single channel conductance of gA, γ, at a given time after addition of PLD. By averaging all current amplitudes within a histogram, we obtained the mean current amplitude of gA events and a standard deviation (STD) for this mean for each trace for a given time after addition of the enzyme. We plotted these mean current amplitudes as a function of the applied voltage for each time point. We obtained a mean value for single channel conductance of gA, γ, at a given time point from the slope of the resulting current versus voltage (I-V) curve in the linear range ≤ |± 100 mV| of the curve.

As demonstrated in Figure 2-9, the current amplitude of gA opening and closing events increased over time after addition of PLD to the bilayer setup. These results were further confirmed by Figure 2-10 which illustrates the distribution of current amplitudes of gA events in a time-dependent manner after addition of PLD to a PC bilayer. In this

figure, a clear shift in the mean current amplitude of gA events reflects a PLD-induced increase in gA conductance.

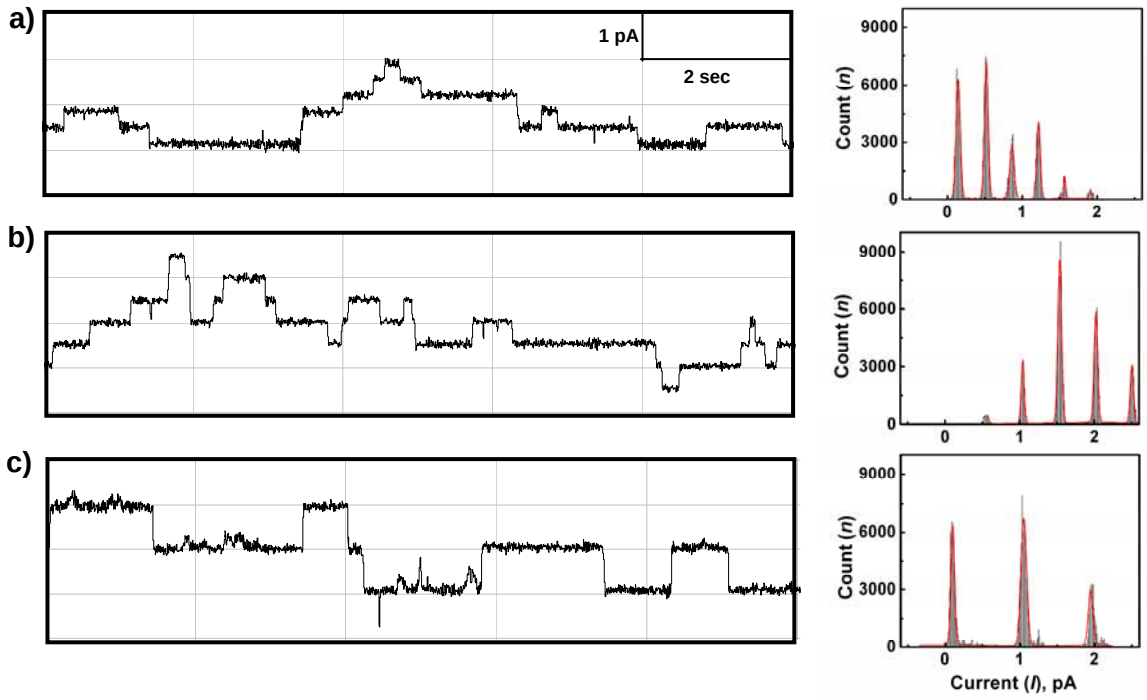

Figure 2-9. Current versus time recordings in a lipid bilayer that contained gA channels (a) before addition of PLD and (b) 5 min, and (c) 13 min after addition of PLD (with a final concentration of 3.1 units·mL^{-1}). Each step increase in current represents the formation of one gA channel and each step decrease represents the dissociation of one gA channel. The corresponding histograms on the right illustrate the distribution of current in each trace. The difference in current between adjacent peaks in these histograms reflects the current amplitude of step-wise gA events. These histograms, therefore, demonstrate a time-dependent increase in current amplitude of gA events.

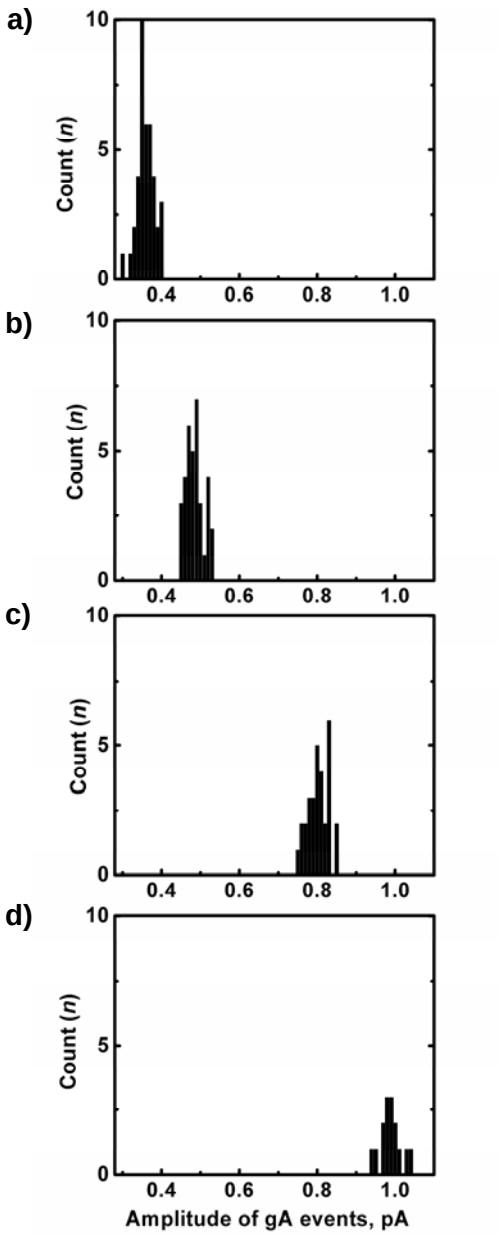

Figure 2-10. Distribution of current amplitudes of gA events at differnt time points after addition of 3.1 units·mL^{-1} PLD to a PC bilayer. Histograms of current amplitudes of individual gA opening and closing events (a) before addition of PLD, (b) 5 min, (c) 7 min, and (d) 13 min after addition of PLD. Ion channel recordings proceeded in an electrolyte solution containing 10 mM CsCl, 0.5 mM $CaCl_2$, and 10 mM cesium acetate at pH 5.5.

Figure 2-11 shows the statistical distribution of current amplitude of gA channels in PC bilayers as a function of the mole fraction of the negatively-charged lipid, PA. These results illustrate the effect of PA lipids in the bilayer on single channel conductance of gA pores and, in combination with the control experiments presented in the main text, confirm that the increase in gA conductance after addition of PLD is a result of the enzymatic activity of PLD that produces negatively-charged PA lipids. These results also confirm that at low mole fraction of PA ($X_{PA} \leq 0.1$) differences in mole fraction of 0.003 could be detected according to a limit of detection, defined as LOD = 3 × STD (see the section on LOD).

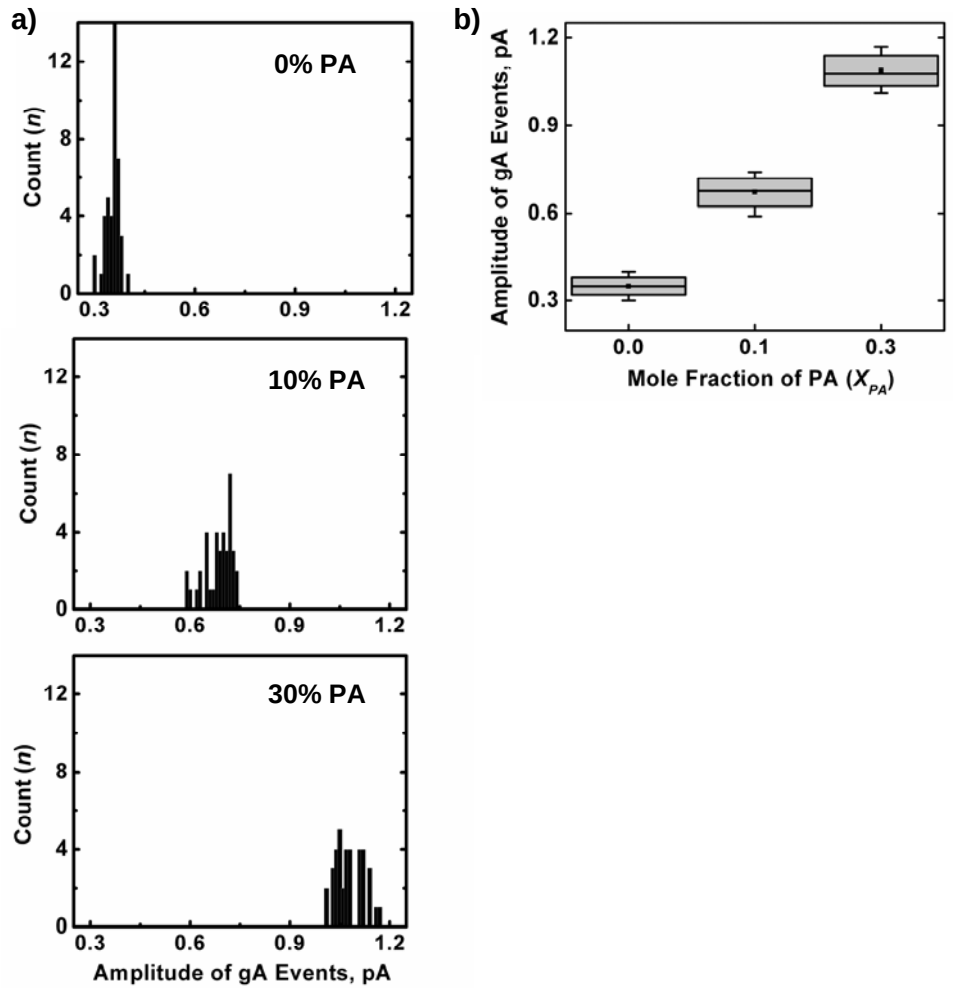

Figure 2-11. Distribution of current amplitudes of gA events in electrically neutral PC bilayers with different contents of negatively-charged PA lipids. (a) Histograms of current amplitudes of gA events in PC bilayers that contained 0, 10, and 30 mol% PA lipids. (b) Box chart showing the distribution of current amplitudes of gA events in these bilayers. Boxes represent the median ± standard deviation (STD). Error bars represent the minimum and maximum current amplitudes. Ion channel recordings proceeded in an electrolyte solution containg 10 mM CsCl, 0.5 mM $CaCl_2$, and 10 mM cesium acetate at pH 5.5.

2.4.6. Cleaning of the Planar Lipid Bilayer Setup

In order to ensure recordings from high quality bilayers without contaminations from previous experiments, we cleaned the bilayer chamber and setup in the following way: We removed the Teflon film that was previously mounted by vacuum grease to separate two compartments of the bilayer setup, and we cleaned the film by several washes with a stream of chloroform from a Teflon squirt bottle, followed by air drying before storage. Second, we rinsed the chamber with deionized water, followed by ethanol, and finally by chloroform. After two chloroform rinses, we used a Kimwipe tissue to clean the inside walls of the chamber such that all the vacuum grease was removed, and we, again, rinsed the chamber with chloroform. We stored the chamber in chloroform between experiments.

Note, all steps with solvents (in particular chloroform) were carried out in a chemical fume hood.

Acknowledgements

We thank Erik Yusko and Alexander MacBriar for their contribution in data collection and analysis and Dr. Jerry Yang for valuable discussions.

References

1. H. A. Brown, L. G. Henage, A. M. Preininger et al., in *Lipidomics and Bioactive Lipids* (2007), Vol. 434, pp. 49.

2. P. Huang and M. A. Frohman, *Expert Opin. Ther. Targets* **11** (5), 707 (2007).

3. S. A. Scott, P. E. Selvy, J. R. Buck et al., *Nat. Chem. Biol.* **5** (2), 108 (2009).

4. P. S. Tappia, M. R. Dent, and N. S. Dhalla, *Free Radical Bio. Med.* **41** (3), 349 (2006).

5. R. A. Deems, B. R. Eaton, and E. A. Dennis, *J. Biol. Chem.* **250** (23), 9013 (1975).

6. M. K. Jain and O. G. Berg, *Biochim. Biophys. Acta* **1002** (2), 127 (1989).

7. J. J. Volwerk, E. Filthuth, O. H. Griffith et al., *Biochemistry* **33** (12), 3464 (1994).

8. T. T. Allgyer and M. A. Wells, *Biochemistry* **18** (24), 5348 (1979).

9. D. Geng, J. Chura, and M. F. Roberts, *J. Biol. Chem.* **273** (20), 12195 (1998).

10. C. Virto, I. Svensson, and P. Adlercreutz, *Chem. Phys. Lipids* **106** (1), 41 (2000).

11. T. Bayburt, B. Z. Yu, I. Street et al., *Anal. Biochem.* **232** (1), 7 (1995).

12. O. H. Griffith and M. Ryan, *BBA-Mol. Cell Biol. L.* **1441** (2-3), 237 (1999).

13. S. Imamura and Y. Horiuti, *J. Biochem.* **83** (3), 677 (1978).

14. K. Kuppe, A. Kerth, A. Blume et al., *Chembiochem* **9** (17), 2853 (2008).

15. J. M. Brake, M. K. Daschner, Y. Y. Luk et al., *Science* **302** (5653), 2094 (2003).

16. D. Hartono, X. Y. Bi, K. L. Yang et al., *Adv. Funct. Mater.* **18** (19), 2938 (2008).

17. S. Blake, T. Mayer, M. Mayer et al., *Chembiochem* **7** (3), 433 (2006).

18. R. Capone, S. Blake, M. R. Restrepo et al., *J. Am. Chem. Soc.* **129** (31), 9737 (2007).

19. C. Danelon, M. Lindemann, C. Borin et al., *IEEE Trans. NanoBiosci.* **3** (1), 46 (2004).

20. M. Mayer, V. Semetey, I. Gitlin et al., *J. Am. Chem. Soc.* **130** (4), 1453 (2008).

21. C. Schmidt, M. Mayer, and H. Vogel, *Angew. Chem. Int. Ed.* **39** (17), 3137 (2000).

22. H. J. Apell, E. Bamberg, and P. Lauger, *Biochim. Biophys. Acta* **552** (3), 369 (1979).

23. T. K. Rostovtseva, V. M. Aguilella, I. Vodyanoy et al., *Biophys. J.* **75** (4), 1783 (1998).

24. D. W. Heinz, L. O. Essen, and R. L. Williams, *J. Mol. Biol.* **275** (4), 635 (1998).

25. A. P. Winiski, A. C. McLaughlin, R. V. McDaniel et al., *Biochemistry* **25** (25), 8206 (1986).

26. O. S. Andersen, R. E. Koeppe, and B. Roux, *IEEE Trans. NanoBiosci.* **4** (1), 10 (2005).

27. These lipid bilayers were typically stable for 1-3 h.

28. J. S. Tou and C. Urbizo, *Cell. Signal.* **13** (3), 191 (2001).

29. M. Madesh and K. A. Balasubramanian, *BBA-Lipid. Lipid Met.* **1389** (3), 206 (1998).

30. L. R. Cambrea, F. Haque, J. L. Schieler et al., *Biophys. J.* **93** (5), 1630 (2007).

31. K. Giger, E. R. Lamberson, and J. S. Hovis, *Langmuir* **25** (1), 71 (2009).

32. S. Blake, R. Capone, M. Mayer et al., *Bioconjugate Chem.* **19** (8), 1614 (2008).

33. B. A. Cornell, V. L. B. Braach-Maksvytis, L. G. King et al., *Nature* **387** (6633), 580 (1997).

34. Q. Hong, T. Stora, L. G. Dover et al., presented at the 1st World Congress of High-Tech Medicine, Hannover, Germany, 2000 (unpublished).

35. M. R. Ghadiri, J. R. Granja, and L. K. Buehler, *Nature* **369** (6478), 301 (1994).

36. S. L. Cockroft, J. Chu, M. Amorin et al., *J. Am. Chem. Soc.* **130** (3), 818 (2008).

37. S. Matile, A. Som, and N. Sorde, *Tetrahedron* **60** (31), 6405 (2004).

38. H. Bayley and P. S. Cremer, *Nature* **413** (6852), 226 (2001).

39. O. S. Andersen, H. J. Apell, E. Bamberg et al., *Nat. Struct. Biol.* **6** (7), 609 (1999).

40. T. A. Cross, A. Arseniev, B. A. Cornell et al., *Nat. Struct. Biol.* **6** (7), 610 (1999).

41. A. Finkelstein and O. S. Andersen, *J. Membr. Biol.* **59** (3), 155 (1981).

42. T. K. Rostovtseva, H. I. Petrache, N. Kazemi et al., *Biophys. J.* **94** (4), L23 (2008).

43. G. A. Woolley and B. A. Wallace, *J. Membr. Biol.* **129** (2), 109 (1992).

44. Y. N. Antonenko, T. I. Rokitskaya, E. A. Kotova et al., *Biochemistry* **43** (15), 4575 (2004).

45. S. B. Hladky and D. A. Haydon, *Nature* **225** (5231), 451 (1970).

46. C. J. Stankovic, J. M. Delfino, and S. L. Schreiber, *Anal. Biochem.* **184** (1), 100 (1990).

47. H. Younus, R. Schops, A. Lerchner et al., *J. Protein Chem.* **22** (6), 499 (2003).

48. T. J. Jeon, J. L. Poulos, and J. J. Schmidt, *Lab on a Chip* **8** (10), 1742 (2008).

49. T. Mach, C. Chimerel, J. Fritz et al., *Anal. Bioanal. Chem.* **390** (3), 841 (2008).

50. M. Kreir, C. Farre, M. Beckler et al., *Lab on a Chip* **8** (4), 587 (2008).

51. Andrea Bruggemann, Cecilia Farre, Claudia Haarmann et al., *Methods Mol. Biol.* **491**, 165 (2008).

52. H. Suzuki, K. V. Tabata, H. Noji et al., *Langmuir* **22** (4), 1937 (2006).

53. M. Winterhalter, *Curr. Opin. Colloid Interface Sci.* **5** (3-4), 250 (2000).

54. M. Montal and P. Mueller, *Proc. Natl. Acad. Sci. U. S. A.* **69** (12), 3561 (1972).

55. J. A. Gowen, J. C. Markham, S. E. Morrison et al., *Biophys. J.* **83** (2), 880 (2002).

56. D. A. Kelkar and A. Chattopadhyay, *BBA-Biomembranes* **1768** (9), 2011 (2007).

57. B. Le Pioufle, H. Suzuki, K. V. Tabata et al., *Anal. Chem.* **80** (1), 328 (2008).

58. D. Wong, T. J. Jeon, and J. Schmidt, *Nanotechnology* **17** (15), 3710 (2006).

59. X. F. Kang, S. Cheley, A. C. Rice-Ficht et al., *J. Am. Chem. Soc.* **129** (15), 4701 (2007).

Chapter 3

Kinetic Parameters of Heterogeneous Catalysis of Phosphatidylcholine by Phospholipase D

Abstract

The enzymatic reaction of interfacial enzymes is an important example of heterogeneous catalysis. Describing the kinetics of these reactions is, hence, a difficult task and requires further theoretical advancements. This chapter presents an attempt to describe the kinetics of the enzymatic reaction of phospholipase D (PLD) using the quantitative results of the gramicidin-based PLD assay introduced previously. We present an adaptation of a basic kinetic model for interfacial reactions to the PLD assay presented in this thesis. Employing this model, we estimated the kinetic parameters of the "specificity constant" and the "apparent interfacial quality" of the PLD enzymatic activity.

3.1. Introduction

Phospholipases form a group of interfacial enzymes that catalyze the hydrolysis of the ester bonds in phospholipids and play an important role in lipid metabolism.[1-4]

While these enzymes are water soluble, their substrates (i.e. phospholipids) are water insoluble. Enzymatic reactions of these enzymes, therefore, depend strongly on the organization of phospholipids in interfacial structures such as liposomes or micelles.[1]

The underlying variables in a microscopically heterogeneous environment are far more complex than those encountered by a soluble enzyme in a homogeneous solution.[1-3,5] Enzymatic reactions of interfacial enzymes, therefore, present an important example of heterogeneous catalysis.

Within the past fourty years, several kinetic models have been developed to describe the enzymatic reaction of interfacial enzymes. Verger *et al.* have proposed the first and simplest kinetic model in which the Michaelis-Menten chemical step and the interfacial activation of the enzyme are combined.[6] Since then, various kinetic models were proposed for various interfacial structures including lipid monolayers, liposomes, micelles, and oil in water emulsions.[3,5,7,8] Examples of these models are the "surface dilution kinetics" that describes catalysis on mixed micelles[3,7,9] and the "scooting and hopping modes" of enzyme action that describes catalysis on liposomes.[5,8]

In the previous chapter, we presented the first assay for phospholipases D and C that is based on planar lipid bilayer systems. In this chapter, we adopt a basic kinetic model for interfacial hydrolysis[6] and apply this model to the assay introduced here. The goal is to obtain kinetic parameters of enzymatic activity of phospholipase D on planar lipid bilayers.

3.2. Kinetic Model

Figure 3-1 illustrates the schematic representation of the simplest adaptation of the Michaelis-Menten model to the interfacial hydrolysis of lipids that was proposed by Verger. *et al*.[6] In this model, the first step is the adsorption of a water-soluble enzyme, E, to the lipid-water interface. This step leads to a more energetically-favorable state, E^*, for binding to the substrate compared to the enzyme in the aqueous phase, E. This step is followed by a two-dimensional Michaelis-Menten catalytic step. The enzyme at the interface, E^*, binds a substrate molecule, S, to form the E^*S complex, followed by its decomposition. As shown in Figure 3-1 this model assumes that the reaction products, P^*, are water-soluble and diffuse away. While valid for short- and medium-chain lipids, this assumption is not valid for natural long-chain phospholipids. In fact, accumulation of reaction products at the interface can dilute the substrate at the surface, inhibit the enzymatic reaction, or accelerate the binding and hence, hydrolysis of the enzyme.[1] Thus, the theoretical analysis of the interfacial hydrolysis of long-chain lipids is very difficult and requires additional kinetic equations to describe the reorganization at the interface and consequent inhibition or acceleration of the hydrolysis reaction.[1] Due to the complexity of the system, this issue has not been addressed; consequently, and simple kinetic models developed for soluble products are the only available alternative for estimating apparent kinetic parameters for interfacial hydrolysis.[1] As described in the following steps, we employ the kinetic model for soluble products, proposed by Verger *et al.*, to estimate the apparent kinetic parameters of hydrolysis of the long-chain lipid, 1,2-diphytanoyl-*sn*-glycero-3-phosphocholine (DiPhyPC), in planar lipid bilayers. Although DiPhyPC is not the optimal substrate with regard to the theoretical analysis, long-chain

lipids are however, the typical substrates of these enzymes in their physiological environment.

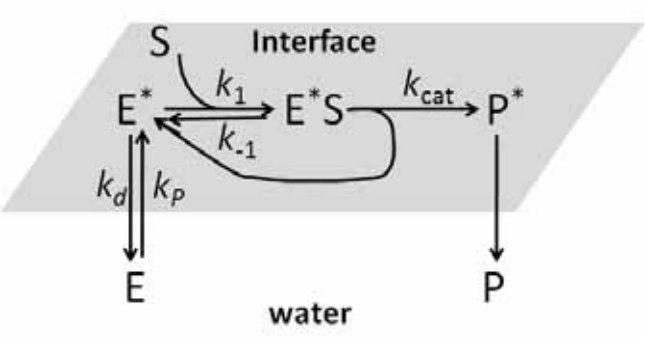

Figure 3-1. Adaptation of the Michaelis-Menten model to the interracial hydrolysis of lipids. This model assumes that the reaction products are soluble. This figure is adopted from Baszkin and Norde, 2000.[1]

As shown in Figure 3-1, the enzymatic reaction of an interfacial enzyme occurs at the interface and, hence, the concentrations of E^*, S, E^*S, and P^* are expressed as surface concentrations Γ_{E^*}, Γ_S, Γ_{E^*S}, and Γ_{P^*} (molecules m^{-2}), while the concentrations of E and P are expressed as bulk concentrations C_E and C_P (mol L^{-1}). The following equations describe the kinetic model shown in Figure 3-1:

$$\frac{d\Gamma_{E^*S}}{dt} = k_1\Gamma_{E^*}\Gamma_S - (k_{cat} + k_{-1})\Gamma_{E^*S}, \tag{5}$$

$$\frac{d\Gamma_{E^*}}{dt} = k_P C_E + (k_{cat} + k_{-1})\Gamma_{E^*} - (k_d + k_1\Gamma_S)\Gamma_{E^*}, \tag{6}$$

$$\frac{d\Gamma_{P*}}{dt} = k_{cat}\Gamma_{E*S}, \tag{7}$$

$$C_{E0}V = C_E V + \Gamma_{E*}A + \Gamma_{E*S}A, \tag{8}$$

where t (min) is time; k_P (m min^{-1}) is the adsorption rate constant; k_d (min^{-1}) is the desorption rate constant; and k_{cat} (min^{-1}) is the catalytic rate constant; k_1 (m^2 molecules^{-1} min^{-1}) and k_{-1} (min^{-1}); V (m^3) is the volume of the aqueous phase and A (m^2) is the surface area of the lipid-water interface.

Solving these equations with the initial condition of $t = 0$, $\Gamma_{P*} = 0$ and assuming that the substrate concentration Γ_S remains constant during the hydrolysis, results in the following equitation:[6]

$$\Gamma_{P*} = \frac{k_{cat}\Gamma_S C_{E0}}{K_m^* \frac{k_d}{k_p} + (K_m^* + \Gamma_S)\frac{A}{V}}\left[\tau + \frac{\tau_1^2}{\tau_1 - \tau_2}(e^{-t/\tau_1} - 1) - \frac{\tau_2^2}{\tau_1 - \tau_2}(e^{-t/\tau_1} - 1)\right], \tag{9}$$

where τ_1 is the induction time, describing the establishment of the adsorption-desorption steady state; τ_2 is the characteristic time of establishment of the interfacial catalytic steady state; C_{E0} represents the initial enzyme concentration in the bulk solution; $\frac{k_d}{k_p}$ (m^{-1}) represents the dissociation constant for binding of enzyme to the membrane that is equal to the ratio of bulk enzyme concentration to surface enzyme concentration, $\frac{C_E}{\Gamma_{E*}}$ (m^{-1}); and $K^*_m = (k_{cat} + k_{-1}) / k_1$ (molecules m^{-2}) is the interfacial Michaelis-Menten

constant. At steady state condition, the following equation for the hydrolysis rate, υ (molecules m^{-2} min^{-1}), can be obtained from Eq. (9):[6]

$$v \equiv \frac{d\Gamma_{P*}}{dt} = \frac{k_{cat}\Gamma_S}{K_m^* \frac{k_d}{k_p} + (K_m^* + \Gamma_S)\frac{A}{V}} C_{E0}. \tag{10}$$

Eq. (10) can, in principle, be adapted to various interfacial structures.[1] We adapt this equation to the ion channel-based assay presented in this work.

In order to employ this equation with mole fractions of substrate and product instead of surface concentrations, we define:

$$X_{p*} = \frac{\Gamma_{P*}}{\Gamma_{p*} + \Gamma_S}, \tag{11}$$

and

$$X_S = \frac{\Gamma_S}{\Gamma_{p*} + \Gamma_S}. \tag{12}$$

Where X_S and X_{P*} are mole fractions of the substrate and product, respectively. Combining Eq. (10), (11), and (12) results in the following equation:

$$v \equiv \frac{d(X_{P*}(\Gamma_{P*} + \Gamma_S))}{dt} = \frac{k_{cat} \times X_S(\Gamma_{P*} + \Gamma_S) \times C_{E0}}{(K_m^* \times \frac{k_d}{k_P}) + (K_m^* + X_S(\Gamma_{P*} + \Gamma_S))\frac{A}{V}}. \tag{13}$$

Assuming that the total concentration of substrate and product at the interface $(\Gamma_{P*} + \Gamma_S)$ remains constant, we obtain:

$$v \equiv (\Gamma_{P*} + \Gamma_S)\frac{dX_{P*}}{dt} = \frac{k_{cat} \times X_S(\Gamma_{P*} + \Gamma_S) \times C_{E0}}{(K_m^* \times \frac{k_d}{k_P}) + K_m^* \frac{A}{V} + \frac{A}{V} X_S(\Gamma_{P*} + \Gamma_S)}. \quad (14)$$

After rearranging this equation, we obtain:

$$v \equiv \frac{dX_{P*}}{dt} = \frac{k_{cat} \times X_S \times C_{E0}}{(K_m^* \times \frac{k_d}{k_P}) + \frac{A}{V}(K_m^* + X_S(\Gamma_{P*} + \Gamma_S))}. \quad (15)$$

A typical range for the partitioning of the enzyme between the aqueous phase and lipid interface at steady state is $\frac{k_d}{k_P} = \frac{C_E}{\Gamma_{E*}} \approx 10^2$ cm^{-1}.[1] In the assay presented here, the area to volume ratio of $\frac{A}{V}$ is estimated to be 0.75 cm^{-1}, considering a chamber with a volume of 3 mL and a lipid-water interface with a surface area of ~2.25×10^{-4} m^2 (obtained by summation of the lipid monolayer formed at the air-water interface and the bilayer formed across the aperture). Therefore, the following inequality is fulfilled:[1,6]

$$K_m^* \times \frac{k_d}{k_P} \gg \frac{A}{V}(K_m^* + X_S(\Gamma_{P*} + \Gamma_S)). \quad (16)$$

Consequently, Eq. (15) can be simplified to the following equation for the hydrolysis rate of the enzyme in the assay presented in the chapter 2:

$$v \equiv \frac{dX_{P*}}{dt} = \frac{k_{cat} \times X_S \times C_{E0}}{K_m^* \times \frac{k_d}{k_P}}. \tag{17}$$

3.3. Results and Discussion

In order to obtain the specificity constant, $\frac{k_{cat}}{K_m^*}$, and the overall kinetic constant called the interfacial quality, $Q_m \equiv \frac{k_{cat}}{K_m^* \times \frac{k_d}{k_P}}$, of the enzymatic reaction of PLD, we plotted the initial hydrolysis rate, v, of PLD as a function of the enzyme concentration in the following graph (all the data is taken from chapter 2).

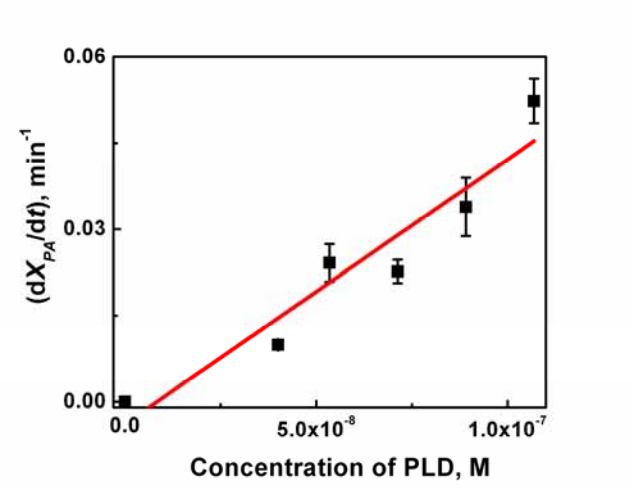

Figure 3-2. Changes in the initial rate of hydrolysis of DiphyPC lipids as a function of PLD concentration in the bulk solution of the bilayer chamber. Data is taken from chapter 2. The solid line represents the best linear fit ($R^2 = 0.89$, $N = 6$) to the data.

Fitting the data in Figure 3-2 to a line revealed a positive slope of 460×10^3 L mol^{-1} min^{-1} for the change in the initial hydrolysis rate as a function of the enzyme concentration. According to Eq. (17), the following can be obtained:

$$\frac{k_{cat}\times X_S}{K_m^*\times\dfrac{k_d}{k_P}} = 460\times10^3 \text{ L mol}^{-1}\text{ min}^{-1} = 7.6\times10^{-22} \text{ m}^3 \text{ molecules}^{-1}\text{ min}^{-1} \qquad (18)$$

The planar lipid bilayers employed here were composed of DiphyPC lipids which corresponded to a mole fraction of substrate, X_S, of 1. We determined the binding affinity of PLD enzyme for DiphyPC bilayers using surface plasma resonance (SPR) and

obtained a dissociation constant of $K_d = 150 \times 10^{-6}$ M. In order to translate this value to $\frac{k_d}{k_P} = \frac{C_E}{\Gamma_{E^*}}$, we assumed that at an enzyme concentration of 150×10^{-6} M, half of the area that is occupied by lipids in a bilayer at the interface are occupied by the enzyme and approximating the size of the enzyme, we estimated the number of the bound enzymes and their surface concentration, Γ_{E^*}. The PLD enzyme employed in the present assay has a molecular weight of ~92 kDa[10] and we approximated the dimensions of this enzyme based on another 92 kDa protein (a 92 kDa fragment of yeast DNA topoisomerase II)[11] and used its crystal dimensions of 120 Å × 120 Å × 50 Å as an estimate for PLD. Assuming a spherical shape for the enzyme, it would cover an area of ~97 nm^2 on the bilayer. If we consider a square unit area of 1 μm^2 and a close hexagonal packing (density of 90.7%) of the PLD enzyme at the interface, at maximal binding there would be ~9.4×10^3 enzymes per μm^2 at the interface. At half-maximal binding, therefore, there would be ~4.7×10^3 enzymes bound per μm^2 at the interface, corresponding to an approximate surface concentration of $\Gamma_{E^*} = 4.7 \times 10^{15}$ enzyme molecules m^{-2}. Thus, at an enzyme concentration, C_E, of 150×10^{-6} M, $\frac{k_d}{k_P} = \frac{C_E}{\Gamma_{E^*}}$ would have a value of 19×10^6 m^{-1}.

By substituting $\frac{k_d}{k_P} = 19 \times 10^6$ m^{-1} and $X_S = 1$ in Eq. (18) we can obtain the specificity constant, which is a measure of catalytic efficiency of the enzyme:

$$\frac{k_{cat}}{K_m^*} = 1.4 \times 10^{-10} \text{ cm}^2 \text{ molecules}^{-1} \text{ min}^{-1} \quad (19)$$

And the apparent interfacial quality, Q_m, can be obtained:

$$Q_m \equiv \frac{k_{cat}}{K_m^* \times \frac{k_d}{k_P}} = 7.6 \times 10^{-16} \text{ cm}^3 \text{ molecules}^{-1} \text{ min}^{-1} \quad (20)$$

The interfacial quality, Q_m, is a global kinetic constant of the hydrolysis that takes into account the influence of the physiochemical properties of the interface on the enzyme activity. The value of the interfacial quality obtained here is comparable to the previously reported value of 4.2×10^{-15} cm^3 molecules^{-1} min^{-1} for hydrolysis of a long-chain lipid by the enzyme phospholipase A, PLA.[1] As mentioned previously, however, this value reflects an apparent kinetic constant (as opposed to a "real" kinetic constant) due to the error introduced by neglecting the effect of insoluble reaction products on the hydrolysis reaction.[1] Recently, addition of a lipolytic product acceptor such as α- and β-cyclodextrin to the aqueous solution was employed to solubilize the products of the hydrolysis reaction of PLA enzymes.[1] This improved approach increased the value of Q_m of the hydrolysis of a long-chain lipid by a PLA enzyme by two orders of magnitude. The resulting Q_m had a value close to the Q_m of the hydrolysis of a medium-chain lipid by the same enzyme.[1]

3.4. Conclusion

In conclusion, this chapter presents an adaptation of a basic kinetic model to the PLD assay presented in chapter 2. Quantitative results of the gramicidin-based assay of

PLD combined with this kinetic model made it possible to estimate the kinetic parameters including the specificity constant, $\frac{k_{cat}}{K_m^*}$, and apparent interfacial quality, Q_m, of the PLD enzymatic activity. Future advancements on theoretical analysis of heterogeneous catalysis may allow us to improve the estimate of these kinetic parameters. Future studies may apply the present kinetic model to the gramicidin-based phospholipase C (PLC) assay introduced in chapter 2. Given the possibility of varying the substrate concentration in the PLC assay, this kinetic model may make it possible to obtain more detailed kinetic information including k_{cat} and the interfacial Michaelis-Menten constant, K_m^*, for PLC enzymatic activity.

Acknowledgements

We thank Erik Yusko and Alexander MacBriar for their contribution in data collection and Dr. Jerry Yang for valuable discussions.

References

1. Adam Baszkin and Willem Norde eds., *physical chemistry of biological interfaces*. (Marcel Dekker Inc., New York, 2000).

2. H. A. Brown, L. G. Henage, A. M. Preininger et al., in *Lipidomics and Bioactive Lipids* (2007), Vol. 434, pp. 49.

3. R. A. Deems, B. R. Eaton, and E. A. Dennis, *J. Biol. Chem.* **250** (23), 9013 (1975).

4. O. H. Griffith and M. Ryan, *BBA-Mol. Cell Biol. L.* **1441** (2-3), 237 (1999).

5. M. K. Jain and O. G. Berg, *Biochim. Biophys. Acta* **1002** (2), 127 (1989).

6. R. Verger, M. C. E. Mieras, and G. H. Dehaas, *J. Biol. Chem.* **248** (11), 4023 (1973).

7. G. M. Carman, R. A. Deems, and E. A. Dennis, *J. Biol. Chem.* **270** (32), 18711 (1995).

8. M. K. Jain, M. H. Gelb, J. Rogers et al., *Enzyme Kinetics and Mechanism, Pt D* **249**, 567 (1995).

9. L. J. Reynolds, L. L. Hughes, and E. A. Dennis, *Anal. Biochem.* **204** (1), 190 (1992).

10. A. J. Morris, J. A. Engebrecht, and M. A. Frohman, *Trends Pharmacol. Sci.* **17** (5), 182 (1996).

11. P. Benedetti, A. Silvestri, P. Fiorani et al., *J. Biol. Chem.* **272** (18), 12132 (1997).

Chapter 4

Quantifying Interactions of Electrically-Charged Bioactive Molecules with Lipid Membranes Using Gramicidin Channels

Abstract

The pharmacologic activity of most drugs involves an initial step of interaction with the cell plasma membrane (either by binding to membranes or by crossing membranes). This interaction, therefore, plays a role in drug selectivity and efficacy. Here, we introduce a gramicidin-based assay to monitor the binding of two electrically-charged drug molecules imipramine and quinine to planar lipid bilayers. We demonstrate that this label-free assay can be employed to quantify the binding of electrically-charged molecules to lipid membranes with various lipid compositions.

4.1. Introduction

Interactions of drug molecules with cell membranes are an important field of study due to the significant role of these interactions in the pharmacologic activity of the drug.[1-3] A large number of drug molecules have ionizable functional groups and at the physiological range of pH (5.5–7.5), they are partially or fully charged.[1,2] Under these

conditions, these molecules are, hence, electrostatically attracted (in the case of positively-charged pharmaceuticals) or repelled (in the case of negatively-charged drugs) by many biological membranes that are composed of acidic lipids, and carry a net negative charge. The interaction of the charged drug molecules with membranes is, therefore, of great interest for pharmacology and medicinal chemistry. These interactions can be studied by various techniques including fluorescence and radioactive assays.[4,5] Here, we introduce a new approach to monitor the binding of electrically-charged molecules to various lipid membranes in real-time and without the need for labeling the drug of interest. This assay detects the binding of these molecules to the membrane through the changes in the ion conductance of the channel forming peptide gramicidin A (gA).[6,7] Binding of electrically-charged molecules to a membrane alters the surface charge density of the membrane and, hence, influences the local concentration of cations near the membrane surface.[1,8] Gramicidin is a cation selective channel[6,9,10] and as previously demonstrated, the single channel conductance of gA, γ, is influenced by the local concentration of cations near the channel entrance.[11-13] The assay presented here, takes advantage of this sensitivity of gA channels and employs these pores to monitor, *in situ*, the changes in the membrane surface charge and hence, binding of the charged molecules onto the membrane.

4.2. Results and Discussion

In order to explore the potential application of a gA-based sensor as a binding assay, we formed planar lipid bilayers of neutral and negatively-charged lipids that

contained gA pores and monitored the single channel conductance, γ, of these pores upon exposure of the lipid bilayer to different concentrations of positively-charged drug molecules. In case of neutral membranes, with an initial surface charge of zero, binding of positively-charged molecules to the membrane creates a positive surface charge. Binding of these drug molecules to negatively-charged membranes with an initial negative surface charge reduces the membrane surface charge by countering the effect of negative charges on the lipids. In both cases, binding of the positively-charged molecules to the membrane leads to a decrease in the concentration of cations close to the membrane. We hypothesized that this change in the local concentration of cations would have a measurable effect on the conductance of gA channels, and hence, the changes in gA conductance would reveal information about these binding events.

We examined the binding of two positively-charged therapeutic compounds, imipramine and quinine. Imipramine (Figure 4-1a) is an amphiphilic drug that belongs to a group of drugs termed tricyclic antidepressants (TCAs) that have been used for treatment of depression for more than 50 years.[4] Having a pK_a value of 9.4, these therapeutic compounds carry a positive charge in aqueous solution at physiological conditions.[4] Fisar *et al.* showed that binding of TCAs to model membranes is strongly affected by the lipid composition of model membranes (with K_d values varying from 10 to1000 nM). This effect was mostly attributed to the role of the negatively-charged lipids.[4] Quinine (Figure 4-1b) is a natural alkaloid that is isolated from the bark of the *cinchona* tree and has been used for reducing fevers and muscle cramps and for treatment of malaria prior to recent development of more effective synthetic drugs.[5] Currently, the side effects and the resistance to these synthesized drugs, has led to a renewed interest in

quinine for treatment of malaria.[5] Quinine has a pK_a of 8.7 and, under physiological condition, bears a positive charge.[14]

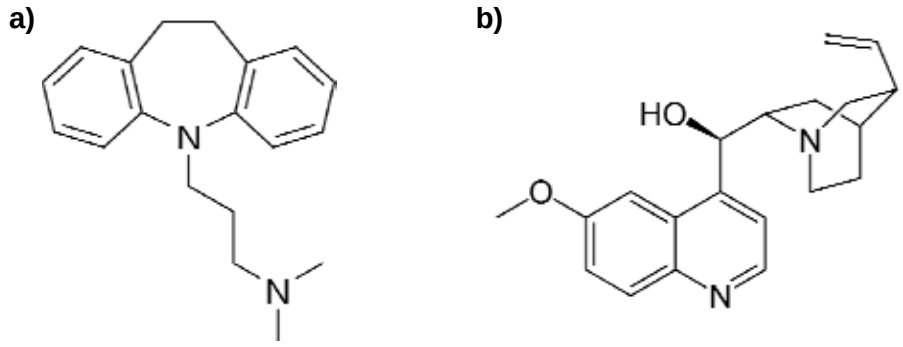

Figure 4-1. Molecular structures of (a) imipramine and (b) quinine.

We examined binding of both of these drugs to lipid membranes composed of either neutral phosphatidylcholine (PC) lipids or composed of 75 mol% PC and 25 mol% negatively-charged phosphatidic acid (PA) lipids. After incorporation of a few gA channels (typically 1-6 at any given time), we exposed the planar lipid bilayers to gradually increasing concentrations of the charged molecules while monitoring the conductance of gA channels. Figure 4-2 illustrates the changes in the single channel conductance of gA, γ, in the examined lipid bilayers as a function of the bulk concentration of quinine and imipramine. As we hypothesized, these plots show that the channel conductance of gA decreased significantly with an increasing concentration of the drug in the solution.

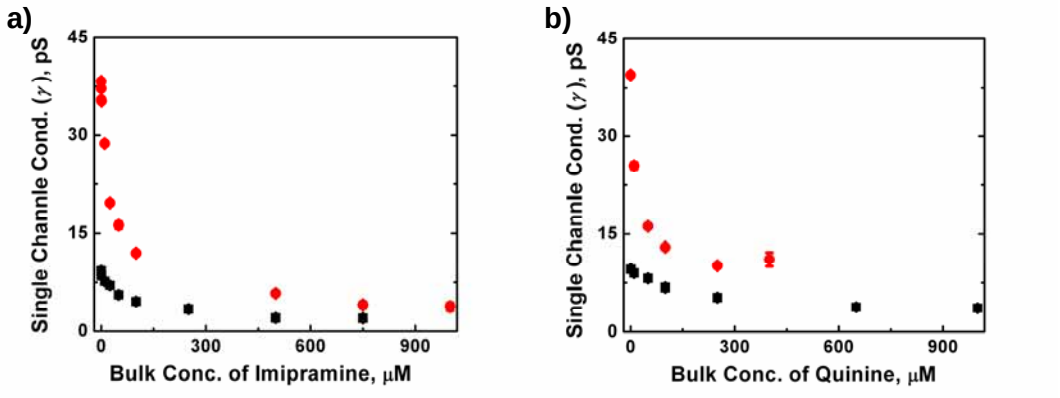

Figure 4-2. Changes in the single channel conductance, γ, of gA pores as a function of the concentration of the positively-charged drugs in the bulk solution. Data show the mean values of γ in lipid bilayers composed of (■) PC lipids and (●) PC and 25 mol% PA lipids as a function of the bulk concentration of (a) imipramine and (b) quinine in the bilayer chamber.

As mentioned previously, this decrease in the conductance of gA is an indirect result of a change in the surface charge density of the membrane.[11-13] Changes in the surface charge density of a membrane, according to the Gouy-Chapman theory, lead to changes in surface potential of the membrane, which influences the distribution of cations and anions in the solution and in vicinity of the membrane.[11-13] The effective surface charge density, σ (C m^{-2}), is a function of both, the amount of negative lipids and the bound positive ions, as described in the following equation:[15]

$$\sigma = (\frac{e_0}{A})(-X_{neg} + \sum_i z_i X_i), \qquad (21)$$

where e_0 (1.60×10^{-19} C) is the elementary charge; A (m^2) is the surface area per lipid molecule (assumed to be the same for PC and PA lipids); X_{neg} is the mole fraction of the negatively-charged lipid in the membrane; X_i is the mole fraction of bound ion i (i.e. moles of bound ion i per mole of total lipid) with valence z_i. This equation assumes that negatively-charged lipids carry only one charge per lipid, which was a good approximation in our case.

In order to quantify the binding of these molecules to the membrane, we first determined the mole fraction of the bound molecules at the membrane. To relate the single channel conductance of gA to the amount of the bound drug to the membrane, we first acquired a calibration curve of γ (in units of pS $=10^{-12}$ Ω^{-1}) as a function of the mole fraction of PA, X_{PA} (unitless), in the membrane. In these experiments, as the mole fraction of the negatively-charged PA lipids in the membrane increases, the surface charge of the membrane becomes more negative and leads to an accumulation of cations (in this case, Cs^+) near the membrane surface. This increased concentration of Cs^+ near the membrane surface and the entrance of gA pores, results in an increase in γ. Figure 4-3 illustrates this calibration curve and Eq. (22) which resulted from the linear fit to the data in this figure, describes this calibration curve:

$$\gamma(\text{pS}) = 118.84 \times X_{PA} + 9.46 \text{ pS}. \qquad (22)$$

The data shown in black and red colors in Figure 4-3 represent two sets of data acquired in slightly different recording buffers. The black data that was acquired initially, showed

a clear linear relationship between γ and X_{PA}, and the red data revealed that a slight change in the recording buffer (while keeping the concentration of Cs^+ constant) made no significant difference in the form of this relationship. We, hence, employed the exact same slope of the linear fit obtained from the data shown in black and only adjusted the y-intercept of this line for a fit to the data shown in red (Eq. (22)). Since the data presented in this chapter was acquired in the same recording buffer as the red data, we employed Eq. (22) to relate the change in the X_{PA} to the measured change in γ.

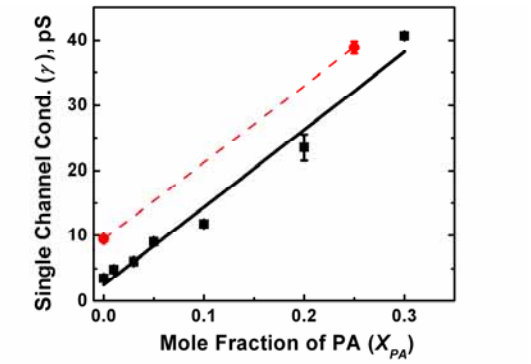

Figure 4-3. Calibration curve of the single channel conductance, γ, of gA as a function of the mole fraction of negatively-charged PA lipids in the membrane. Graph shows the mean values of γ in PC lipid bilayers that contained various amounts of PA in a recording buffer that contained (■) 10 mM cesium chloride and 10 mM cesium acetate with a pH value of 5.5, and (●) 20 mM cesium chloride and 10 mM HEPES with a pH value of 7.4. Error bars represent the standard error of the mean ($N \geq 3$). The solid black line represents the best linear fit to the data shown in black ($\gamma(\text{pS}) = 118.84 \times X_{PA} + 2.50$ pS, $R^2 = 0.97$, $N = 7$). The resulting black line was shifted in the y-axis to fit the data shown in red ($\gamma(\text{pS}) = 118.84 \times X_{PA} + 9.46$ pS), and the shifted line is shown as a dashed red line.

Using this calibration curve, we translated the changes in the single channel conductance of gA to the changes in the amount of PA lipids in the membrane. Converting γ values in Figure 4-1 to X_{PA}, we observed a similar decrease in X_{PA} as a function of the bulk concentration of drug molecules in the bilayer chamber. In the experiments with drug molecules, however, the amount of X_{PA} in the membrane was constant throughout the experiment, and thus, the *apparent* change in the X_{PA} (that is change predicted by the calibration curve) in fact, reflects the amount of positive ions that are bound to the membrane. Therefore, by computing the difference between X_{PA} in the examined membrane and the X_{PA} predicted by the calibration curve ($X_{PA,\ pred.}$), we obtained the amount of bound cations to the membrane, as following:

$$X_{PA} - X_{PA,pred.} = \sum_i X_i z_i, \tag{23}$$

where X_i represent the mole fraction of the ith cation bound to the membrane and z_i represents the valence of the ion. The buffer solution used in the study presented here contained 20 mM CsCl and 10 mM HEPES with a pH of 7.4; the major cations in the solution included Cs^+ and the positively-charged drug molecules. While monovalent cations including Cs^+ usually do not bind to neutral lipids such as PC,[16] these ions bind to the headgroup of negatively-charged lipids such as PA.[16] Approximating the binding constant of Cs^+ to PA lipids with the binding constant of Cs^+ to the negatively-charged phosphatidylserine (PS) lipids ($K = 0.05\ M^{-1}$ corresponding to a dissociation constant of

20 M)[16], at the low (0.02 M) bulk concentration of Cs^+ used in the present experiments, the amount of bound Cs^+ at the membrane is negligible. Thus, the amount of cations bound to the membrane solely reflects the amount of the cationic drug molecules. Eq. (23) can, hence, be written as:

$$X_{PA} - X_{PA,pred.} = X_D z_D, \tag{24}$$

where X_D represents the mole fraction of the charged drug bound to the membrane, and z_D represents the valence of the charged drug.

We employed Eq. (22) to compute $X_{PA,pred}$, and by replacing the obtained values of $X_{PA,pred}$ in Eq. (24), we obtained $X_D\, z_D$ as a function of the drug concentration. Figure 4-4 illustrates the changes in $X_D\, z_D$ as a function of the bulk concentration of the drug for neutral and negatively-charged lipid membranes.

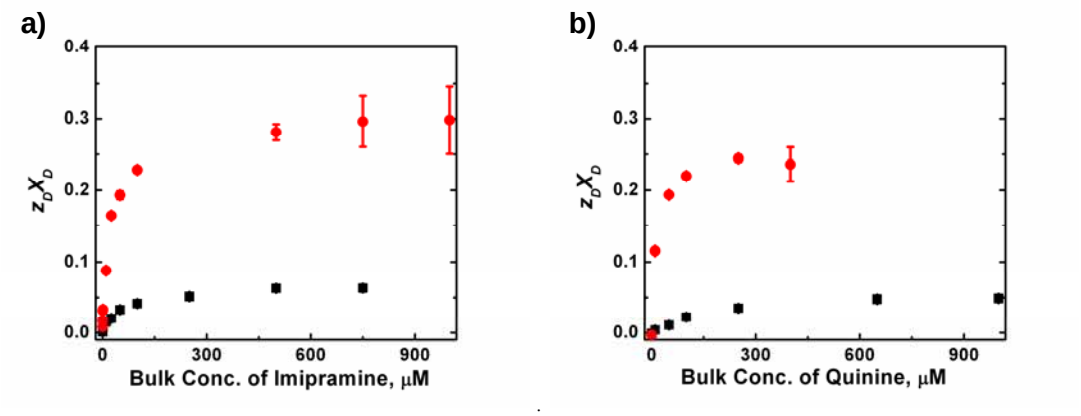

Figure 4-4. Changes in the amount of binding of cationic drug bound to lipid bilayers as a function of the concentration of these drugs in the bulk solution. Data shows the mean values of $X_D z_D$ as obtained from Eq. (24) in lipid bilayers composed of (■) PC lipids and (●) 75 mol% PC and 25 mol% PA lipids as a function of the bulk concentration of (a) imipramine and (b) quinine in the bilayer chamber.

Imipramine has a pK_a value of 9.4[4] and thus, according to the Henderson–Hasselbalch equation, at a pH of 7.4, approximately 99% of the drug molecules in bulk solution bear a positive charge corresponding to an effective charge of z_i, = +0.99. Quinine has a pK_a value of 8.8[14] and at pH of 7.4 approximately 96% of the quinine molecules in bulk solution bear a positive charge corresponding to an effective charge of z_i = +0.96. Using these z_i values, from the data in Figure 4-4, we obtained the mole fraction of the bound drug molecule.

Binding of these drug molecules to lipid bilayers can be described by a Langmuir binding isotherm:

$$B = \frac{B_{\max} C_D}{(C_D + K_d)}, \tag{25}$$

where B (unitless) is the amount of the bound drug (in moles) per mole of lipids at free drug concentration of C_D (M); B_{max} (unitless) represents the maximum amount of drug bound per mole of lipid; K_d represents the dissociation constant for the binding of drug molecules to the membrane. Given the mole fraction of the bound drug molecule as a function of the drug concentration, we can obtain the binding isotherm of these binding events. Due to the ion concentration profile in the vicinity of every charged membrane,[8] however, the binding association constant ($1/K_d$) of charged drug molecules is determined not by the bulk concentration of the drugs but by the local concentration of the charged drug molecules near the membrane. According to the Boltzmann equation (Eq. (26)), the local concentration of any ion at a distance X from the membrane surface, C_X (mol L^{-1}), at a given electric potential of Ψ_X (V), can be computed from the bulk concentration of that ion, C_b (mol L^{-1}):[8,15,16]

$$C_X = C_b \exp(\frac{-zF\psi_X}{RT}), \tag{26}$$

where z is the valence of the ion; F (96,485 C mol^{-1}) is the Faraday constant; R (8.31 N m mol^{-1} K^{-1}) is the gas constant and T (K) is the temperature. Thus, the concentration of the cationic form of the drug in the vicinity of the membrane, C_m, can be obtained as following:

$$C_m = C_b \exp(\frac{-zF\psi_0}{RT}), \tag{27}$$

where Ψ_0 (V) represents the surface potential of the membrane. Given the bulk concentration of the drug, we need the membrane surface potential to be able to compute the local concentration of the drug near the membrane. We obtained the membrane surface potential as described in the following steps.

Gramicidin channels are permeable to monovalent cations[6,9,17] such as Cs^+ and K^+ and the conductance of these pores in the recording buffer used in the present study (20 mM CsCl and 10 mM HEPES with a pH of 7.4) is dominated by the passage of Cs^+ through gA channels with a minor contribution of protons (which are at a concentration of 10^{-7} M). Assuming that the single channel conductance of gA, γ, is linearly proportional to the local concentration of the permeant ion Cs^+ at the membrane, the following relationship can be written:[8,18]

$$\gamma \propto [Cs^+]_m. \tag{28}$$

The concentration of Cs^+ near the membrane, $[Cs^+]_m$, at a given membrane surface potential can be obtained by the Boltzmann equation:

$$[Cs^+]_m = [Cs^+]_b \exp(\frac{-zF\psi_0}{RT}), \tag{29}$$

where $[Cs^+]_b$ represents the bulk concentration of cesium ions. Combing Eq. (28) and (29) results in:

$$\gamma \propto [Cs^+]_b \exp(\frac{-zF\psi_0}{RT}). \tag{30}$$

The ratio of the single channel conductance of gA in two different bilayers, γ_1 and γ_2, can be written as:

$$\frac{\gamma_1}{\gamma_2} = \frac{[Cs^+]_{b,1} \exp(\frac{-zF\psi_{0,1}}{RT})}{[Cs^+]_{b,2} \exp(\frac{-zF\psi_{0,2}}{RT})}, \tag{31}$$

where $[Cs^+]_{b,1}$ and $[Cs^+]_{b,2}$ are the bulk concentration of cesium ions and given these concentrations are identical for both bilayers, Eq. (31) can be simplified to:

$$\frac{\gamma_1}{\gamma_2} = \exp(\frac{-zF(\psi_{0,1} - \psi_{0,2})}{RT}). \tag{32}$$

Since the surface potential of a neutral membrane is considered to be zero ($\psi_{0,n} = 0$), the ratio of the single channel conductance of gA in a charged membrane, γ_C, to the gA conductance in a neutral membrane, γ_n, will be:

$$\frac{\gamma_C}{\gamma_n} = \exp(\frac{-zF\psi_{0,C}}{RT}), \tag{33}$$

where $\psi_{0,C}$ is the surface membrane potential of the charged membrane. Solving Eq. (29) for $\psi_{0,C}$, we obtain:

$$\psi_{0,C} = \frac{-zF}{RT}\ln(\frac{\gamma_C}{\gamma_n}). \tag{34}$$

Assuming that a lipid membrane composed of PC lipids is completely neutral and has a surface potential of 0, we can convert the changes in the single channel conductance of gA to the changes in surface potential of the membrane using Eq. (34). Substituting the following constant values in Eq. (34) results in Eq. (35):

$z = +1$, $F = 96{,}485$ C mol^{-1}, $R = 8.31$ N m mol^{-1} K^{-1}, $T = 298$ K

$$\psi_{0,C} = -25.7 \text{ mV} \times \ln(\frac{\gamma_C}{\gamma_n}). \tag{35}$$

Obtaining the membrane surface potential using Eq. (35), we computed the local concentration of the drug at the membrane by the Boltzmann equation (Eq. (27)) for different bulk concentrations of the drug. By plotting the mole fraction of the charged drug molecules bound to the membrane as a function of the drug concentration near the membrane, and fitting the data to Eq. (25), we can obtain the binding dissociation constant K_d and the binding capacity B_{max} for these binding events.

Figure 4-5 depicts the mole fraction of the bound drug molecules to neutral and negatively-charged lipid membranes as a function of the local concentration of the drug near the membrane. Values of K_d and B_{max} that resulted from best curve fits in Figure 4-5 are summarized in Table 4-1.

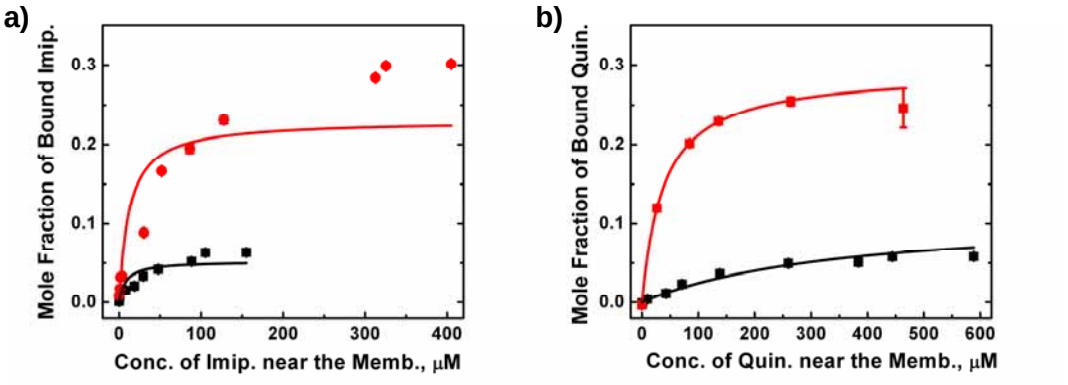

Figure 4-5. Changes in the mole fraction of the cationic drug that is bound to lipid membranes as a function of the local concentration of the positively-charged drug in the vicinity of the membrane. The data show the mean values of the mole fraction of bound drug to lipid bilayers composed of (■) PC lipids and (●) 75 mol% PC and 25 mol% PA as a function of the local concentration of (a) imipramine and (b) quinine near the membrane. Error bars represent the standard error of the mean. Solid curves represent the best fit of the data to the Langmuir isotherm binding equation of $B = \frac{B_{\max} C_D}{(C_D + K_d)}$, where B is the mole faction of bound drug molecules per mole of lipids, and C_D is the concentration of unbound drug.

Table 4-1. Parameters of binding of the cationic form of imipramine and quinine to neutral and negative-charged lipid bilayers.

Lipid bilayer	Imipramine K_d (μM)	Imipramine B_{max} (mol/mol)	Quinine K_d (μM)	Quinine B_{max} (mol/mol)
PC	8 ± 5	0.05 ± 0.01	368 ± 160	0.11 ± 0.07
75% PC/25% PA	12 ± 8	0.23 ± 0.14	38 ± 21	0.29 ± 0.20

Since this gA-based assay relies on changes in the surface potential of the lipid membrane to detect the binding of molecules to the membrane, the resulting binding parameters only describe the binding of the charged form of the examined drugs. As previously mentioned, under the experimental condition of the present study, about 99% of imipramine molecules and 96% of quinine molecules carry a positive charge in the bulk solution and the remaining fraction of molecules carry no electrical charge. Having their charge lost, this fraction of drug molecules interact differently with the lipid membrane and may, for example, accumulate in the hydrophobic core of the membrane. Although, we would expect the charged and the uncharged from of drug to reach an equilibrium in the membrane as well. This equilibrium will depend on the pk_a of the drug in the membrane environment. It is possible that the uncharged form of the drug is solubilized in the membrane which would alter the pk_a.

The K_d value of 38 μM that was obtained here for binding of quinine to PC/PA bilayers is in relatively good agreement with a previously reported value of K_d = 10 μM for binding of quinine to lipid vesicles that contained 100 mol% PA lipids under similar

experimental conditions.[19] The difference by a factor of ~4 weaker binding determined here, might in part be due to the fact that the bilayer contained 25 mol% PA instead of 100 mol%. A previous study on binding of imipramine to lipid membranes using a radioligand binding assay has reported K_d values of 0.01-1.2 μM for binding of this drug to PC and PC/PS bilayers.[4] While the value of K_d obtained here for binding of imipramine to PC/PA bilayers (12 μM) is approximately 10-fold higher than these reported values, the K_d obtained for binding of imipramine to PC bilayers (8 μM) is three orders of magnitude larger than the reported value of ~10 nM. One possible factor for this difference is the inappropriateness of the binding model employed here to describe the binding of imipramine to the membrane as the fits in Figure 4-5a do not seem to describe the data well. This difference may also be due to the fact that the present gA-based assay probes only the binding of the charged fraction of drug. Therefore, the difference between the results presented here and reported values may reflect a significant difference between the binding affinity of uncharged form of the drug to the membrane and that of the charged form of the drug. The difference between the acyl chain structure of lipids may also contribute to the difference between the present and previous reports.

We have also explored the application of this binding assay by monitoring the binding of a negatively-charged detergent sodium dodecyl sulfate (SDS) to neutral lipid bilayers and, as expected, observed a gradual increase in single channel conductance of gA with an increasing concentration of SDS in the bilayer chamber (data not shown). This result showed that this gA-based assay may also be employed to detect the binding of negatively-charged molecules to lipid membranes.

4.3. Conclusion

In conclusion, we introduced a gramicidin-based assay to monitor the binding of the cationic form of two therapeutic drugs, quinine and imipramine, to planar lipid bilayers. We related the change in the single channel conductance of gA pores to the change in the mole fraction of the positively-charged drug molecules bound to the membrane. Employing the obtained mole fractions, we quantified the monitored binding events and revealed the dissociation constant (K_d) and the maximum binding of drug per lipid (B_{max}).

This label-free assay is based on single channel recordings of gA pores and monitors, *in situ* and in real time, the binding of electrically-charged molecules to lipid membranes through the changes in surface potential of the membrane. This assay is, hence, limited to detection of the charged species in the membrane.

4.4. Experimental Section

4.4.1. Materials

We purchased imipramine hydrochloride, quinine, and SDS from Sigma Aldrich; cesium chloride (CsCl) from International Biotechnologies, Inc.; calcium chloride ($CaCl_2$), pentane, and hexadecane from Fluka; and HEPES from Fisher Scientific. Gramicidin A (gA) was purchased as gramicidin D from Sigma Aldrich and purified by silica chromatography as described previously[20] to afford a final purity of 97% of gA. We purchased the following phospholipids form Avanti Polar Lipids, Inc.: 1,2-diphytanoyl-

sn-glycero-3-phosphocholine (DiPhyPC), 1,2-diphytanoyl-*sn*-glycero-3-phosphate (sodium salt) (DiPhyPA).

4.4.2. Formation of Planar Lipid Bilayers

We formed planar lipid bilayers with the "folding technique" in a custom-made bilayer setup fabricated in Teflon with two compartments of 3 or 4 mL capacity. We separated these two compartments by a thin Teflon film that contained one aperture with a diameter of ~100 μm (Eastern Scientific Inc.). We used vacuum grease (Corning) to attach the Teflon film to the chamber and to create a water tight seal between the two compartments. To facilitate bilayer formation, we pretreated the area surrounding the aperture of the Teflon film on each side with 2 μL of 5% (v/v) hexadecane in pentane. After addition of 1 mL of appropriate electrolyte (see below) to each compartment, we spread 3-5 μL of a lipid solution in pentane (25 mg mL^{-1} for DiPhyPC or 5 mg mL^{-1} for mixtures containing 90 mol% DiphyPC and 10 mol% phosphatidylinositol) at the air-water interface of the electrolyte solution and raised the liquid level by adding another 2 or 3 mL (depending on the compartment size) of electrolyte. Raising the liquid level in these two compartments above the aperture in the Teflon film resulted in the formation of a lipid bilayer from apposition of two lipid monolayers as described originally by Montal and Mueller. If raising the liquid level did not immediately result in formation a bilayer over the aperture, we lowered the liquid level in one or both compartments, followed by raising the electrolyte solution again. We repeated this cycle until we obtained a bilayer with a minimum capacitance of 70 pF.

The electrolyte solution for the experiments in this study contained 20 mM cesium chloride (CsCl) and 10 mM HEPES with a pH of 7.4. We chose electrolytes with low ionic strength for these single channel recordings because the charge-induced local increase in cation concentration close to a membrane affects the gA conductance more significantly under conditions of low ionic strength compared to conditions of high ionic strength.

4.4.3. Single Channel Recordings

Once a stable lipid bilayer was obtained, we gradually added small volumes (0.1 μL) of a solution of 10 ng mL^{-1} gA in isopropanol (Acros Organics) to both compartments of the bilayer setup until one to six gA channels were inserted in the bilayer at the same time. After each addition of gA, we mixed the bilayer chambers by stirring the solutions in both compartments for at least 3 min (we confirmed previously that a small droplet of food dye was completely mixed in the setup within 2 min of stirring). In these experiments the final concentration of gA in the bilayer chamber was in the range of 0.1-2.0 pM. This range of gA concentration corresponds to 0.3-8 femtomoles of gA in the chamber with a volume of 3-4 mL; the total amount of lipid in each compartment was ~150 nanomoles, leading to a lipid to gA ratio of ~10^8. To measure the single channel conductance of gA pores, we recorded current traces versus time while applying different voltages in the range of ±100 mV. We performed these single channel recordings in "voltage clamp mode" using Ag/AgCl pellet electrodes (Warner Instruments) in both compartments of the bilayer setup. Data acquisition and storage was

carried out using a custom software written in Labview by Daniel J. Estes in combination with a Geneclamp 500 amplifier from Axon Instruments (set to a gain of 100 mV pA^{-1} and a filter cutoff frequency of 2 kHz). The data acquisition board (National Instruments) that was connected to the amplifier was set to a sampling frequency of 15 kHz. All recordings were carried out at a temperature of ~22º C.

We performed the analysis of the single channel current traces by computing histograms of the currents from the original current versus time traces with Clampfit 9.2 software (Axon Instruments). From these histograms, we extracted the mean current amplitude of gA channel opening and closing events. All conductance values were obtained from the slopes of current amplitudes versus voltage (I-V) curves (see the next section for more details on this analysis).

In order to reduce the noise in these single channel recordings, we mounted the bilayer setup on a low noise stir plate (Stir-2, Warner Instruments), which was placed on a bench top vibration isolation platform (50 BM-4, Minus K Technology) inside a Faraday cage from Warner Instruments. In addition, we found that we reached the minimum noise level by placing the aforementioned setup on top of a second vibration isolation table (63-500 series from TMC) with a Faraday cage.

4.4.4. Monitoring Changes in gA Conductance Induced by Binding of Drugs and Statistical Data Analysis

We gradually exposed a bilayer that contained gA pores to the drug by a step by step addition of the drug to the bilayer chamber. After each addition, the bilayer chamber

was stirred for 3 min to mix the drug inside the chamber. For each concentration of the drug, we recorded current traces at different applied voltages. To analyze these current versus time traces, we first obtained a histogram that represented the distribution of currents for each current trace. The difference in current between adjacent peaks in these histograms represented the current amplitude of single gA channel openings. These current amplitudes, therefore, reflect the single channel conductance of gA, γ, at a given concentration of the drug. By averaging all current amplitudes within a histogram, we obtained the mean current amplitude of gA events and a standard deviation (STD) for this mean for each trace for a given drug concentration. We plotted these mean current amplitudes as a function of the applied voltage for each concentration. We obtained a mean value for single channel conductance of gA, γ, at a given drug concentration from the slope of the resulting current versus voltage (I-V) curve in the linear range $\leq |\pm 100$ mV| of the curve.

Acknowledgements

We thank Nashmia Khalid for her contribution in data collection.

References

1. D. Barthel, O. Zschoernig, K. Lange et al., *Biochim. Biophys. Acta* **945** (2), 361 (1988).

2. J. M. Carrozzino and M. G. Khaledi, *J. Chromatogr. A* **1079** (1-2), 307 (2005).

3. J. K. Seydel and M. Wiese, *Drug-Membrane Interactions*

(Wiley-VCH, Weinheim, 2002).

4. Z. Fisar, K. Fuksova, and M. Velenovska, *Gen. Physiol. Biophys.* **23** (1), 77 (2004).

5. I. Porcar, A. Codoner, C. M. Gomez et al., *J. Pharm. Sci.* **92** (1), 45 (2003).

6. O. S. Andersen, R. E. Koeppe, and B. Roux, *IEEE Trans. NanoBiosci.* **4** (1), 10 (2005).

7. T. A. Cross, A. Arseniev, B. A. Cornell et al., *Nat. Struct. Biol.* **6** (7), 610 (1999).

8. S. G. A. Mc Laughlin, G. Szabo, and G. Eisenman, *J. Gen. Physiol.* **58** (6), 667 (1971).

9. O. S. Andersen, *Annu. Rev. Physiol.* **46**, 531 (1984).

10. O. S. Andersen, H. J. Apell, E. Bamberg et al., *Nat. Struct. Biol.* **6** (7), 609 (1999).

11. H. J. Apell, E. Bamberg, and P. Lauger, *Biochim. Biophys. Acta* **552** (3), 369 (1979).

12. R. Capone, S. Blake, M. R. Restrepo et al., *J. Am. Chem. Soc.* **129** (31), 9737 (2007).

13. T. K. Rostovtseva, V. M. Aguilella, I. Vodyanoy et al., *Biophys. J.* **75** (4), 1783 (1998).

14. M. Srinivas, M. G. Hopperstad, and D. C. Spray, *Proc. Natl. Acad. Sci. U. S. A.* **98** (19), 10942 (2001).

15. P. M. Macdonald and J. Seelig, *Biochemistry* **26** (5), 1231 (1987).

16. M. Eisenberg, T. Gresalfi, T. Riccio et al., *Biochemistry* **18** (23), 5213 (1979).

17. E. Bamberg, K. Noda, E. Gross et al., *Biochim. Biophys. Acta* **419** (2), 223 (1976).

18. M. J. Kell and L. J. Defelice, *J. Membr. Biol.* **102** (1), 1 (1988).

19. J. Pedros, I. Porcar, C. M. Gomez et al., *Spectrochimica Acta Part a-Molecular and Biomolecular Spectroscopy* **53** (3), 421 (1997).

20. C. J. Stankovic, J. M. Delfino, and S. L. Schreiber, *Anal. Biochem.* **184** (1), 100 (1990).

Chapter 5

Fabrication of Arrays of Supported Lipid Membranes for Screening of Drug-Membrane and Protein-Membrane Interactions

Abstract

This chapter describes a rapid, reproducible, and straightforward method to form copies of functional membrane arrays with various lipid compositions and the application of these arrays for screening of drug-membrane and protein-membrane interactions. We employed topographically patterned agarose gels to stamp spatially-addressable arrays of supported bilayers on glass and confirmed the fluidity of these membranes by fluorescence recovery experiments. We took advantage of the storage capability of hydrogels and demonstrate that inking posts on an agarose stamp with extremely small volumes ($\leq$ 1 μL) of a solution containing liposomes was sufficient to transfer at least 100 copies of a membrane array without the need for re-inking. We used stamped membrane arrays for screening the interactions of a protein (annexin V) and an anti-inflammatory drug (nimesulide) with bilayers of various lipid compositions and discovered that the interaction of the prescription drug nimesulide with membranes depends on their cholesterol content.

5.1. Introduction

Interest in supported bilayers[1-3] includes studies of the dynamic structure of membranes,[4,5] their self-assembly,[5] lipid-protein interactions,[5] ligand-receptor interactions,[5-8] development of membrane-based biosensors,[5,9-15] and drug discovery.[16] In addition, many pharmaceuticals are known to interact with biological membranes and assays for testing drug-membrane interactions are important for a better understanding of drug activity, targeting, and toxicity.[17] In order to use supported bilayers efficiently for studying the aforementioned processes, the membranes must be fluid[1,16,18,19] and mechanically stable[19]. Techniques currently employed to form arrays of supported membranes use deposition of droplets of liposome solution onto surfaces,[6,18] vesicle fusion from bulk solution onto patterned substrates,[20,21] delivery of liposomes by microfluidic channels,[22,23] and microcontact printing with poly (dimethylsiloxane) (PDMS).[24]

Considering the application of membrane arrays for screening protein-membrane or drug-membrane interactions, an ideal fabrication method would rapidly create many functional copies of an array of different bilayers while consuming minimal amounts of lipids. Among the existing methods, microcontact printing has the ability to create many spots of membranes in parallel. To prepare arrays with various compositions, however, posts of the stamp used for microcontact printing have to be inked individually. Such an inking procedure can be time consuming and introduce heterogeneity in the stamped arrays. It would therefore be advantageous if a biocompatible stamp – once inked –

would store the inking solution and allow multiple transfers without the need for re-inking.

Here, we demonstrate that stamping with hydrogel stamps allows multiple stamping while using minute amounts of material. We fabricated stamps from 4% agarose gel, which has a pore size that is sufficiently large to allow for the diffusion of macromolecules and small liposomes (the pore size of 2% agarose gel is ~ 470 nm[25]). This capability makes it possible to store inking solution in the stamp while replenishing molecules at the surface of the stamp and thus to perform multiple stamping of biomolecules.[25] Recently agarose stamps[26,27] have been applied to pattern arrays of proteins,[28,29] bacteria,[30] and mammalian cells.[31] Here we present the first attempt to use hydrogel stamps to create functional arrays of fluid lipid membranes.

5.2. Results and Discussion

To form arrays of lipid bilayers, we inked each post on the agarose stamp with a sub-microliter volume of liposome suspension and after the posts absorbed the solution, we placed the inked stamp in contact with glass slides for 5-10 sec (see experimental section for details and stamp dimensions). Immediately after removing the stamp we immersed the patterned substrates in deionized water or PBS buffer. We hypothesize that during stamping, supported membranes form by diffusion of small liposomes (diameter 20-80 nm)[32] through the pores of the agarose stamp and by subsequent spreading of liposomes onto the regions of contact with the glass. Since the agarose stamps used in this method consisted mostly (≥ 96% w/w) of water, we suggest that the mechanism of

bilayer formation was similar to the mechanism of the established method of vesicle fusion from solution.[16]

We examined the structure of the stamped lipid bilayer spots on the glass substrate by atomic force microscopy (AFM) experiments. The AFM results revealed a smooth surface of bilayer with scattered defects. Figure 5-1a shows an AFM image of a stamped bilayer composed of 99% (w/w) egg PC and 1% (w/w) rh-PE on a glass substrate. Figure 5-1b shows a height profile of the stamped bilayer using a defect site as a reference.[6] The area of the defect sites was ≤ 23 % of the total imaged bilayer area. Cross-section analysis of the defects revealed a thickness of 4.3 ± 0.8 nm, which corresponds to the height of a single lipid bilayer.[6]

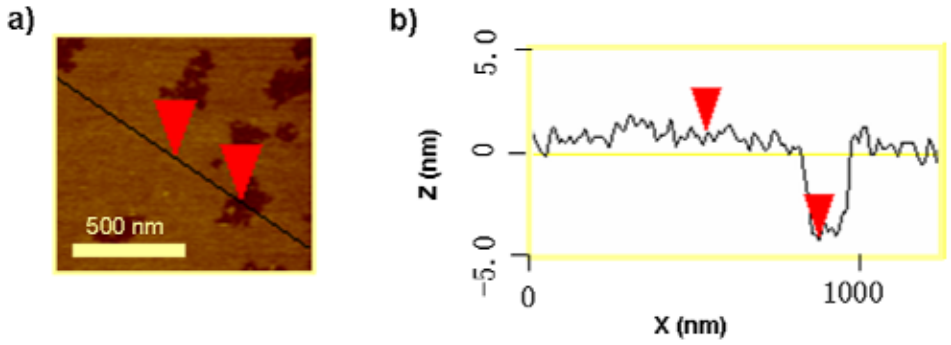

Figure 5-1. (a) AFM image of a potion of a stamped spot of bilayer composed of 99% (w/w) egg PC and 1% (w/w) rh-PE. The area of defects within this image is ~ 14%. (b) Height profile of the supported lipid bilayer along the black line in (a). The step height indicated by the markers is 4.5 nm.

To investigate the capability of agarose stamps to store small liposomes, we used a stamp which was inked once and stamped 100 times without intermediate re-inking. This stamp was inked with a solution of liposomes composed of L-α-phosphatidylcholine from chicken egg (egg PC) and 1% (w/w) 1,2-dipalmitoyl-*sn*-glycero-3-phosphoethanolamine-*N*-(lissamine–rhodamine B sulfonyl) (rh-PE). We found no significant loss in the fluorescence intensity of the spots over 100 stamping events (Figure 5-2a). Figure 5-2b and c show fluorescent micrographs of membrane arrays on glass obtained after 6 and 100 stamping events. To test the fluidity of the stamped bilayers, we performed fluorescence recovery after photobleaching (FRAP) experiments (see experimental sections for details). Figure 5-2d shows the recovery of a photobleached spot in a bilayer of the last (100^{th}) array. Fluorescence recovery of the bilayers in this array was similar to the recovery of the bilayers in the 6^{th} array (difference in diffusion constant $\leq$ 5%) indicating that the quality of the stamped arrays remained constant over ~100 stamping events. The fluorescence intensity in the photobleached spot recovered to ~90% of its original intensity, a value typical for supported membranes of high quality.[6]

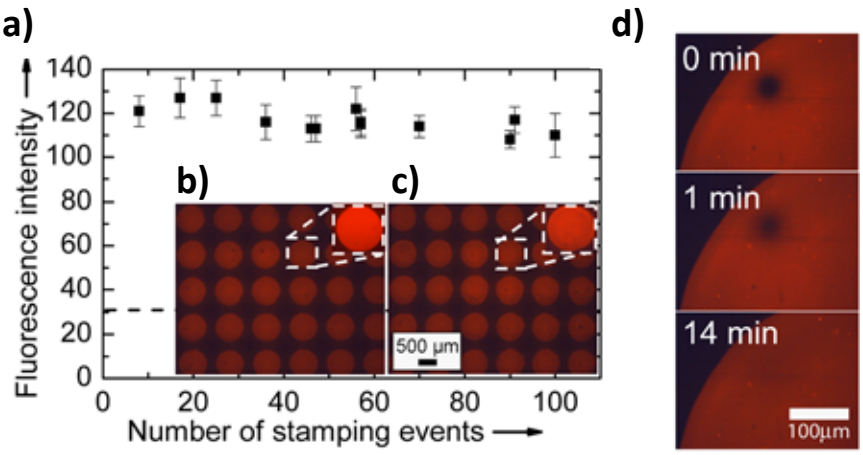

Figure 5-2. Fluorescence intensity after stamping of 100 arrays of membranes using a hydrogel stamp without intermediate inking and test of bilayer fluidity. Bilayers composed of egg PC and 1 % (w/w) rh-PE were stamped on glass slides. (a) Mean fluorescence intensity of supported bilayers as a function of the number of stamping events. The error bars represent the standard deviation of the fluorescence intensity of all spots in each array and the dashed line represents the mean fluorescence intensity of the background. The standard deviation of the fluorescence intensity within any individual spot was less than 9.5% and from spot to spot in an array it was less than 9%. (b) Micrograph of spots of supported bilayers after the 6th and (c) 100th stamping event. (d) Fluorescence images from a FRAP experiment performed on the array from the last (100th) stamping event after photobleaching for 8 min.

We used a stamp with posts with a diameter of 200 µm to explore the potential of this method for producing membrane arrays with high density. Figure 5-3a shows a resulting array with a density of 600 membrane spots per cm^2. If such a stamp would be inked using robotics, it should, in principle, be possible to stamp multiple copies of high-density arrays with various membrane compositions.[29] Figure 5-3b shows an array of

bilayers with two different fluorescently-labeled lipids. These spots were transferred in parallel from the same stamp.

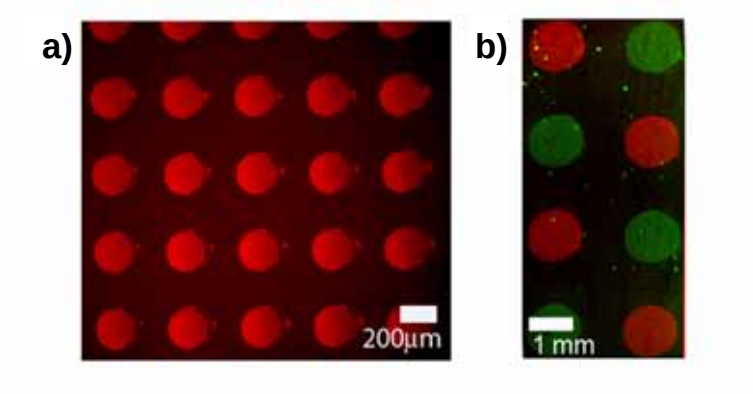

Figure 5-3. Stamped high-density array of supported bilayers and membrane arrays with various compositions. (a) Fluorescent micrograph of a patterned array of bilayers composed of egg PC with 1% (w/w) rh-PE using an agarose stamp with a post size of 200 µm. (b) Fluorescent micrograph of an array of bilayers containing egg PC and 1% (w/w) rh-PE (red) and 3% (w/w) NBD-PE (green).

To demonstrate the ability of this method to create, in parallel, bilayers with different lipid compositions, we transferred arrays of supported membranes using liposomes containing 0-50% negatively-charged lipids and 0-50% cholesterol. Remarkably, hydrogel-stamping resulted in membrane arrays of high quality on glass substrates even when the bilayers contained 50 % negatively-charged lipids (Figure 5-4a).

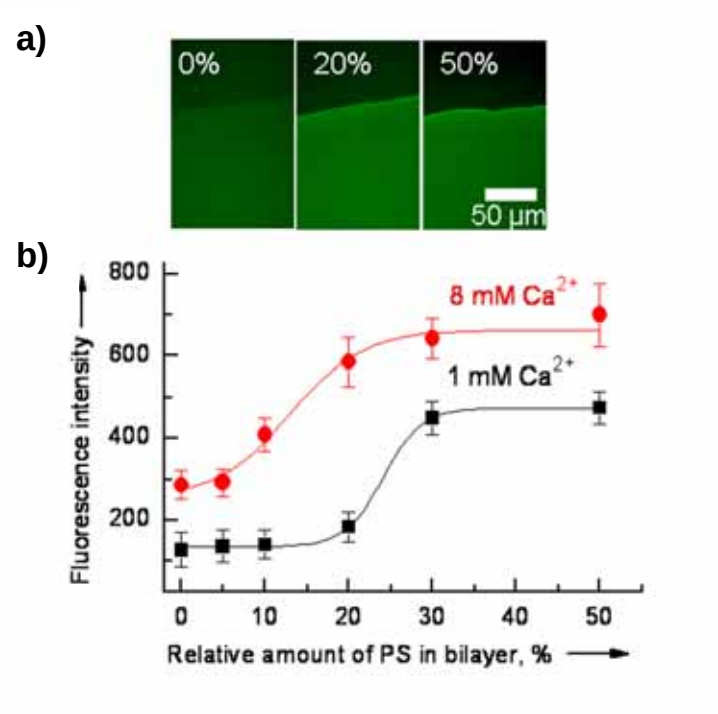

Figure 5-4. Binding of the protein annexin V to bilayers with different PS content. (a) Micrographs of binding of fluorescently-labeled annexin V to bilayers containing 0, 20, and 50% (w/w) DOPS. (b) Increase of fluorescence intensity due to binding of annexin V to an array of bilayers with a gradient in DOPS. Binding of annexin V is calcium-dependent; data were obtained in (■) 1 mM and (●) 8 mM Ca^{2+}. Error bars represent standard deviations of fluorescence intensity.

To study if liposomes with different lipid compositions are transferred differentially from the agarose stamp to the glass slide, we inked the posts of a stamp with mixtures of two different liposome populations. Liposomes composed of 99% (w/w) egg PC and 1% (w/w) rh-PE (population A) and liposomes composed of 50% (w/w) egg PC and 50% (w/w) DOPS (population B) were prepared separately and mixed in different ratios shortly before the inking procedure. Only liposomes of the population A were

fluorescently labeled and therefore the fluorescence intensity of the resulting supported bilayers represented the percentage of the transferred liposomes from this population. Five different mixtures of the two aforementioned liposome populations were used to ink the posts on a stamp, the ratios were: 100% A, 0% B; 80% A, 20% B; 50% A, 50% B; 30% A, 70% B; 0% A, 100% B. **Figure 5-5** shows fluorescent micrographs of the resulting array and the graph represents the mean fluorescence intensity in the bilayer spots which resulted from inking solutions with varying ratios of fluorescently-labeled liposomes. These results showed that the fluorescence of the transferred bilayers was proportional to the ratio of the two liposome populations in the inking solution, suggesting no significant preference of transfer between neutral and negatively-charged liposomes.

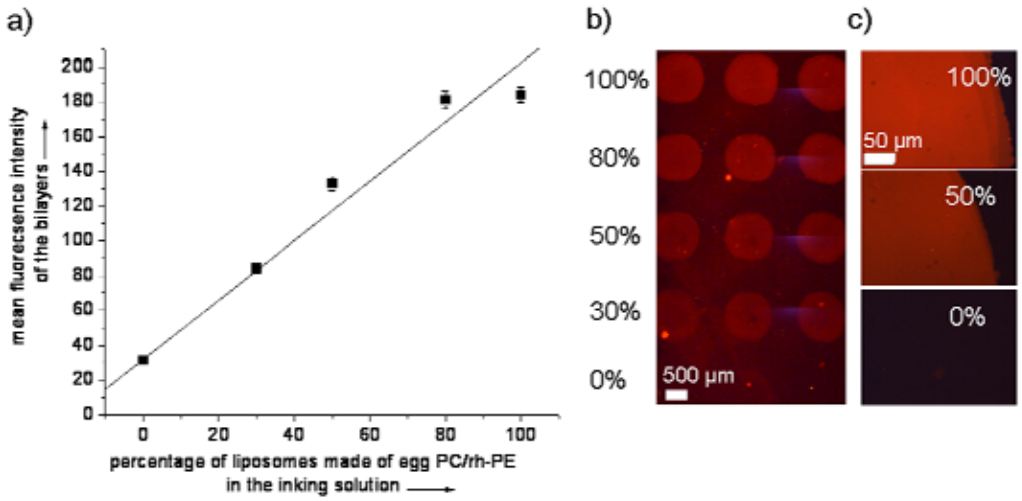

Figure 5-5. Transfer of liposomes from a mixture of liposome preparations which were used for inking of an agarose stamp. (a) Graph showing the mean fluorescence intensity of bilayers transferred from the posts which were inked with mixtures containing different ratios of fluorescent liposomes of population A and non-fluorescent liposomes of population B. Error bars represent standard deviations of fluorescence intensity. (b) Fluorescent micrograph of the array of bilayers with various compositions. Spots of each row have the same composition. The corresponding posts on the stamp were inked with (from top) first row: 100% population A, second row: 80% population A and 20% population B, third row: 50% population A and 50% population B, forth row: 30% population A and 70% population B, and fifth row: 100% population B. (c) Fluorescent images of a portion of bilayer spots of the array shown in (b) at higher (40×) magnification.

To explore the application of membrane arrays with various compositions for screening of protein-membrane interactions, we formed arrays from egg PC with a gradient in the negatively-charged lipid, DOPS, and measured the binding of annexin V

to theses bilayers. Annexin V is a calcium-dependent binding protein that interacts with negatively-charged lipids.[33] Figure 5-4a shows micrographs of binding of fluorescently-labeled annexin V to supported bilayers with three different concentrations of DOPS. Figure 5-4b illustrates that binding of annexin V to supported membranes increased with increasing concentration of both, DOPS in the bilayer, and calcium ions in solution. These results show that stamped arrays of supported membranes can be used effectively to quantify protein-membrane interactions.

In addition to investigating protein-membrane binding, membrane arrays may be useful for screening drug-membrane interactions. These interactions can depend on the composition of the lipid membrane[17] (e.g. the content of cholesterol) and they can induce a change in the fluidity of the bilayer.[34] The therapeutic and toxic effects of many drugs are affected by interactions with lipid membranes.[17,34] To demonstrate the influence of the lipid composition on drug-membrane interactions, we studied the fluidity changes introduced by a non-steroidal anti-inflammatory drug (NSAID), nimesulide, in bilayers with various contents of cholesterol. NSAIDs, (e.g. aspirin or ibuprofen) are the most important drugs for treatment of inflammation, pain, and fever.[34]

Lucio *et al.* reported that nimesulide increases the fluidity in membranes composed of egg PC.[34] Here, we incubated stamped membrane arrays of egg PC containing various cholesterol contents in solutions containing 0, 50, and 100 μM nimesulide for 2 hrs and monitored the changes in fluidity by FRAP experiments. Figure 5-6 shows the fluorescence recovery of bleached spots in the presence of nimesulide.

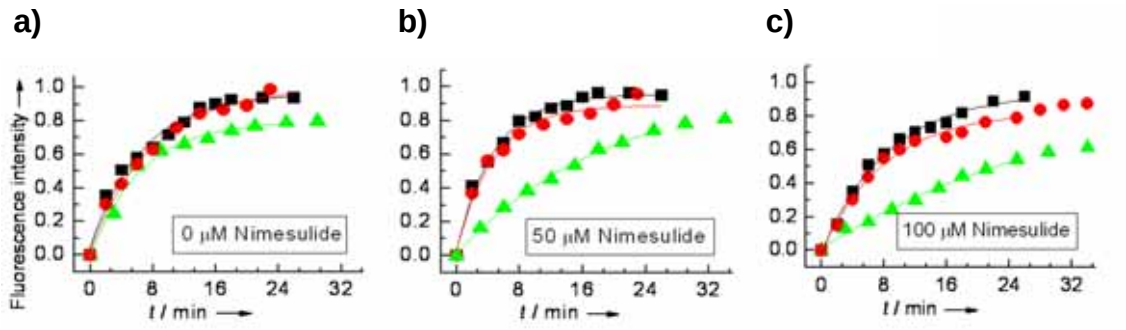

Figure 5-6. Influence of nimesulide on the fluidity of stamped lipid bilayers with various cholesterol contents. Recovery curves of supported lipid bilayers of egg PC and 1 % (w/w) rh-PE containing (■) 0 % cholesterol, (●) 20 % cholesterol, and (▲) 50 % cholesterol in the presence of (a) 0 µM, (b) 50 µM, and (c) 100 µM nimesulide.

In agreement with Lucio *et al.*[34] We found that 50 µM nimesulide increased the fluidity in egg PC membranes. We discovered the same effect with bilayers containing moderate cholesterol content (≤ 20%). Surprisingly, however, nimesulide had the opposite effect, namely a decrease in fluidity, on bilayers with high cholesterol content (≥ 50%). Also unexpectedly, nimesulide decreased the fluidity of all examined bilayers when added at a concentration of 100 µM (Figure 5-6c). The diffusion coefficients of fluorescently-labeled lipids in these bilayers are summarized in Table 1.

Table 5-1. Diffusion coefficients, *D* of supported membranes composed of egg PC and 1% (w/w) rh-PE with various cholesterol contents in the presence of nimesulide.

Cholesterol content (%)	*D* ($cm^2 s^{-1}$) as a function of the		
	0	50	100
0	2.0×10^{-9}	2.7×10^{-9}	1.4×10^{-9}
20	1.8×10^{-9}	2.4×10^{-9}	1.2×10^{-9}
50	1.5×10^{-9}	0.7×10^{-9}	0.4×10^{-9}

The errors of the diffusion coefficients are ≤ ±7 %. The errors were obtained by measuring the difference between diffusion coefficients of fluorescently-labeled lipids in bilayers made from the same lipid composition but stamped on different days.

5.3. Conclusion

In conclusion, we present a strikingly simple and reproducible method to obtain copies of functional membrane arrays from a range of lipids (including up to 50% negatively-charged lipids). This method is capable of fabricating at least 100 copies of a bilayer array while using only picomolar amounts of lipids per spot – a characteristic that may be particularly beneficial for stamping precious membrane preparations that can often only be obtained in limited quantities, such as cellular membrane fragments. Binding assays with these arrays elucidated an unknown effect of cholesterol on the interaction of a prescription drug with bilayers and we expect liposome stamping to be very useful for the rapidly growing interest in drug membrane interactions,[17,34] protein-membrane interactions,[5] and arrays of membrane proteins.[6]

5.4. Experimental Section

5.4.1. Fabrication of Agarose Stamps

We prepared agarose stamps according to the procedure described by Mayer *et al.*[29] Briefly, we heated an aqueous solution containing 4% (w/v) of high-gel strength agarose (OmniPur; Merck, Darmstadt, Germany) in 0.15 M KCl to the boiling point and cast it onto a patterned PDMS master at room temperature. Then we allowed the solution to gel at room temperature and peeled off the PDMS master to obtain the agarose stamps (Figure 5-7a). Depending on the desired dimensions of the agarose stamps, we used different PDMS masters to mold the stamps. The PDMS master for stamps with posts with 1 mm diameter was a replica (positive) of a PDMS replica (negative) of a standard 1536-well plate (polystyrene) with flat bottoms (Corning, Cambridge, MA, USA).[29] We also used masters prepared by photolithography[29] for stamps with posts with diameter of 200 and 700 μm. Depending on the PDMS master used for casting, arrays of posts on the agarose stamp, were (i) 200 μm in diameter, 130 μm in height, and spaced 200 μm from each other, (ii) 700 μm in diameter, 700 μm in height, and spaced 300 μm from each other; or, (iii) 1 mm in diameter, 1.5 mm in height, and spaced 1 mm from each other.

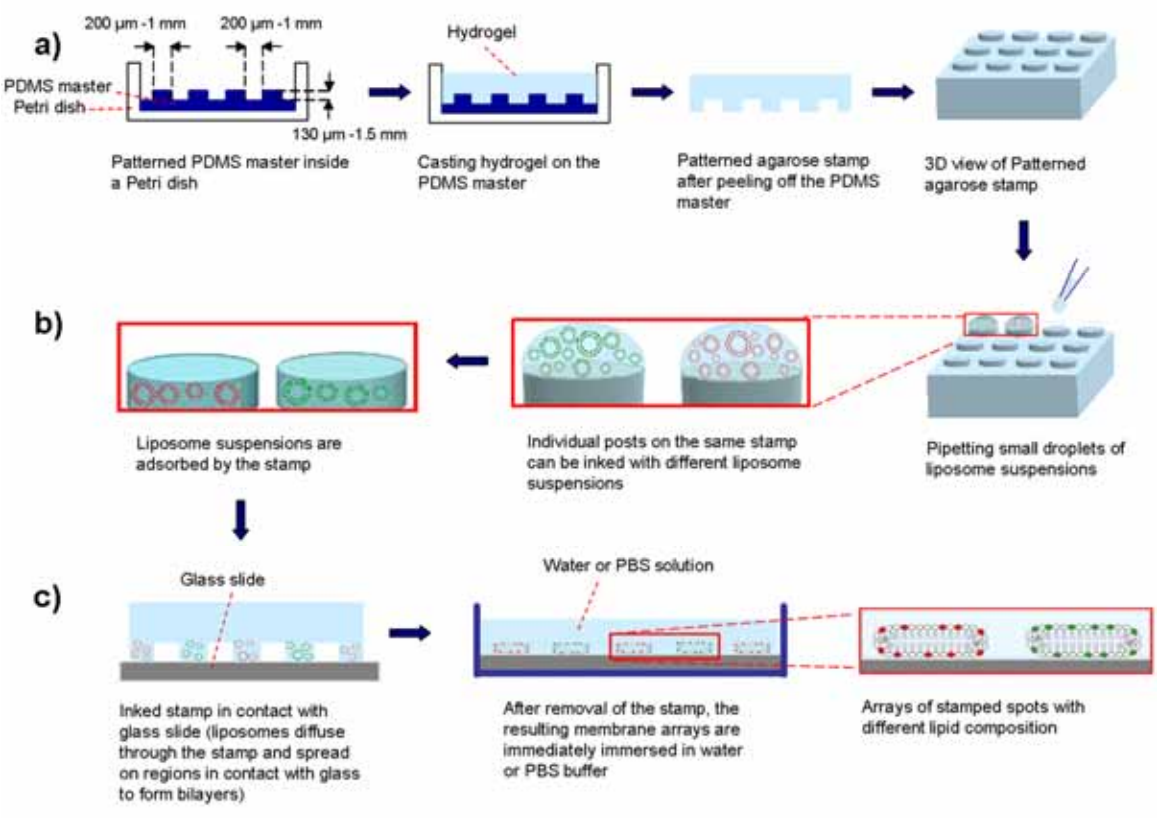

Figure 5-7. Schematic representation of the fabrication of agarose stamps, the inking process, and the stamping procedure. (a) Casting agarose gel onto a patterned PDMS master and peeling off the PDMS master from the agarose gel resulted in a topographically patterned agarose stamp. (b) In order to ink the posts of the stamp manually, the stamps were turned upside down such that posts were facing upwards and small droplets (~ 0.2 µL) of liposome suspensions were added on top of each post. Small liposomes inside the droplet diffused into the agarose gel and the solution of the liposome suspension was absorbed by the gel. (c) Supported lipid bilayer spots were formed by diffusion of liposomes through the gel and subsequent spreading of these liposomes onto the glass slide at the areas of contact between the stamp and glass slide. Stamped membrane arrays on glass slides were immersed in water or PBS buffer immediately after removal of the stamp from the substrate. The membrane arrays were then ready for inspection, binding assays, or storage.

5.4.2. Preparation of Liposomes

Lipid mixtures used to prepare liposomes were: 99% L-α-phosphatidylcholine form chicken egg (egg PC; Sigma Aldrich) and 1% (w/w) 1,2-dipalmitoyl-*sn*-glycero-3-phosphoethanolamine-*N*-(lissamine–rhodamine B sulfonyl) (rh-PE; Avanti Polar Lipids); 97% egg PC and 3% NBD-labled PE (NBD-PE; Avanti Polar Lipids); mixtures of egg PC / rh-PE or NBD-PE / 1,2-dioleoyl-*sn*-glycero-3-[phospho-L-serine] (DOPS; Avanti Polar Lipids), and mixtures of egg PC / rh-PE / cholesterol (Avanti Polar Lipids). The respective mixing ratios are mentioned in the main text. Small unilamellar liposomes were produced by tip sonication using a Branson Sonifier 150 (Branson Ultrasonics Corporation, Danbury, USA) of 1 mg lipid in 500 µL of an aqueous solution containing 0.15 M KCl, for 2-6 minutes (with ~ 5 watts output energy). Before sonication, the lipids were dissolved in chloroform and 100 µL of a 10 mg/mL lipid solution in chloroform was used to deposit a lipid film on the wall of a 5 mL round bottom flask using a rotatory evaporator under vacuum (starting form -300 torr and going up to -740 torr). Residual traces of chloroform were removed by desiccation under vacuum (~ -740 torr) for at least 1 hour.

5.4.3. Cleaning of Microscope Glass Slides

Microscope glass slides (Microslides, No. 2974, Corning, N.Y.) were cleaned with fresh piranha solution (mixture of concentrated sulfuric acid and 30 % hydrogen peroxide) followed by washing with deionized water at least eight times and drying at 180° C for 2 hours.

5.4.4. Inking and Stamping Procedure

To ink the agarose stamps with 1 mm or 700 μm posts, we turned the stamp upside down in a Petri dish containing a solution of 0.15 M KCl, such that ~ ¾ of the thickness of the stamp was immersed the KCl solution and the posts (which were facing upwards) were out of the KCl solution. We inked these posts individually by pipetting ~ 0.2 μL of liposome suspension on top of each post (Figure 5-7b). Neighboring posts on the same stamp could be inked with different liposome suspensions. Once the solution was adsorbed by the hydrogel (typically after ~ 4 minutes), we added another droplet of ~ 0.2 μL of solution on top of each post and this process was repeated for 4 or 5 times. In case of stamps with smaller posts (200 μm in diameter), we inked the agarose stamp by immersing the posts in a solution of liposomes for ~ 30 min. After inking we turned these stamps upside down (200 μm posts facing upwards) and after the stamp adsorbed all solution, we used it for stamping. In the beginning of a stamping series, we stamped 4-7 times on clean glass slides to remove excess solution of liposomes from the stamp.

To form arrays of lipid bilayers, we placed the inked agarose stamp in contact with clean glass slides for 5-10 sec (Figure 5-7c). After removing the stamp from the slides, the glass slides were immediately immersed in water or PBS solution. All stamping procedures were carried out at room temperature in a small room with ≥ 55 % humidity. We found that carrying out the stamping procedure in humidity < 50 % resulted in supported bilayers with reduced fluidity. The stamped spots of lipid bilayers retained their fluidity even after storing them for two weeks in buffer solution.

5.4.5. Atomic Force Microscopy (AFM) Experiments

We performed AFM experiments to examine the structure of the stamped lipid bilayers on the glass slides.[35] These experiments were carried out on a Nanoscope IIIA Multimode AFM (Veeco Metrology) in the tapping mode. All AFM experiments were performed in deionized water at room temperature using a commercially available fluid cell, sealed by an O-ring. The images were collected at 256 × 256 pixel resolution at a scan rate of 2.39 Hz using the Olympus Biolevers tips (Asylum Research). The spring constant of the cantilever was 0.027 N/m and the imaging frequency was 7 - 9 kHz.

5.4.6. Fluorescence Recovery after Photobleaching (FRAP) Experiments

FRAP experiments were performed on stamped supported lipid bilayers on glass slides (immersed in water or PBS) using a Nikon E600FN epifluorescence microscope equipped with an Evolution MP (Media Cybernetics, Canada) camera. The rhodamine label of lipids was excited using standard filter settings for rhodamine. Using a 40× water-immersion objective a spot with a diameter of ~ 30 μm was photobleached for 6-9 minutes with the aperture of the microscope closed as much as possible and all neutral density filters taken out of the light path. Fluorescence recovery of the bleached spot was then monitored with the same 40× objective. The recovery process was imaged with the aperture open and a ND4 neutral density filter in the light path to minimize further photobleaching. FRAP experiments were carried out in a dark room and the shutter for excitation was open only during image acquisition to minimize further photobleaching.

Images were analyzed by calculating the difference between the mean fluorescence intensity of the photobleached spot and a fluorescent spot in the same

bilayer (a spot within the bilayer that had not been bleached) and then normalized to the maximum difference between these two intensities. Diffusion coefficients of stamped membranes were compared to the diffusion coefficient of a control bilayer prepared on the same glass slides by the established vesicle fusion method.[36] Diffusion coefficients were calculated by the equation, D (cm^2 s^{-1}) = 0.224 ω^2 (cm)^2 / $t_{1/2}$ (s), where ω is the radius of the bleached spot and $t_{1/2}$ is the half time of the fluorescence recovery.[37,38] We obtained the value of $t_{1/2}$ from an exponential curve fit through the data.

Acknowledgements

We thank Jerry Yang, Irina Gitlin, and Adam Urbach for valuable discussions.

References

1. E. Sackmann, *Science* **271** (5245), 43 (1996).

2. H. M. McConnell, T. H. Watts, R. M. Weis et al., *Biochim. Biophys. Acta* **864** (1), 95 (1986).

3. M. Tanaka, A. P. Wong, F. Rehfeldt et al., *J. Am. Chem. Soc.* **126** (10), 3257 (2004).

4. S. J. Johnson, T. M. Bayerl, D. C. McDermott et al., *Biophys. J.* **59** (2), 289 (1991).

5. M. L. Wagner and L. K. Tamm, *Biophys. J.* **79** (3), 1400 (2000).

6. Y. Fang, A. G. Frutos, and J. Lahiri, *J. Am. Chem. Soc.* **124** (11), 2394 (2002).

7. C. Bieri, O. P. Ernst, S. Heyse et al., *Nature Biotech.* **17** (11), 1105 (1999).

8. S. Heyse, T. Stora, E. Schmid et al., *Biochim. Biophys. Acta* **1376** (3), 319 (1998).

9. E. Sackmann and M. Tanaka, *Trends Biotechnol.* **18** (2), 58 (2000).

10. P. Fromherz and W. Arden, *J. Am. Chem. Soc.* **102** (20), 6211 (1980).

11. H. Kiefer, B. Klee, E. John et al., *Biosens. Bioelectron.* **6** (3), 233 (1991).

12. U. Radler, J. Mack, N. Persike et al., *Biophys. J.* **79** (6), 3144 (2000).

13. S. M. Schiller, R. Naumann, K. Lovejoy et al., *Angew. Chem. Int. Ed.* **42** (2), 208 (2003).

14. K. Morigaki, T. Baumgart, A. Offenhausser et al., *Angew. Chem. Int. Ed.* **40** (1), 172 (2001).

15. H. Bayley and P. S. Cremer, *Nature* **413** (6852), 226 (2001).

16. J. T. Groves, *Curr. Opin. Drug Disc.* **5** (4), 606 (2002).

17. J.K. Seydel and M. Wiese, *Drug-membrane Interactions*. (Wiley-VCH, Weinheim, 2002).

18. P. S. Cremer, J. T. Groves, L. A. Kung et al., *Langmuir* **15** (11), 3893 (1999).

19. Y. Fang, A. G. Frutos, and J. Lahiri, *ChemBioChem* **3** (10), 987 (2002).

20. J. T. Groves, N. Ulman, and S. G. Boxer, *Science* **275** (5300), 651 (1997).

21. L. A. Kung, J. T. Groves, N. Ulman et al., *Adv. Mater.* **12** (10), 731 (2000).

22. L. Kam and S. G. Boxer, *J. Am. Chem. Soc.* **122** (51), 12901 (2000).

23. T. L. Yang, S. Y. Jung, H. B. Mao et al., *Anal. Chem.* **73** (2), 165 (2001).

24. J. S. Hovis and S. G. Boxer, *Langmuir* **17** (11), 3400 (2001).

25. A. Pluen, P. A. Netti, R. K. Jain et al., *Biophys. J.* **77** (1), 542 (1999).

26. M. Fialkowski, C. J. Campbell, I. T. Bensemann et al., *Langmuir* **20** (9), 3513 (2004).

27. B. A. Grzybowski, Kyle J. M. Bishop, C. J. Campbell et al., *Soft Matter* **1** (2), 114 (2005).

28. B. D. Martin, B. P. Gaber, C. H. Patterson et al., *Langmuir* **14** (15), 3971 (1998).

29. Michael Mayer, Jerry Yang, Irina Gitlin et al., *Proteomics* **4** (8), 2366 (2004).

30. D. B. Weibel, A. Lee, M. Mayer et al., *Langmuir* **21** (14), 6436 (2005).

31. M. M. Stevens, M. Mayer, D. G. Anderson et al., *Biomaterials* **26** (36), 7636 (2005).

32. M. A. Cooper, *J. Mol. Recognit.* **17** (4), 286 (2004).

33. J. F. Tait, D. F. Gibson, and C. Smith, *Anal. Biochem.* **329** (1), 112 (2004).

34. M. Lucio, H. Ferreira, Jlfc Lima et al., *Phys. Chem. Chem. Phys.* **6** (7), 1493 (2004).

35. K. Morigaki, H. Schonherr, C. W. Frank et al., *Langmuir* **19** (17), 6994 (2003).

36. P. S. Cremer and T. L. Yang, *J. Am. Chem. Soc.* **121** (35), 8130 (1999).

37. D. Axelrod, D. E. Koppel, J. Schlessinger et al., *Biophys. J.* **16** (9), 1055 (1976).

38. D. M. Soumpasis, *Biophys. J.* **41** (1), 95 (1983).

Chapter 6

Generating Arrays with High Content and Minimal Consumption of Functional Membrane Proteins

Abstract

This chapter introduces a widely-accessible and straight-forward technique for fabricating membrane protein arrays. This technique employs topographically-patterned agarose gels to deliver various membrane preparations to glass substrates in a rapid and parallel fashion. It can fabricate more than 30 identical copies of a membrane protein array while requiring only femtomoles of protein. Taking advantage of on-stamp preconcentration, it is able to pattern arrays of multilayered membrane spots with more than 20-fold increased content of membrane proteins compared to existing methods.

6.1. Introduction

Membrane proteins play a prominent role in cellular function and therefore attract strong interest as therapeutic targets;[1-5] a great portion of the currently marketed therapeutic drugs target membrane proteins.[1,2,4] To identify new drug candidates by high throughput screening, the pharmaceutical industry would benefit from arrays that display

functional membrane proteins.[1-5] In addition, supported membranes[6-15] as well as arrays of membranes,[16-25] membrane proteins,[1-4,26] or native vesicles[5,27] are increasingly employed in academic research laboratories for studies of interactions between proteins and lipids,[28,29] proteins and membrane proteins,[1,2,4,26] as well as between therapeutic drugs and biomembranes.[21,22,30]

Despite their significance, membrane proteins are notoriously difficult to prepare in sufficient quantities and in correctly-folded, functional, and pure form.[2,3,15,31] Fabrication of arrays of these proteins has, therefore, remained challenging and limited to a few expert research groups.[1-4,11,26] Among the fabrication techniques developed to date,[1-3,26] robotic spotting is most common.[2-4] In this method, a robotic pin printer deposits small droplets of membrane suspensions onto substrates to create an array of membrane proteins.[2] Despite its usefulness, this method requires a robotic system and is hence not accessible to most academic research laboratories. In contrast, microcontact printing[20,32-35] is an accessible, simple, and well-established arraying technique that has been applied for fabrication of a variety of arrays, including arrays of supported lipid bilayers[20,34] and arrays of soluble proteins[32-34]. This technique has not, however, been adopted for direct fabrication of arrays of membrane proteins, presumably because stamping with poly (dimethylsiloxane) (PDMS) stamps requires drying of the ink on the posts of the stamp in order to preserve the fidelity of the micro pattern. In the case of preparations of fragile membrane proteins, this drying step can result in protein denaturation and is therefore typically avoided.[3]

Here we introduce a novel, straight-forward, and efficient method that employs hydrogel-based microcontact printing[21,28,36-41] to fabricate arrays of various membrane

proteins in a parallel and rapid fashion. The unique characteristics of hydrogel stamps provide a hydrated and biocompatible environment that makes it possible to employ microcontact printing for direct and rapid fabrication of membrane protein arrays. We demonstrate the capability of this technique to fabricate these arrays by two distinct approaches with complimentary benefits. In one approach, hydrogel stamps store small proteoliposomes and deliver them onto glass substrates. This procedure consumes a minimal amount of precious membrane preparations while fabricating multiple copies (at least 30) of a membrane protein array. In the other approach, which addresses the challenge of fabricating arrays from low abundance membrane proteins, hydrogel stamps preconcentrate and deliver relatively large membrane fragments (from mammalian cells) to bare or chemically-activated glass substrates. This procedure patterns multilayered membrane structures with more than 20-fold increased protein contents per area of the spot compared to existing methods. We employed the resulting membrane protein arrays to carry out ligand-binding assays with a fluorescently-labeled ligand and demonstrated excellent signal to background ratio of fluorescence.

Recently, we introduced a method that used topographically-patterned agarose gels to fabricate arrays of various lipid bilayers with up to 600 spots cm^{-2}.[21] We demonstrated that this method can create more than 100 copies of an array of functional[28] and fluid supported lipid bilayers[42] while using only picomoles of lipids.[21] This method was, however, limited to generating spots of lipid bilayers; it did not generate membrane spots that contained embedded transmembrane proteins. Here we expand the scope of this method to the important application of generating arrays of membrane proteins that are embedded functionally in lipid membranes. In addition, we demonstrate a novel aspect of

hydrogel stamps, namely preconcentration of large membrane fragments, that made it possible to generate arrays of multilayered membranes with high content of functional membrane proteins.

6.2. Results and Discussion

In order to generate arrays of membrane proteins, we used detergent dialysis to reconstitute an integral membrane protein, human tissue factor (TF), into small liposomes with a protein to lipid ratio of 1:5000 (containing 3% fluorescently-labeled lipids) and used the resulting proteoliposomes to ink an agarose stamp (Figure 6-1a). The small size of these proteoliposomes (diameter ~50 nm)[43] allowed them to diffuse into agarose stamps (364±8 nm pore size[44]) where these proteoliposomes were stored in a biocompatible and hydrated environment. Consequently, the inked stamp could be used to pattern 100 copies of a membrane protein array without intermediate re-inking. As shown in Figure 6-2a, the comparison between the mean fluorescence intensities of stamped membranes (by epifluorescence microscopy) within the 100 arrays revealed no significant decrease in the fluorescence intensity of lipids with increasing number of stamping event (except for the first 2-5 stamping events in which we always observed fluorescence intensities that were higher than the following arrays; this effect was probably due to transfer of excess material on the surface of the stamps during the very first stamping events). We also examined the fluidity of the stamped membranes by performing fluorescence recovery after photobleaching (FRAP) experiments (as described previously[21]) on membrane spots within different stamped arrays. These

experiments confirmed the mobility of lipid molecules within the stamped membrane spots (Figure 6-2b), indicating that at least 85 stamping events could be performed without loss in quality of the lipids in the stamped arrays.

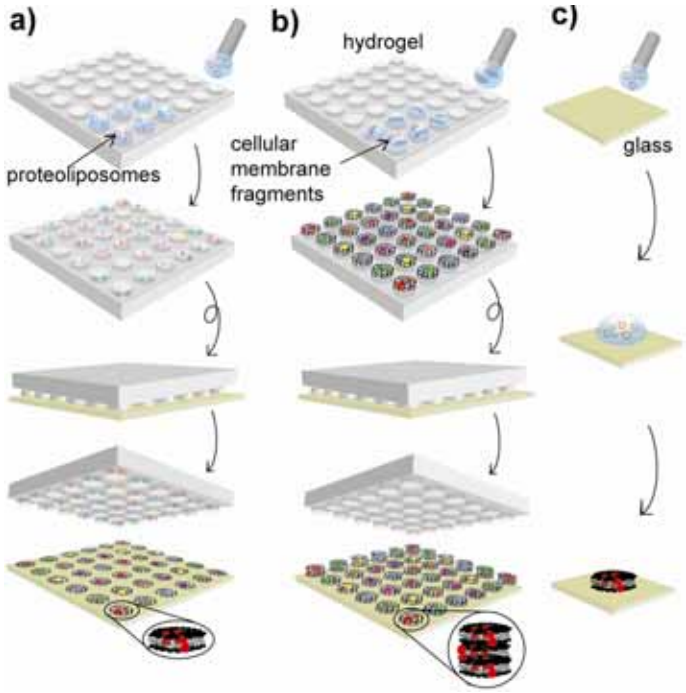

Figure 6-1. Cartoon comparing hydrogel stamping with spotting of membranes. (a) Storage of small proteoliposomes inside the posts of a stamp affords multiple printing of *single* lipid bilayers with embedded membrane proteins without intermediate re-inking. (b) Preconcentration of relatively large membrane fragments on the posts of the stamp affords patterning of arrays of *multilayered* cell membrane fragments with high protein content. (c) Preparation of droplet-derived membrane spots by deposition (spotting) of a droplet of a suspension of membrane preparations onto substrate. This droplet was incubated for 1h in a humid chamber to avoid drying by evaporation. Note, the resulting membrane arrays or spots were immersed in an aqueous solution immediately after their generation.

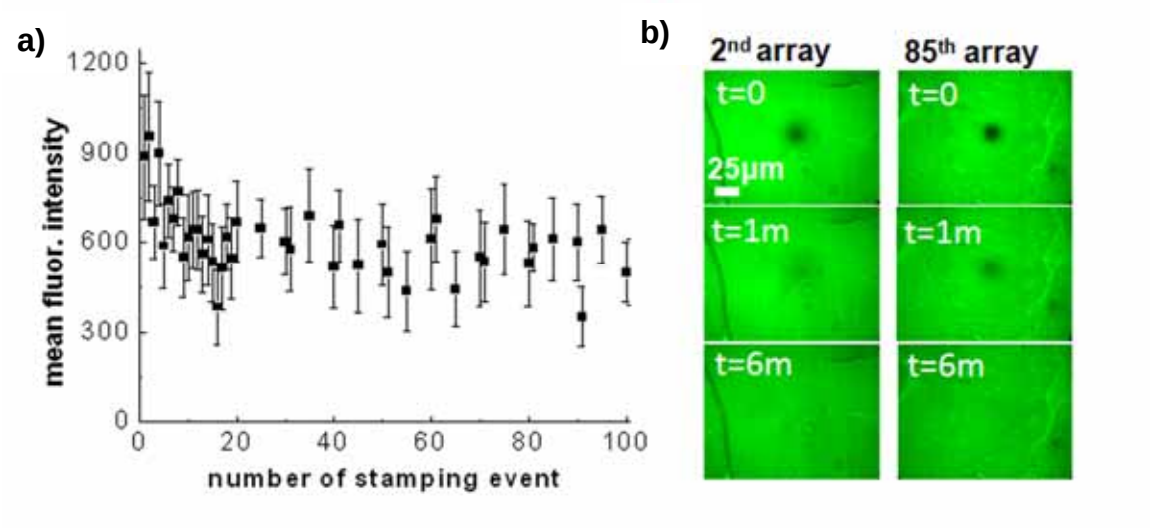

Figure 6-2. Multiple stamping of membrane arrays and comparison of lipids in membrane spots of 100 stamped membrane arrays. (a) Mean fluorescence intensity of fluorescently-labeled lipids (NBD-PE) in stamped membrane protein arrays as a function of the number of stamping events without intermediate re-inking. The error bars represent the standard error of the mean intensities of several of the membrane spots within each array. (b) Fluorescent micrographs from a FRAP experiment performed on a membrane from the 2nd and 85th stamped arrays.

In order to confirm the presence of TF proteins in these arrays, we added a primary antibody (pAb) against TF followed by exposure to a fluorescently-labeled secondary antibody (sAb*). Figure 6-2a shows that the fluorescent signal (and hence the content of TF in the membranes) remained close to constant during the first 30 stamped arrays. We also compared the fluorescent signal of these stamped membrane spots with control spots of supported membranes that we prepared by placing small droplets of solutions of membrane preparations on glass or γ-aminopropylsilane (GAPS) coated substrates (Figure 6-1c; this technique is similar to the method of robotic spotting[2] and

we refer to the resulting spots as “droplet-derived spots”, see Experimental Section for details).

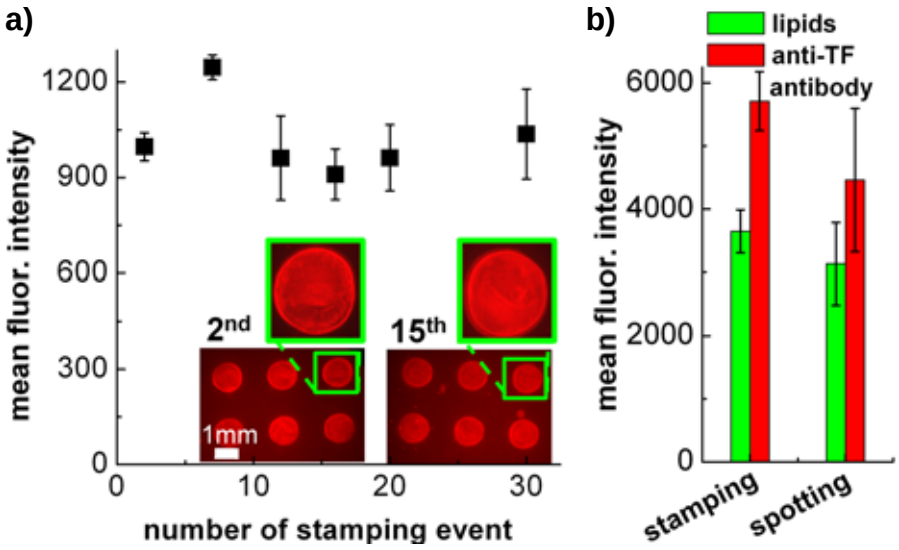

Figure 6-3. Multiple stamping of a membrane protein array using a stamp that was inked once and comparison of stamped membranes with droplet-derived membranes. (a) Mean fluorescence intensity of antibodies bound to TF proteins in membrane spots of arrays as a function of the number of stamping events. Error bars represent the standard error of the mean intensity of several spots in each array. Insets show fluorescent micrographs of two of these arrays. (b) Comparison of the fluorescence intensity of labeled-lipids (green) and antibodies bound to TF (red) in stamped membranes with droplet-derived membranes. Error bars represent the standard deviation of mean fluorescence intensities.

This comparison showed no significant difference between the stamped membrane spots and droplet-derived membrane spots (Figure 6-3b). We examined the

specificity of antibody binding to the TF-containing membrane spots by exposing one of these membrane spots only to the sAb* and detected no fluorescent signal in the absence of pAb against TF. Figure 6-4 shows fluorescent micrographs of two similar TF-containing membrane spots. One of these membrane spots was exposed to an anti-TF antibody followed by exposure to a fluorescent secondary antibody (Figure 6-4a), while the other spot was only exposed to the fluorescently labeled secondary antibody (Figure 6-4b). These images confirmed the specificity of antibody binding interactions.

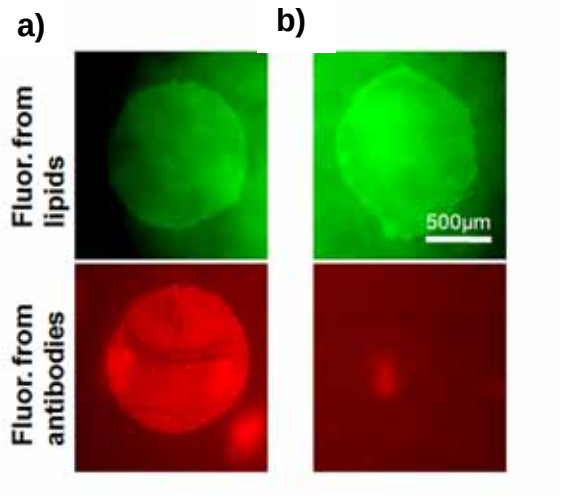

Figure 6-4. Fluorescent micrographs of two TF-containing membrane spots after exposure to (a) anti-TF primary antibody and fluorescent secondary antibody, and (b) fluorescent secondary antibody only (control experiment). Micrographs in the top row show the signal from the fluorescently-labeled lipids (NBD-PE) in these membranes (images taken with FITC filter setting). These images confirmed the similarity of these two membrane spots. Micrographs in the bottom row show the signal from fluorescent antibodies bound to TF in these membrane spots.

Stamping of small proteoliposomes, thus, made it possible to generate rapidly up to 30 copies of a membrane protein array while using a stamp that was inked only once with a total amount of 0.4 picomoles of TF per post of the stamp (i.e. ~13 femtomoles corresponding to ~ 470 pg of TF per spot). As shown in the Figure 6-5a, we observed no significant loss in fluorescent signal from the membranes within the first 30 stamped arrays. During further stamping events, however, this trend changed and the fluorescence intensity (and, hence, the amount of TF in membranes) started to decrease in a linear fashion. Despite this decrease, the signal that we detected from the antibodies bound to TF protein in the membrane spots of the 30^{th}-100^{th} arrays may be sufficient for some applications; Figure 6-5b shows a fluorescent micrograph of the 100^{th} stamped array and illustrates detectability of the membrane spots in this array even when using non-optimal optics (here a 2× objective).

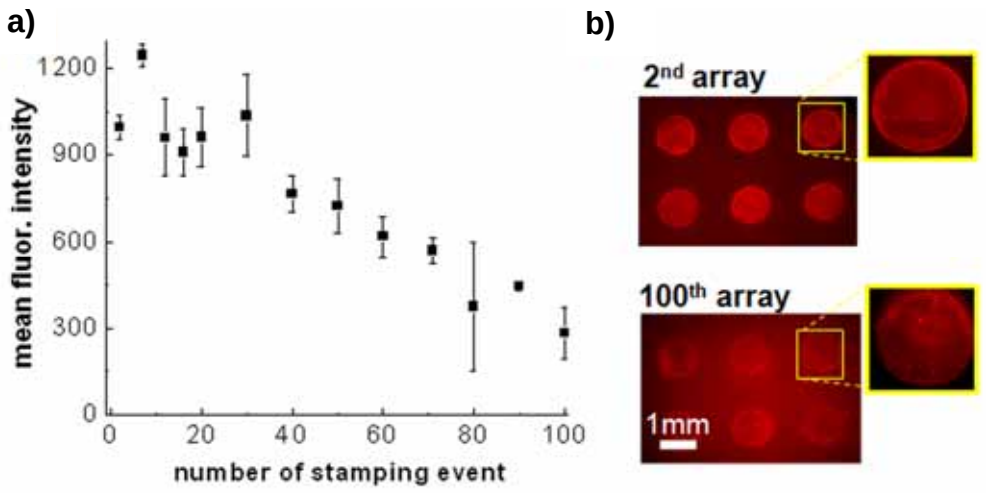

Figure 6-5. Multiple stamping of membrane arrays and comparison of TF proteins in membrane spots of 100 stamped arrays. (a) Mean fluorescence intensity of fluorescent antibodies bound to TF proteins in stamped membrane protein arrays as a function of the number of stamping events. The error bars represent the standard error of the mean intensities of several of the membrane spots within each array. (b) Fluorescent micrographs of the 2nd and 100th stamped membrane array. Note, images of the 100th array were acquired with more sensitive camera settings than the other images to obtain the fluorescence intensities shown in (a).

The results in Figure 6-2 and Figure 6-5, show that the fluorescent signal from the lipids and hence the amount of lipids remained almost constant during 100 stamping events while the amount of proteins decreased after 30 stamping events. We attribute this difference to the difference in size and mass and, hence, diffusivity of proteoliposomes compared to liposomes (without TF protein) in the agarose gel. An increased size and mass of proteoliposomes may slow their diffusion through the gel network compared to

other liposomes (that may have a low or no protein content) in the preparation. We, therefore, hypothesized that the smaller average size of liposomes without protein facilitated their diffusion through the gel and provided a sustained supply for stamping, while proteoliposomes diffused slower and therefore provided a limited supply for stamping. The long-lasting plateau in intensity from fluorescence of lipids (Figure 6-2a) compared to the initial plateau and gradual reduction of signal from antibody-labeled TF proteins supports this hypothesis (Figure 6-5a).

In order to extend this patterning method to membrane preparations that are typically used for drug binding studies,[2] we obtained membrane fragments from mammalian cells that contained the human nicotinic acetylcholine receptor (AChR) and reconstituted this transmembrane receptor into small liposomes. We inked agarose stamps with these proteoliposomes and stamped multiple arrays of membranes. Using epifluorescence microscopy, we found close to constant fluorescence intensity from the fluorescent lipids that we included during the reconstitution procedure in the membranes of these arrays. Immunofluorescence assays with pAb against AChRs and sAb*, however, revealed no detectable AChR in these membranes. We attribute the low fluorescent signal to the low initial concentration of AChRs in the original preparation of membrane fragments (<1 nM).

In order to maximize the protein concentration in the membrane preparation while simplifying the procedure and keeping the manipulation of membrane proteins to a minimum, we used cell membrane fragments directly and omitted the dialysis reconstitution step. We, thus, inked individual posts of agarose stamps with suspensions of membrane fragments that contained either AChRs or human dopamine transporters

(DATs) and printed several membrane arrays on glass or GAPS coated slides. Figure 6-6a and b show fluorescent micrographs of two arrays that were exposed to pAb against either AChR or DAT (both pAbs were from rat), followed by incubation with sAb*. The remarkably strong fluorescent signal from only one group of membrane spots in each of these arrays illustrated the specificity of binding interactions; pAb against AChR did not bind to DAT and pAb against DAT did not bind to AChR (Figure 6-6a, b). We compared the fluorescent signal of these stamped membrane spots with droplet-derived membrane spots. This comparison showed that hydrogel-stamped membrane spots containing AChR (Figure 6-6c) resulted in at least 20 times stronger fluorescence intensity upon binding of labeled antibodies against AChR compared to the intensity from droplet-derived spots. Figure 6-6d illustrates the fluorescence intensities from a similar comparison for DAT-containing membrane spots, revealing, again, at least 20-fold higher content of DAT in stamped spots compared to droplet-derived spots. The remarkably strong fluorescence intensity from antibodies bound specifically to AChRs or DATs in membranes of these stamped arrays (Figure 6-6a, b) suggested the presence of multilayer membranes with concomitant high protein contents in the stamped arrays. We hypothesized that the large size of membrane fragments impeded their diffusion into the network of the agarose gel (pore diameter of 243±5 nm for a 4% gel)[44] and that membrane fragments thus preconcentrated at the surface of the posts of the agarose stamps while excess liquid from the membrane preparation adsorbed into the gel (Figure 6-1b). Once we brought the inked stamps into contact with clean glass slides for 5-20 sec, the agarose posts transferred the preconcentrated membrane fragments onto the substrate, forming multilayer membrane structures with embedded membrane proteins (Figure 6-1b).

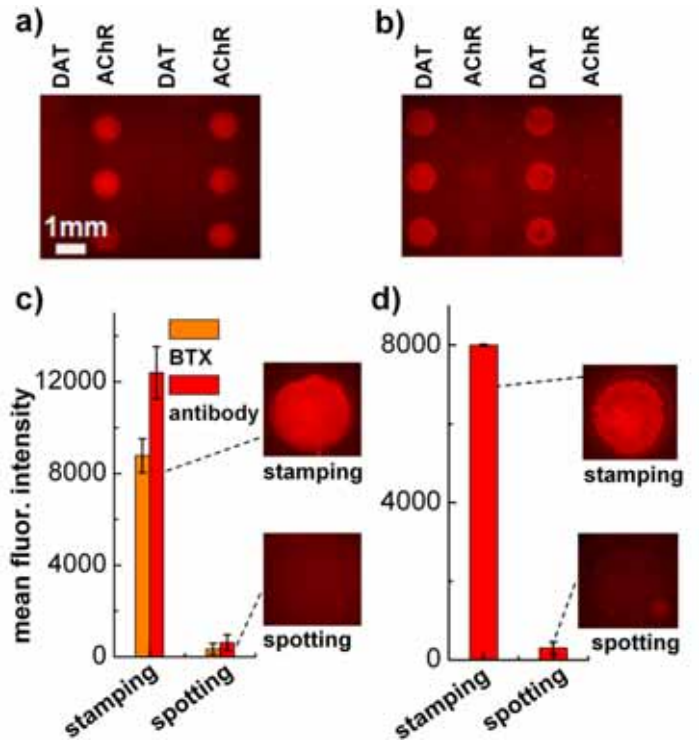

Figure 6-6. Stamped arrays of two different membrane proteins and comparison of stamped spots with droplet-derived spots. Fluorescence micrographs of arrays with alternating columns of DAT-containing and AChR-containing membranes after exposure to fluorescent antibodies against (a) AChR, and (b) DAT. (c) Comparison of fluorescence intensity from antibodies (red) or BTX (orange) bound to AChRs in stamped membranes with droplet-derived membrane spots. (d) Comparison of fluorescence intensity of antibodies bound to DATs in stamped membranes with droplet-derived membrane spots. Bar graphs show fluorescence intensities (after background subtraction) of stamped spots and droplet-derived spots. Error bars represent standard deviation of mean fluorescence intensities.

We confirmed the multilayered structure of these membranes by confocal microscopy (Figure 6-7) (see Experimental Section for details). Immunofluorescence

assays revealed that the employed stamp delivered almost all membrane fragments during the first stamping event; almost no membrane fragments were delivered during the following stamping events. This result confirms the hypothesis of preconcentration and subsequent multilayer-transfer.

For applications in the pharmaceutical industry it is important that membrane protein arrays can be used to carry out functional binding assays of ligands, agonists, or antagonists.[2-4] We investigated the suitability of the stamped membrane arrays for these assays by probing the binding of a fluorescently-labeled derivative of the neurotoxin α-bunguratoxin (BTX) to AChRs. Figure 6-6c compares the fluorescent signal from BTX bound to AChRs in stamped membranes with the signal from BTX bound to droplet-derived spots. The fluorescence intensities from bound BTX were in good agreement with the results from antibody binding and demonstrated at least a 20-fold higher content of AChR in stamped membrane spots compared to droplet-derived spots (Figure 6-6c). Moreover, this approach (i) directly employed cell membrane fragments with the benefit of minimized processing of membrane preparations, (ii) patterned multilayer spots of membranes with high protein contents, and (iii) minimized undesired and potentially denaturing interaction of membrane proteins with the supporting substrate[1,2,4,8-11,45] due to the presence of multilayer membranes.

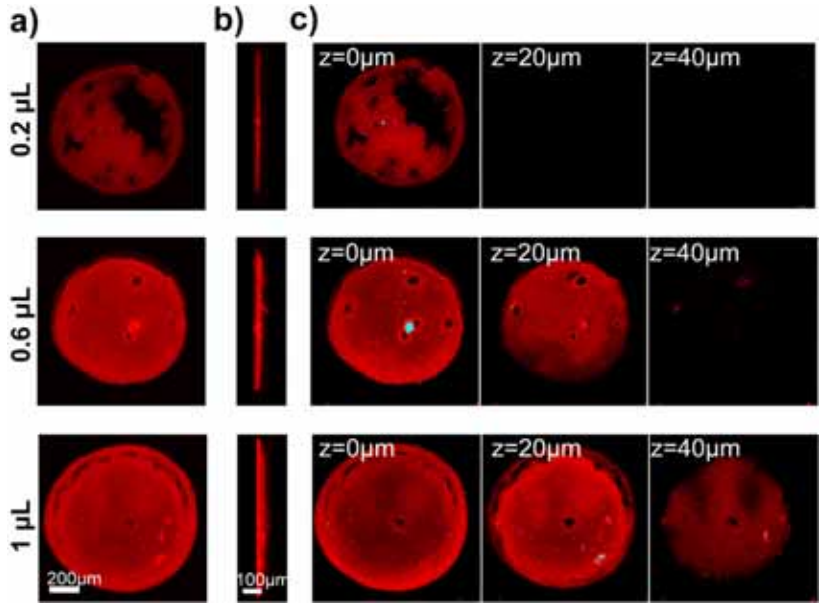

Figure 6-7. Confocal images of stamped membrane fragments containing AChR on a glass slide after exposure to fluorescent antibodies. These membrane spots were transferred from a stamp on which the posts were inked with 0.2 µL (first row of images), 0.6 µL (second row of images), or 1 µL (third row of images) of a solution of cell membrane fragments. (a) Top view, and (b) side view of rendered z-scans of the stamped membrane spots. (c) Confocal scans of these membrane spots at different distances (in z-direction) from the surface of the glass substrate confirming the multilayered nature of the spots. Note the exceptionally strong signal to background ratio of these multilayered membrane spots.

6.3. Conclusion

In conclusion, we present the first demonstration of microcontact printing of proteoliposomes and cell membrane fragments by taking advantage of the storage and preconcentration capability of biocompatible hydrogels. The method presented here is a

remarkably simple, efficient, and cost-effective method that requires only standard laboratory equipment and chemicals to fabricate membrane protein arrays in any laboratory within less than three hours. We carried out ligand-binding assays and showed that the resulting supported membrane proteins were functional and retained their binding activity. We employed this method for two distinct approaches to fabricate arrays of membranes with integral membrane proteins. One approach takes advantage of the storage capability of agarose stamps and minimizes the required time and amount of membrane proteins by generating multiple copies of a membrane protein array. This approach is particularly beneficial when membrane proteins can be reconstituted in relatively high concentrations and when fabrication of several copies of a membrane protein array is desirable. The other approach preconcentrates membrane fragments to generate arrays of multilayered membranes with high contents of embedded proteins and, thus, achieves more than 20-fold enhanced detection sensitivity while requiring only femtomoles of membrane proteins. This second approach is most beneficial when membrane proteins are sensitive to reconstitution or can be obtained only in low concentrations. The advantageous characteristics of these two complementary approaches make biocompatible hydrogel stamping compelling for fabrication of arrays of precious membrane proteins. We expect hydrogel-based microcontact printing of membrane protein preparations to be useful for the steadily growing interest in drug-membrane interactions and drug-protein interactions in industrial and academic research.

6.4. Experimental Section

6.4.1. Materials

We obtained high-gel strength agarose powder from OmniPur (Merck, Darmstadt, Germany). All the lipids, including 1-Palmitoyl-2-Oleoyl-*sn*-Glycero-3-Phosphocholine (POPC), porcine brain L-α-Lysophosphatidylserine (L-α-PS), and 1,2-Dimyristoyl-*sn*-Glycero-3-Phosphoethanolamine-N-(7-nitro-2-1,3-benzoxadiazol-4-yl) (NBD-PE) were obtained from Avanti Polar Lipids (Alabaster, AL, USA). We purchased recombinant human tissue factor (TF) and mouse monoclonal anti-TF antibody from Calbiochem (San Diego, CA, USA). We obtained cell membrane fragments containing human dopamine transporter (DAT) (transporter concentration of ~14.5 nM) and membrane fragments containing human acetylcholine receptor (AChR) (receptor concentration of ~1 nM) from PerkinElmer Life and Analytical Sciences (Boston, MA, USA). We purchased rat monoclonal anti-DAT antibody from Abcam (Cambridge, MA, USA), and rat monoclonal anti-AChR antibody from Sigma-Aldrich (St Louis, MO, USA). Alexa-fluor 555 goat anti-mouse antibody and alexa-fluor 555 goat anti-rat antibody were purchased from Molecular probes (Eugene, OR, USA). We purchased the detergent *n*-octyl-β-D-glucopyranoside (OG) from Sigma-Aldrich (St Louis, MO, USA) and the blocking solution of casein in phosphate buffered solution (PBS) from Pierce (Rockford, IL, USA). Buffer A solution contained 100 mM NaCl, 20 mM Hepes/NaOH buffer, pH 7.5, and 0.02% (w/v) sodium azide.

6.4.2. Fabrication of Agarose Stamps

We prepared agarose stamps with a concentration of 2-4% (w/v), as previously described.[21,39] We used 2% agarose stamps (pore size of 364±8 nm[44]) for multiple stamping applications and 4% agarose stamps (pore size of 243±5 nm[44]) for preconcentration applications. Briefly, we added agarose powder to a solution of 150 mM KCl, 10 mM Hepes, pH 7.4 and heated the mixture (in a microwave oven) to the boiling point, while shaking the beaker occasionally, until the agarose powder was completely dissolved. Then we immediately poured the hot solution onto a patterned PDMS master (placed inside a Petri dish) and quickly degassed the solution in a desiccator that was connected to a diaphragm vacuum pump to remove all air bubbles from the wells of the PDMS master (such bubbles can result in defective posts on the resulting stamp and must be removed). The PDMS master which contained wells with 1 mm diameter (and was used as the mold for agarose stamps) was a replica (positive) of a PDMS replica (negative) of a standard 1536-well plate (polystyrene) with flat bottoms (Corning, Cambridge, MA, USA).[21,39] The advantage of using a PDMS replica of a 1356-well plate, instead of the plate itself, is that the PDMS mold is elastomeric, which facilitates removal of the agarose stamp from the mold. We allowed the gel to form at 4˚C for one hour and peeled off the PDMS master to obtain topographically patterned agarose stamps.

6.4.3. Preparation of Small Proteoliposomes

We prepared small proteoliposomes containing human tissue factor (TF) by a detergent dialysis method as described by Neuenschwander *et al*.[46] Briefly, we generated

a lipid film by depositing a total of 0.65 micromoles of lipids composed of 77% (mol %) POPC, 30% L-α-PS, and 3% NBD-PE dissolved in chloroform in a round-bottom flask followed by pulling a vacuum while rotating the flask. We hydrated this lipid film with 100 μL of a freshly prepared solution of 100 mM OG in buffer A. In order to obtain a TF to lipid ratio of 1:5000, we added 189 μL of 1 mg mL^{-1} TF in deionized (DI) water to this mixture. The resulting mixed micelles containing lipids, TF, and OG were incubated at room temperature for 30 min followed by dialysis with a dialysis cassette (0.1-0.5 mL, 10,000 molecular weight cutoff) from Pierce in 1 L of buffer A. We replaced the buffer solution every 24 h for 72 h.

6.4.4. Preparation of Glass Substrates

We cleaned all microscope glass slides (pre-cleaned slides from Corning Inc., Corning, NY, USA) by immersing them in a freshly prepared Piranha solution (2:1 concentrated sulfuric acid and 30% hydrogen peroxide) for ~10 min. We rinsed these slides with copious amounts of DI water and stored them in DI water until use.

Glass slides coated with γ-aminopropysilane (GAPS II)[47,48] were purchased from Corning Inc. and we used them as obtained.

6.4.5. Inking and Stamping Procedure

We performed the inking and stamping procedure as previously described.[21] Briefly, once the agarose gel formed on the PDMS master, we peeled off the PDMS master and placed the resulting agarose stamp in a Petri dish containing water (with the

posts facing upwards) such that ~ 2/3 of the height of the stamp was immersed in DI water. We inked individual posts of the stamp by manually pipetting small droplets (~ 0.1 μL) of the desired solutions on top of each post. We often inked each post 2-4 times to supply adequate amounts of material (particularly for multiple stamping applications). Once no more excess liquid was visible on the surface of the posts, we employed the stamp to pattern an array of membranes. After removal of the stamp, we immediately immersed the patterned glass or GAPS II slides in water or buffer. For the multiple stamping experiments, when we inked the stamps with small proteoliposomes, we carried out the stamping procedure in a room with a humidity of >65% to avoid possible dehydration. As opposed to stamped arrays from small proteoliposomes, we found that stamped arrays from relatively large membrane fragments were not sensitive to humidity and we carried out these experiments in a standard laboratory without humidity control. We think that the transfer a multilayer of membranes retained adequate humidity to prevent dehydration. This characteristic of the novel concept of stamping multilayered membrane preparations is advantageous because it simplifies the procedure for stamping multilayered membrane arrays.

6.4.6. Preparation of Droplet-Derived Membrane Spots

We prepared droplet-derived membrane spots that are similar to spots produced by the method of robotic spotting,[47,48] as control for the stamped membrane spots. As reported by Lahiri and coworkers,[47,48] in the robotic spotting method, a robotic pin deposits small droplets of solutions of membrane preparations on a substrate (mostly, γ-

aminopropylsilane coated slides (GAPS II)). These authors incubated the patterned substrates in a humid chamber for 1 h and then employed them for ligand binding assays.[47,48] Attempting to follow this procedure to prepare droplet-derived membrane spots, we deposited small droplets (0.2-1 μL) of membrane preparations on a clean glass slide or on a GAPS II slide. To provide a defined border for these membrane spots, we often deposited the droplets inside a poly (dimethyl siloxane) (PDMS) frame (with a punched out hole in the center) that we sealed previously on the substrate. We matched the type of membrane preparations (small proteoliposomes versus cell membrane fragments) as well as the amount of material used to prepare these control membrane spots to the membrane preparation that we used to ink posts on the stamps. We left these membrane preparations in contact with glass for 1, 10, 40, and 60 min in a chamber with >85% humidity to protect the spots from drying (we always checked the droplets at the end of this incubation time to confirm that there was still liquid present on the spots). To wash away the excess solution of membrane preparations at the end of the incubation time, we immersed the entire setup in a large volume (~10 mL) of PBS and stored the resulting membrane spots in PBS solution for microscopy, imaging, and binding assays. Due to the surprisingly low signals (upon performing immunofluorescence assays) from these control experiments with droplet-derived spots, we decided to examine a few samples in which we deliberately dried out the droplets that contained the membrane preparations. To do so, we left a few droplets in the humid chamber for more than 5 h until they dried out and then processed them in the same way as the wet samples. Employing the resulting membrane spots on the glass slides for immunofluorescence assays, we noticed that this procedure resulted in almost no signal (probably because the

membrane was washed away from the substrate during wash steps). In case of GAPS II slides, however, immunofluorescence assays revealed a significantly higher signal compared to the samples that we kept wet at all times.

6.4.7. Microscopy and Imaging

To carry out imaging, we used an upright E600FN Nikon microscope equipped with an XCite 120 lamp (EXFO Life Sciences, Ontario, Canada) and a Coolsnap camera (Photometrics, Tucson, AZ). We acquired images using Metamorph 7 software (Universal Imaging, Downingtown, PA). All of the fluorescent micrographs presented in this work are false color images. We acquired images of NBD labeled lipids with filter settings for fluorescein and images of alexa-fluor 555 labeled antibodies with filter settings for rhodamine. We performed confocal microscopy with an inverted TE2000-U Nikon microscope equipped with an Argon 488 laser and a Helium-Neon 543 laser and a Nikon scan head. Confocal images were acquired by Nikon EZ-C1 3.5 software. (Image Systems, Inc., Columbia, MD).

6.4.8. Immunofluorescence Assays

As mentioned previously, patterned glass or GAPS II slides were immersed in PBS immediately after removal of the stamp. After performing epifluorescence microscopy on these arrays (to probe the quality of lipids in stamped membranes by imaging the fluorescent lipids in these preparations), we incubated these arrays in a solution of casein in PBS for 1 h to block the bare glass. We then incubated these arrays

in PBS solutions containing either anti-TF antibody (1.5 μg mL^{-1}), anti-DAT antibody (5.8 μg mL^{-1}), or anti-AChR antibody (0.75 μg mL^{-1}) followed by a fluorescently labeled secondary antibody; we used alexa-fluor 555 goat anti-mouse antibody (5.5 μg mL^{-1}), or alexa-fluor 555 goat anti-rat antibody (5 μg mL^{-1}). We carried out the incubation with antibodies at room temperature for 5-15 h with the primary antibody and for 1-3 h with the secondary antibody. We did not rinse the slides between these incubations and only rinsed them with PBS prior to imaging.

6.4.9. Characterization of Multilayered Membranes by Confocal Microscopy

In order to confirm the multilayer structure of stamped membrane fragments from cell preparations, we performed confocal microscopy on these membranes and used rendered z-scans of stamped membrane spots to probe the thickness of these spots. Figure 6-7 shows confocal images of stamped membrane spots that were transferred from a stamp on which each post had been inked with different amounts of membrane preparations. The membrane spots shown in Figure 6-7a, b, and c were transferred from posts that were inked with 0.2 μL, 0.6 μL, and 1 μL of solution of AChR-containing membrane fragments, respectively. In order to image one membrane spot completely in each image, we employed a 10× objective for this series of confocal images. Figure 6-7c shows z-scans of each of these three membrane spots at different distances from the glass surface and demonstrates the difference in thickness of these membrane spots. This figure clearly illustrates an increase in thickness of stamped membrane spots with increasing

amount of membrane preparations used to ink the corresponding posts on the stamp. These results confirm the multilayer structure of the stamped membrane spots.

6.4.10. Physical Properties of Membrane Arrays from Stamping Small Proteoliposomes

In previous work, we examined the structure and morphology of stamped spots of supported lipid bilayers (without embedded membrane proteins) by AFM,[21] these experiments revealed the presence of a single lipid bilayer on the solid substrate. We concluded that liposomes, once transferred to the solid substrate, fused with each other and with the surface by rupturing and forming individual supported lipid bilayers. We confirmed the presence of a continuous and fluid lipid bilayer within the stamped spots by demonstrating fluorescence recovery after photobleaching (FRAP).[21] If the liposomes would have remained as intact, individual liposomes, then we would not have observed recovery of fluorescence in the photobleached spot as demonstrated previously by Bourdillon's group.[15,49] Figure 6-2 demonstrates that stamping fluorescent lipids which were embedded along with membrane proteins in the small proteoliposomes that we used to ink the hydrogel stamps also recovered after photobleaching; this result suggests that hydrogel stamping of small proteoliposomes generated confluent membrane spots rather than individual intact liposomes[5,27].

Acknowledgements

We thank Dr. R.F. Capone and A.M. Sauer for their help and valuable discussions. This work was supported by Thermo Fisher and the Center for Chemical Genomics, University of Michigan, Ann Arbor.

References

1. C. Bieri, O. P. Ernst, S. Heyse et al., *Nat. Biotechnol.* **17** (11), 1105 (1999).
2. Y. Fang, A. G. Frutos, and J. Lahiri, *J. Am. Chem. Soc.* **124** (11), 2394 (2002).
3. V. Yamazaki, O. Sirenko, R. J. Schafer et al., *BMC Biotechnol.* **5** (2005).
4. Y. L. Hong, B. L. Webb, H. Su et al., *J. Am. Chem. Soc.* **127** (44), 15350 (2005).
5. H. Pick, E. L. Schmid, A. P. Tairi et al., *J. Am. Chem. Soc.* **127** (9), 2908 (2005).
6. Y. H. M. Chan and S. G. Boxer, *Curr. Opin. Chem. Biol.* **11** (6), 581 (2007).
7. F. Giess, M. G. Friedrich, J. Heberle et al., *Biophys. J.* **87** (5), 3213 (2004).
8. M. Tanaka and E. Sackmann, *Nature* **437** (7059), 656 (2005).
9. W. W. Shen, S. G. Boxer, W. Knoll et al., *Biomacromolecules* **2** (1), 70 (2001).
10. I. K. Vockenroth, P. P. Atanasova, A. T. A. Jenkins et al., *Langmuir* **24** (2), 496 (2008).
11. M. L. Wagner and L. K. Tamm, *Biophys. J.* **79** (3), 1400 (2000).
12. M. Merzlyakov, E. Li, I. Gitsov et al., *Langmuir* **22** (24), 10145 (2006).
13. S. Chiantia, J. Ries, G. Chwastek et al., *BBA-Biomembranes* **1778** (5), 1356 (2008).
14. B. Sanii, A. M. Smith, R. Butti et al., *Nano Lett.* **8** (3), 866 (2008).
15. C. Elie-Caille, O. Fliniaux, J. Pantigny et al., *Langmuir* **21** (10), 4661 (2005).
16. J. S. Hovis and S. G. Boxer, *Langmuir* **17** (11), 3400 (2001).
17. S. Lenhert, P. Sun, Y. H. Wang et al., *Small* **3** (1), 71 (2007).
18. C. K. Yee, M. L. Amweg, and A. N. Parikh, *J. Am. Chem. Soc.* **126** (43), 13962 (2004).

19. J. J. Shi, J. X. Chen, and P. S. Cremer, *J. Am. Chem. Soc.* **130** (9), 2718 (2008).

20. J. T. Groves, N. Ulman, and S. G. Boxer, *Science* **275** (5300), 651 (1997).

21. S. Majd and M. Mayer, *Angew. Chem. Int. Ed.* **44** (41), 6697 (2005).

22. J. T. Groves, *Curr. Opin. Genet. Dev.* **5** (4), 606 (2002).

23. M. A. Holden, S. Y. Jung, T. L. Yang et al., *J. Am. Chem. Soc.* **126** (21), 6512 (2004).

24. Y. Deng, Y. Wang, B. Holtz et al., *J. Am. Chem. Soc.* **130** (19), 6267 (2008).

25. A. R. Sapuri, M. M. Baksh, and J. T. Groves, *Biophys. J.* **82** (1), 166A (2002).

26. C. J. Kastrup, M. K. Runyon, F. Shen et al., *Proc. Natl. Acad. Sci. U S A* **103** (43), 15747 (2006).

27. D. Stamou, C. Duschl, E. Delamarche et al., *Angew. Chem. Int. Ed.* **42** (45), 5580 (2003).

28. S. Majd, D. J. Estes, and M. Mayer, *Calcium Binding Proteins* **1** (1), 26 (2006).

29. T. J. McIntosh and S. A. Simon, *J. Gen. Physiol.* **130** (2), 225 (2007).

30. Y. L. Hong, B. L. Webb, S. Pai et al., *J Biomol Screen* **11** (4), 435 (2006).

31. H. Bayley and P. S. Cremer, *Nature* **413** (6852), 226 (2001).

32. A. Bernard, E. Delamarche, H. Schmid et al., *Langmuir* **14** (9), 2225 (1998).

33. C. D. James, R. C. Davis, L. Kam et al., *Langmuir* **14** (4), 741 (1998).

34. L. A. Kung, L. Kam, J. S. Hovis et al., *Langmuir* **16** (17), 6773 (2000).

35. M. Tanaka, A. P. Wong, F. Rehfeldt et al., *J. Am. Chem. Soc.* **126** (10), 3257 (2004).

36. C. J. Campbell, S. K. Smoukov, K. J. M. Bishop et al., *Langmuir* **21** (7), 2637 (2005).

37. G. Mahmud, K. J. M. Bishop, Y. Chegel et al., *J. Am. Chem. Soc.* **130**, 2146 (2008).

38. B. D. Martin, B. P. Gaber, C. H. Patterson et al., *Langmuir* **14** (15), 3971 (1998).

39. M. Mayer, J. Yang, I. Gitlin et al., *Proteomics* **4** (8), 2366 (2004).

40. M. M. Stevens, M. Mayer, D. G. Anderson et al., *Biomaterials* **26** (36), 7636 (2005).

41. D. B. Weibel, A. Lee, M. Mayer et al., *Langmuir* **21** (14), 6436 (2005).

42. L. K. Tamm and H. M. McConnell, *Biophys. J.* **47** (1), 105 (1985).

43. S. A. Smith and J. H. Morrissey, *J. Thromb. Haemost.* **2** (7), 1155 (2004).

44. N. Pernodet, M. Maaloum, and B. Tinland, *Electrophoresis* **18** (1), 55 (1997).

45. A. J. Diaz, F. Albertorio, Susan Daniel et al., *Langmuir* **24** (13), 6820 (2008).

46. P. F. Neuenschwander, M. M. Fiore, and J. H. Morrissey, *J. Biol. Chem.* **268** (29), 21489 (1993).

47. Y. Fang, A. G. Frutos, Y. L. Hong et al., *Microarray Technology and Its Applications*, 309 (2005).

48. Y. Fang, A. G. Frutos, and J. Lahiri, *Chembiochem* **3** (10), 987 (2002).

49. A. Berquand, P. E. Mazeran, J. Pantigny et al., *Langmuir* **19** (5), 1700 (2003).

Chapter 7

Conclusion and Future Work

In this work, we developed two platforms for studying molecular interactions on model lipid membranes. The first part of this work introduces an ion channel-based sensor for monitoring the activity of membrane-active enzymes and the binding of bioactive molecules at the surface of the membrane. The second part of this work presented a straightforward approach to fabricate arrays of lipid bilayers and arrays of membrane proteins for screening of lipid-protein interactions and drug-membrane interactions. The concluding remarks and the future work of each of these two parts of this work are discussed in the following sections.

7.1. Gramicidin-Based Sensors for Quantifying Enzyme Activity and Molecular Interactions on Membranes

Gramicidin channel is well-studied ion pore with a great potential for sensing applications due to its small size, availability, and the relative ease with which chemical modifications on the channel can be performed.[1-7] In the first part of this thesis, we developed a novel sensor based on gramicidin channels and applied this sensor as an enzymatic assay to study the activity of phospholipases C and D and also as a binding

assay to screen the binding of quinine and imipramine to lipid membranes. In the following section, we mention two potential applications of this gA-based assay.

Monitoring Molecular Interactions through gA Kinetics

In this work, we demonstrated that gA channels can effectively report the activity of phospholipases D and C on lipid bilayers as well as the binding of charged molecules to lipid bilayers. To extract information about these interactions on the membrane, we monitored only changes in the single channel conductance of gA. Many pharmaceuticals are, however, known to alter the packing and order of lipids in the plasma membrane.[8] Interactions of these molecules with cellular membranes may, therefore, result in changes in membrane properties such as fluidity.[8] Considering the sensitivity of gA channels to membrane properties such as thickness and stiffness,[7,9] simultaneous screening of different aspects of gA channels including their single channel conductance, life time, opening and closing probability, and frequency may, in future, reveal more information on molecular interactions on the membrane through the changes in one or more of these gA characteristics.

Monitoring the Interactions of Hydrophobic Molecules with Membranes

In Chapter 4, we explored the application of the gA-based sensor developed in this thesis for screening the binding of electrically-charged molecules to lipid membranes. We demonstrated that the binding of charged molecules to lipid membranes results in a change in the surface charge density of the membrane and can be detected through the change in the single channel conductance of gA pores. For this application,

we assumed that the examined drug molecules bound only to the surface of the lipid membrane and did not penetrate into the bilayer and hence, did not alter the surface area of the membrane. For molecules with a relatively large hydrophobic part, this penetration would not, however, be negligible and may significantly increase the surface area of the membrane. In a membrane with a given net charge, an increase in the surface area of the membrane would lead to a decrease in the surface charge density of the membrane and would influence the gA conductance. Future studies might consider the effect of penetration of charged molecules into the bilayer on the conductance of gA and modify the theoretical approach of the binding assay presented in Chapter 4 accordingly. Future work might also take advantage of this effect to employ this gA-based sensor for probing the interactions of neutral molecules that are hydrophobic with charged membranes. When a neutral and hydrophobic molecule interacts with a membrane with a known amount of charge, although the binding of the neutral molecule to the membrane does not alter the net charge on the membrane, we hypothesized that penetration of the molecule into the bilayer reduces the surface charge density of the membrane and consequently, the conductance of gA. If feasible, this approach will broaden the scope of the presented binding assay in Chapter 4 and will enable this gA-based assay to screen the interactions of charged and neutral molecules with lipid membranes.

Application as a Flippase Assay

As demonstrated in Chapter 2, Figure 2-7, the gramicidin-based sensor presented in this thesis, could detect the transverse asymmetry in a lipid bilayer. This unique capability of this sensor platform may be applicable to study the enzymatic activity of

lipid flippases. Flippases are lipid transporters that play a pivotal role in cell homeostasis and belong to various subfamilies of the P-type ATPases and ATP-binding cassette (ABC) transporters.[10-12] These proteins are involved in regulating lipid asymmetry, cellular signaling, vesicle budding, and protein synthesis.[12] As a result, dysfunction of flippases causes different diseases including cholestasis, atherosclerosis, and visual impairment.[12] Established techniques employed to probe the activity of these proteins include fluorescent[13-16] and radioactive[17-19] assays. These assays rely on extraction,[14,17,18,20-22] fluorescent quenching,[13,15,16,21,22] or hydrolysis[23] of the labeled lipids in the outer leaflet of liposomes. Most of these techniques are, however, non-continuous and require labeling of lipid molecules. While combining some of these techniques (e.g. extraction and fluorescent quenching) with the stopped-flow kinetics[20,22] or florescence resonance energy transfer (FRET)[20] has enabled *in situ* monitoring of flippase activity, the need for labeling of lipids has remained the main drawback for this group of assays. An attempt to address this issue was recently reported where the activity of a flippase was monitored *in situ* and without labeling through the changes in shape of giant liposomes.[24] The gA-based sensor developed in this thesis might also present a label-free and sensitive platform assay for monitoring the activity of flippase proteins *in situ* and in real-time.

We have demonstrated that the conductance of gramicidin A (gA) channels is affected by electrical charges near the entrance of the channel and not by those near the exit of the channel. Since gA is a cation selective channel, the entrance of gA is always located in the positively polarized compartment of the bilayer setup and can be switched from one compartment to the other based on the polarity of the applied voltage. As such, gA channels embedded in an asymmetric lipid bilayer with one leaflet containing charged

lipids and one leaflet containing neutral lipids, have two different conductances depending on the polarity of the applied voltage. Enzymatic activity of a flippase on a lipid bilayer that contains charged lipids would result in a change in charge distribution between the two leaflets. This change would lead to a differential behavior in gA conductance depending on the polarity of the applied voltage and may, hence, be monitored through the single channel conductance of gA pores.

7.2. Hydrogel Stamping for Fabrication of Arrays of Membranes and Membrane Proteins

In summary, hydrogel-based microcontact printing method presented in the second part of this thesis is a simple and unique technique that makes it possible to fabricate multiple copies of microarrays of membranes with and without membrane proteins and even cell membrane fragments while consuming minimal amounts of these extremely expensive and hard to obtain biomolecules. The method is designed to prevent denaturation of fragile membrane proteins by taking advantage of the biocompatible and hydrated nature of agarose gels. This method has the potential to reduce the costs as well as to simplify, miniaturize, and accelerate HTS applications for both academic research and pharmaceutical drug discovery. In the following section, we mention some of the potential applications of hydrogel stamping method as well as the potential studies on this topic.

Arrays of Membrane Fragments from Human Organ Cells

We have demonstrated the ability of hydrogel-based microcontact printing to pattern arrays of lipid bilayers as well as arrays of cell membrane fragments that contained transmembrane proteins. Future work should, therefore, be able to employ this unique approach to produce arrays of membrane spots that represent the plasma membranes from human organ cells, in a rapid and parallel fashion while consuming minimal amounts of these membrane preparations. An array of micron-size membrane fragments, each from a different cell type from one of the body organs, would present a valuable test platform for drug discovery and development. Such a miniaturized and compact chip may be applied for rapid screening of interactions between potential therapeutic compounds and cell membranes of various cell types in human body.

Supported Membranes with Raft-Like Domains

Another future application of hydrogel-based microcontact printing is the fabrication of supported membranes that contain raft-like domains. As mentioned previously, lipid rafts are microdomains of elevated cholesterol levels within cell membranes that play a prominent role in a range of biological processes such as endocytosis and cell signaling.[25-27] These domains have also been implicated in a number of diseases such as AIDS, diabetes, and Alzheimer's.[25-27] While the significant role of lipid rafts in different diseases makes them attractive study subjects, their small size, divers molecular composition, and dynamic nature make studies of rafts in biological membranes challenging. A simple, well-defined, and stable system for investigating these microdomains would, therefore, be valuable in the field of biology. The hydrogel

stamping method can pattern domains of supported membranes with desired compositions of raft-forming lipids. Backfilling the resulting arrays by spreading various liposomes between the raft-like domains will form a continuous supported lipid bilayer with well-defined model rafts. In this thesis, we demonstrated the ability of hydrogel stamps to create multiple copies of a membrane array with various lipid compositions. Inking the posts on a hydrogel stamp with various liposomes, therefore, makes it possible to create rapidly many arrays of lipid rafts with various compositions. Applying different liposome solutions to backfill each stamped array would result in the formation of supported lipid membranes that can vary in both, the lipid composition of the raft, and the lipid composition of the supporting membrane.

Such raft-containing membranes can be employed to study the partitioning of different proteins into the rafts and the effect of different drugs on rafts. An interesting application of these raft-containing membranes is to study the role of lipid rafts in the formation of amyloid plaques that are the main hallmarks of the Alzheimer's disease.[25] Considering the possible role of lipid rafts in a range of other diseases including AIDS, diabetes, and asthma,[25-27] a well-defined and high-throughput system to study lipid rafts may provide a general platform to study the molecular details that are involved in these diseases and to find effective therapeutic targets.

Application in Industry

Hydrogel stamping method, as presented here, is a simple and low-tech technique that requires no special equipment, chemical or even surface treatment and makes it possible to fabricate multiplexed arrays of membrane preparations in almost any

laboratory within few hours. The current hydrogel stamping method, however, requires manual pipetting of the ink solutions onto individual posts of a stamp, which may be challenging and time-consuming for certain large-scale applications. In order to transfer this technology to industrial research, therefore, future work may address this issue by employing robotic pin printing technology[28] for the inking procedure.

Hybrid Surfaces with Patterned Conductive Polymers

Furthermore, future work may employ hydrogel stamping to modify solid substrates with patterned conducting polymers. Once brought into contact with a conductive substrate (e.g. glass coated with gold), a hydrogel stamp that is loaded with desired monomers can act as an aqueous solution with a defined shape and contact area. Applying an appropriate voltage between the conductive substrate and an electrode inserted into the hydrogel stamp would, hence, initiate polymerization at the regions of contact between the stamp and the substrate. Given the growing application of conductive polymers for biomedical applications, such a controlled patterning method might provide a unique tool to create new hybrid substrates.

References

1. O. S. Andersen, *Annu. Rev. Physiol.* **46**, 531 (1984).
2. O. S. Andersen, R. E. Koeppe, and B. Roux, *IEEE Trans. NanoBiosci.* **4** (1), 10 (2005).
3. H. J. Apell, E. Bamberg, and P. Lauger, *Biochim. Biophys. Acta* **552** (3), 369 (1979).
4. S. Blake, R. Capone, M. Mayer et al., *Bioconjugate Chem.* **19** (8), 1614 (2008).
5. R. Capone, S. Blake, M. R. Restrepo et al., *J. Am. Chem. Soc.* **129** (31), 9737 (2007).

6. T. K. Rostovtseva, V. M. Aguilella, I. Vodyanoy et al., *Biophys. J.* **75** (4), 1783 (1998).

7. T. K. Rostovtseva, H. I. Petrache, N. Kazemi et al., *Biophys. J.* **94** (4), L23 (2008).

8. J. K. Seydel and M. Wiese, *Drug-Membrane Interactions* (Wiley-VCH, Weinheim, 2002).

9. D. A. Kelkar and A. Chattopadhyay, *BBA-Biomembranes* **1768** (9), 2011 (2007).

10. D. L. Daleke, *J. Biol. Chem.* **282** (2), 821 (2007).

11. P. F. Devaux, *FEBS Lett.* **234** (1), 8 (1988).

12. T. Pomorski and A. K. Menon, *Cell. Mol. Life Sci.* **63** (24), 2908 (2006).

13. P. D. W. Eckford and F. J. Sharom, *Biochemical Journal* **389**, 517 (2005).

14. P. Natarajan and T. R. Graham, *Methods* **39** (2), 163 (2006).

15. Y. Romsicki and F. J. Sharom, *Biochemistry* **40** (23), 6937 (2001).

16. R. A. Vishwakarma, S. Vehring, A. Mehta et al., *Organic & Biomolecular Chemistry* **3** (7), 1275 (2005).

17. C. G. Frank, S. Sanyal, J. S. Rush et al., *Nature* **454** (7204), E3 (2008).

18. S. Sanyal, C. G. Frank, and A. K. Menon, *Biochemistry* **47** (30), 7937 (2008).

19. S. Sanyal and A. K. Menon, *Proceedings of the National Academy of Sciences of the United States of America* **106** (3), 767 (2009).

20. U. Marx, G. Lassmann, H. G. Holzhutter et al., *Biophysical Journal* **78** (5), 2628 (2000).

21. Q. L. Chang, S. N. Gummadi, and A. K. Menon, *Biochemistry* **43** (33), 10710 (2004).

22. S. Vehring, L. Pakkiri, A. Schroer et al., *Eukaryotic Cell* **6** (9), 1625 (2007).

23. S. N. Gummadi and A. K. Menon, *Journal of Biological Chemistry* **277** (28), 25337 (2002).

24. A. Papadopulos, S. Vehring, I. Lopez-Montero et al., *Journal of Biological Chemistry* **282** (21), 15559 (2007).

25. H. P. Cheng, K. S. Vetrivel, P. Gong et al., *Nature Clinical Practice Neurology* **3** (7), 374 (2007).

26. E. C. Jury, F. Flores-Borja, and P. S. Kabouridis, *Seminars in Cell & Developmental Biology* **18** (5), 608 (2007).

27. K. Simons and L. Rajendran, *Journal of Neurochemistry* **108**, 43 (2009).

28. V. Yamazaki, O. Sirenko, R. J. Schafer et al., *Bmc Biotechnology* **5** (2005).